EVALUATION OF METAL DUSTING OF NICKEL-CHROMIUM-IRON BASED ALLOYS IN A LABORATORY ENVIRONMENT

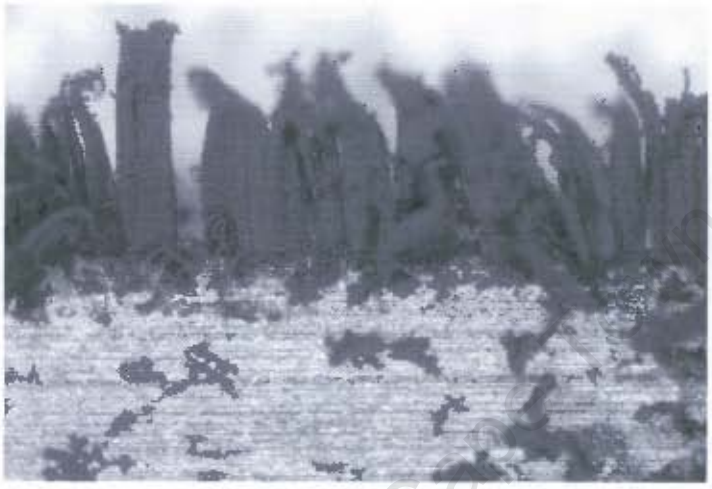

BY

MPHO DAVID MAREKWA

A thesis submitted to the Faculty of Engineering and Built Environment of the University of Cape Town in fulfilment of the requirement for the degree of Master of Science in Applied Science in Materials Engineering

Centre for Materials Engineering
Department of Mechanical Engineering
University of Cape Town

July 2006

UNIVERSITY OF CAPE TOWN

ACKNOWLEDGEMENTS

I would like to thank my family for their help and encouragement throughout my project. Without them, it would not have been completed.

I would like to express my sincere gratitude to the following people for their significant contribution during this research project:

- My supervisor, Dr K. Marcus, for his encouragement and guidance throughout this project.
- Mr E. Filmalter at PetroSA for supporting the project and providing the financial support.
- Mr G. Newins and Mr P. Jacobs for manufacturing my fixtures.
- Mrs M. Waldron for her assistance in using the electron microscope.
- Mrs N. Africa for her administrative assistance.
- Mrs P. Park-Ross for her assistance and advice with equipment in the laboratory.
- Dr S. Kwofie for his advice and guidance.
- Mr Neville Thomas (Special Metals, UK) and Mr Ken Perel (Multi-alloys, RSA) for supplying the metal alloys.
- Mr A. Pietersen at the SA Naval Laboratories for his assistance with spark emission spectroscopy compositional analysis of the specimens.
- Staff and students at the Centre for Materials Engineering for their support and encouragement.
- The financial support of the NRF is gratefully acknowledged.

ABSTRACT

The deposition of carbon from a carbon-rich environment onto structural materials is prevalent in petrochemical and chemical industries such as in the production of syngas, iron reduction plants, petroleum refineries, carbon dioxide cooled nuclear plants, fuel cells using molten salts and hydrocarbons, and the recycle–gas loop equipment of coal–gasification units. The consequence of carbon deposition is a metal related degradation phenomenon known as "Metal dusting". Metal dusting results in rapid material wastage and/or thinning of material, producing hemispherical pits and grooves as the affected material disintegrates into a mixture of carbon and metal particles.

The aim of this study was to elucidate material factors that cause or contribute to metal dusting. This was achieved by refurbishing the in-built metal dusting rig to carry out experimental tests on a laboratory scale. The objectives of this research were to simulate a metal dusting environment, characterize the resistance of various alloys to metal dusting, and to evaluate the effects of surface treatment and temperature on metal dusting. Metal dusting was induced on a wide variety of nickel-based and iron-based alloys which were capable of forming chromium oxide scales in a flowing CO-H_2-H_2O atmosphere at 650°C and 500°C. Some of the alloys were heat treated at 850°C for an hour prior to exposure and others were ground to 600 grit SiC. Some degree of metal dusting attack was observed for all alloys tested except for an alloy with high chromium and nickel content. The results indicated that metal dusting is much more aggressive at lower temperatures than at high temperatures. It was also observed that the surface working of the alloys had a very significant effect to metal dusting resistance as well as the amount of scale forming elements additions and the presence of certain carbides forming elements. The preheat treatment seemed not to have a significant effect on the resistance to metal dusting.

GLOSSARY

PetroSA	**Petroleum Oil and Gas Corporation of South Africa**
LPG	**Liquid Petroleum Gas**
CO	**Carbon monoxide**
H_2	**Hydrogen**
CH_4	**Methane**
Cr_2O_3	**Chromium oxide**
SiO_2	**Silicon oxide**
Al_2O_3	**Aluminium oxide**
CO_2	**Carbon dioxide**
°C	**Degrees Celsius**
CH_4	**Methane**
Fe_3C	**Iron carbide or Cementite**
J	**Diffusion flux**
m	**meter**
s	**seconds**
K	**Kelvin**
D	**Diffusion coefficient**
dC/dx	**Concentration gradient**
D_0	**Temperature independent pre-exponential**
Q_d	**Activation energy for diffusion**
R	**Universal gas constant**
T	**Temperature**
a_C	**Carbon activity**
Kg	**Kilograms**
P_{CO}	**Partial pressure of carbon monoxide**
P_{CO_2}	**Partial pressure of carbon dioxide**
P_{CH_4}	**Partial pressure of methane**

P_{H_2O}	**Partial pressure of water**
P_{O_2}	**Partial pressure of oxygen**
K_i	**Equilibrium constant of the reaction**
CPT	**Carbon precipitation temperature**
H_2S	**Hydrogen sulphide**
S	**Sulphur**
$S_{(ad)}$	**Adsorbed sulphur**
GRD	**Ground samples**
ARD	**As-received samples**
HT	**Heat-treated samples**
ΔG°	**Standard Gibbs free energy change**
SEM	**Scanning electron microscopy**
EDS	**Energy dispersive spectroscopy**
VHN	**Vickers's micro-hardness number**

TABLE OF CONTENTS

CHAPTER ONE

GENERAL INTRODUCTION

1.1 METAL DUSTING BACKGROUND

Carbon is regarded as a very important alloying element in steels and alloys because of its significant influence on the mechanical properties [1]. For example, increasing the carbon level of steels increases the hardness and strength. It can also have an influence on the corrosion behaviour of steels and alloys. In chromium-alloyed steels, carbon reduces the resistance of corrosion by forming carbides and locally depleting the metal matrix of chromium [2-4].

The process of increasing the carbon level in steels is known as carburization. The deposition of carbon from a carbon-rich environment onto structural materials is prevalent at petrochemical and chemical industries such as in the production of syngas, iron reduction plants, petroleum refineries, carbon dioxide cooled nuclear plants, fuel cell using molten salts and hydrocarbons, and the recycle–gas loop equipment of coal–gasification units [5-7]. The consequence of carbon deposition is a carbon related degradation phenomenon known as a "metal dusting".

Lately, intensive research on metal dusting was done by Grabke *et al* and Pippel *et al* [8,9]. Metal dusting is described as a catastrophic form of carburization which occurs under conditions where the carbon activity (a_c) of the gaseous atmosphere is greater than one [6]. This results in rapid material wastage and/or thinning of material, producing hemispherical pits and grooves as the affected material disintegrate into a mixture of carbon and metal particles. Metal dusting occurs in intermediate temperatures of 450°C - 800°C [8]. This corrosion phenomenon has become a serious problem in recent years.

The main cause of metal dusting is the growth of graphite in the metal, leading to the disintegration of the metal. However, the mechanism and type of attack are different depending on the metal composition and temperature of the environment.

1.2 INDUSTRIAL EXPERIENCE ON METAL DUSTING

The combination of natural gas or methane with steam at high temperature produces a mixture of gases commonly known as "syngas" which contains H_2, CO, CO_2, H_2O, and CH_4 [10]. Metal dusting is prevalent in such gas mixtures at a temperature range of about 450°C to 800°C. Iron and nickel-based alloys are susceptible to metal dusting [11]. The alloys that are commonly used in petrochemical and chemical industries are Ni-Cr-Fe based alloys such as Inconel ® alloy 600 (Alloy 600), Incoloy ® alloy 800 (Alloy 800), and Inconel ® alloy 601 (Alloy 601).

An adherent, protective, self-repairing oxide scale is said to protect the alloy surface against metal dusting [6,10-12]. For greater efficiency of the plant, the amount of steam is often decreased, leading to lower steam-to-hydrogen ratios (H_2O/H_2). The amount of CO content in syngas is increased as a result of high pressures required for greater efficiency of the plant. The combination of the lower H_2O/H_2 ratios and CO/CO_2 ratios results in lower O_2 partial pressures and high carbon activities [10]. Consequently, the metal dusting propensity and severity is increased.

A heat exchanger made up of Alloy 800 (20% Cr-32% Ni) failed after 23 000 hours by local wastage [6]. The wall of Alloy 800 was wasted from 10 mm to 3 mm and a weldment in the wall of Alloy 800 which was made up of Alloy 600 (15% Cr-72% Ni) was less attacked than Alloy 800. Failure of structural components in industries has been reported in detail by Grabke *et al* in gas heaters of direct reduction plants, platform units in refinery, direct reduction furnaces, and heat exchangers of an ammonia plant [6]. Metallic interconnects in solid oxide fuel cells (SOFC) are susceptible to metal dusting since they act as gas separators and

distributors. The environment in which metallic interconnects operate contains natural gas or methane at temperature ranges of 550°C to 800°C [12].

Metal dusting is prevalent in transfer lines and ferrules since syngas is produced above the critical metal dusting temperature (>>800°C) and transferred to a boiler via a transfer line where it is rapidly quenched to a temperature below the critical metal dusting temperature range (<800°C) [10,13]. Under such conditions carbon deposition is theoretically possible and metal dusting can occur. Alloy ferrules that are used in the transfer line do often experience metal dusting and are periodically replaced. Figure 1.1 shows a metal dusted ferrule from the PetroSA plant in Mossel Bay. The arrows show the severity of corrosion on the ferrule.

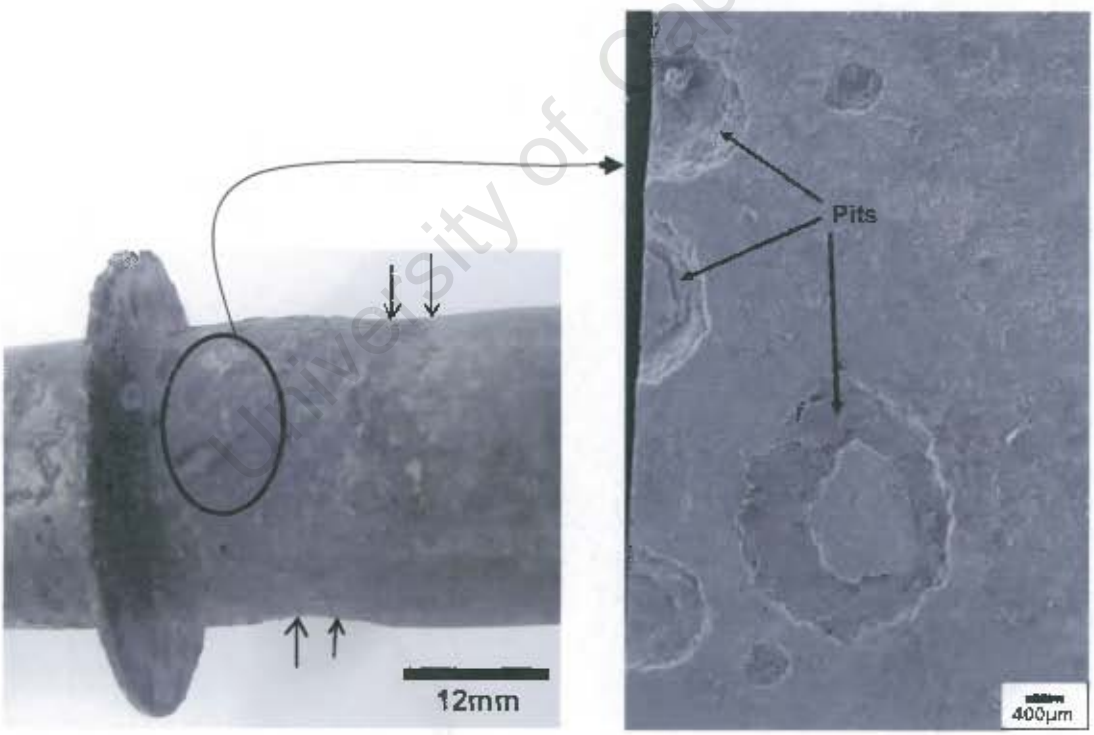

Figure 1.1: The double arrows shows deformation of a ferrule (Alloy 600) and the type of damage such as pits. It was used to protect the tube sheet from the gas temperature. The sample was received from the PetroSA plant in Mossel Bay.

A tube built of Alloy 800 from the secondary reformer was also attacked by metal dusting, see Figure 1.2. The arrows shows a cross-section of the material where it was not attacked and a region where it was attacked. The pit depth and width ranged from about 0.5 to 5 mm.

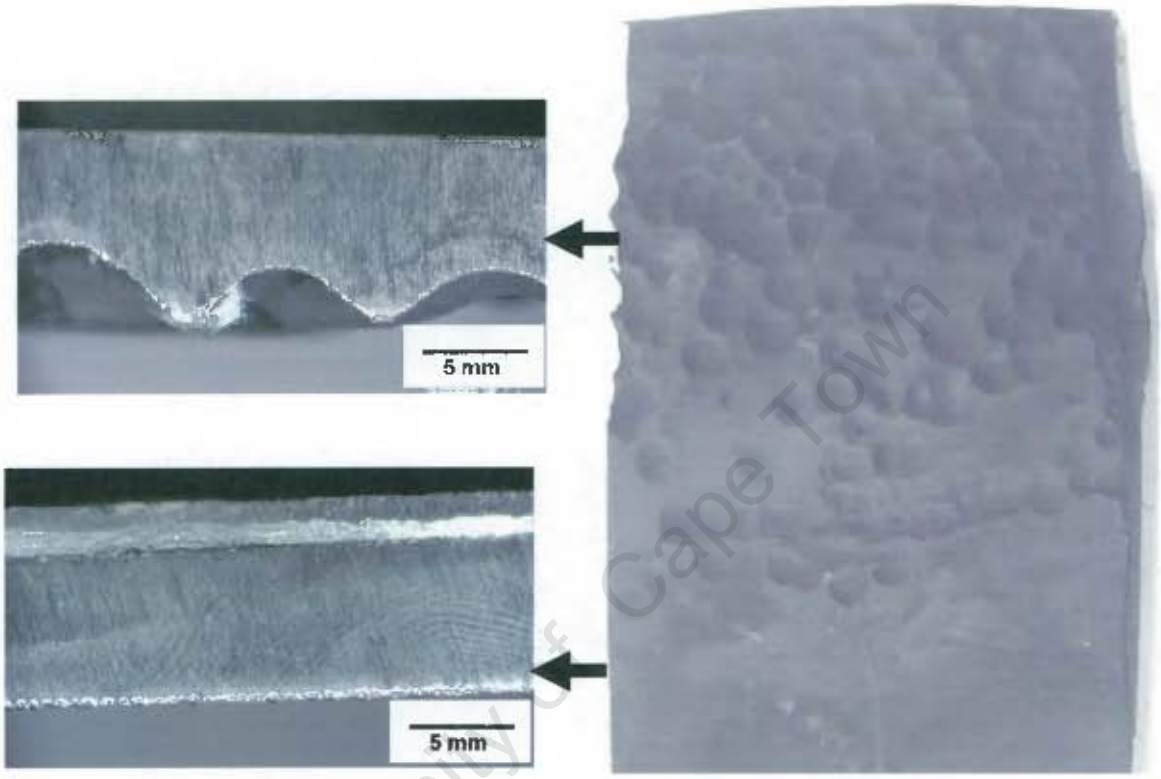

Figure 1.2: Photographs of Alloy 800 showing local pits on its surface. Uniform wastage was observed at certain areas on the alloy surface.

Alloy 600 liners inside the neck of the reformer had been affected by metal dusting and a big chunk of it came out and was lodged in a burner/mixer arrangement. Alloy 600 was metal dusted whereas Alloy 800 was not affected by metal dusting. These two alloys were exposed to the same environment [14]. A similar phenomenon of Alloy 800 outperforming Alloy 600 was observed in quite a number of cases at the PetroSA plant. The theory predicts that Alloy 600 should resist metal dusting much better than Alloy 800. Failure of Alloy 800 has been reported by numerous researchers before. A rather random attack of metal dusting experienced across all types of plants makes it difficulty to propose a resistant material.

Grabke *et al* emphasized that in principle no metallic material which can dissolve carbon, is resistant to disintegration by metal dusting and long term suppression of metal dusting is only possible by a stable oxide scale and retardation is possible by low carbon solubility and diffusivity and high content of carbide forming elements [11].

1.3 PROJECT MOTIVATION

In South Africa, PetroSA converts natural gas from sub-sea wells located 85 km south of Mossel Bay to synthetic fuels [14]. Natural gas and associated condensate are pumped from the sub-sea wells, and transferred to the processing plant for conversion to petrol, diesel, kerosene, alcohol and liquid petroleum gas (LPG). The methane rich natural gas is reformed to syngas by reaction with steam and oxygen at high temperature in the secondary reformer. The secondary reformer is regarded as the heart of the plant. A super heater in a secondary reformer was affected by metal dusting. Consequently, metal dusting has been causing unscheduled process unit shut downs at the PetroSA plant. The plant was shut down for three months to replace the affected super heater. It cost PetroSA 51.6 million rands to replace the super heater excluding loss of profit during that three months of repairing.

Transfer lines and ferrules often experiences metal dusting and are periodically replaced. However, that does not solve the problem as metal dusting often causes unscheduled process shut downs and increases maintenance expenditure. Prevention of this requires investigations of materials that will resist metal dusting. Past research has shown that such materials include alloys containing good combinations of Cr, Si, Al, Ni and carbide forming elements [6,15-17]. The microstructure and surface finish of such alloys also have an effect on the resistance to metal dusting.

Available information on the resistance to metal dusting may be misleading because, for example, Alloy 800 was reported to be less resistant to metal dusting than Alloy 600. Failure of Alloy 800 and Alloy

600 due to metal dusting has been reported [6,12,16-18]. At PetroSA, Alloy 800 was not attacked by metal dusting whereas Alloy 600 was attacked although they were exposed to the same environment [14]. This contrasting information has led to a decision to conduct an alloy exposure programme on a laboratory scale to compare the performance of different alloys. The results will be compared with those described in published literature on metal dusting and recommendations will be made to reduce or eliminate the problem of metal dusting at the PetroSA plant.

1.4 AIMS OF THE PROJECT

The aim of this project is to elucidate material factors that cause or contribute to metal dusting. The findings will help plant designers to choose the right alloys for metal dusting resistance and would add more knowledge on the behaviour of nickel-iron-chromium alloys in a atmosphere containing CO-H_2-H_2O gas mixture. This entails carrying out experimental tests on a laboratory scale by building a simulation rig. The major objectives of this research project are:

- To simulate the metal dusting environment.
- To evaluate the reliability of mass loss/gain as a measure of the resistance to metal dusting.
- To characterize the resistance of various alloys to metal dusting.
- To evaluate the effects of surface treatment and temperature on metal dusting.

1.5 LIMITATION OF THIS THESIS

The limitation of this thesis is that it is mainly experimentally based. In this regard no modelling software has been used.

1.6 OUTLINE OF THIS THESIS

The thesis begins with a literature review, *Chapter Two.* The literature review discusses the cause of metal dusting corrosion and methods of suppressing it. *Chapter Three* describes all the test fixtures that were designed by the author to carry out the experiments of this project and describes all the experimental techniques employed in this thesis. All the results are shown in *Chapter Four* and discussed in *Chapter Five.* The conclusions that were drawn from *Chapter Four* and *Five* are stated in *Chapter Six.* Recommendations for future work are listed in *Chapter Seven*.

CHAPTER TWO

LITERATURE REVIEW

2.1 INTRODUCTION

Corrosion is a naturally occurring degradation mechanism that is defined as the destructive and unintentional attack of a metal [19]. It can cause extensive and costly damage to structural metals. Corrosion is prevalent and takes many forms. Its occurrence cannot be eradicated completely. Corrosive environments include the atmosphere, aqueous solutions, soil, acids, bases, inorganic solvents, molten salts and the human body [19]. The variables in the corrosion environment, which includes fluid velocity, composition and temperature, can have a certain influence on the corrosion properties of the metal that are in contact with it. Corrosion occurs on the unprotected surface. Different environments can cause different types of corrosion attack that may vary in nature and appearance. The several forms of corrosion that can occur on metals depending on the environment are:

- Uniform or General corrosion
- Galvanic corrosion
- Crevice corrosion
- Pitting corrosion
- Intergranular corrosion
- Selective leaching corrosion
- Stress corrosion cracking
- Corrosion fatigue
- Erosion corrosion

All these corrosion forms have been studied for years and the literature on them are widely available [19,20].

2.1.1 Uniform or General Corrosion

Uniform corrosion is a uniform attack of the entire metal surface characterized by the rusting of steel [19,20]. Other forms of general corrosion are tarnishing of silver or green patina associated with the corrosion of copper. This type of attack is mostly found where a metal is in contact with an acid or a humid atmosphere. It is the least harmful because the rates of corrosion can be measured and predicted. Some common methods used to prevent or reduce uniform corrosion are coatings, cathodic protection and inhibitors.

2.1.2 Galvanic Corrosion

Galvanic corrosion occurs when two different metals are in electrical contact and immersed in the same corrosive solution or environment [19,20]. When dissimilar metals are placed in an electrolyte, they assume different corrosion potentials. Hence, the potential difference is the driving force for galvanic current flow [19]. The less noble metal in the galvanic couple will become the anode and experience corrosion, while the more noble metal (cathode) will be protected from corrosion. Common methods used to reduce or prevent this type of corrosion are to choose the metals that are close together in the galvanic series, use an anode area as large as possible, insulate dissimilar metals from each other, and cathodic protection [19,20].

2.1.3 Crevice Corrosion

Crevice corrosion is a form of localized corrosion which occurs in a crevice formed between two surfaces, one at least of which is a metal [19,20]. It

is caused by depletion of oxygen in the crevice. Consequently oxidation of the metal occurs and electrons from this electrochemical reaction are conducted through the metal to the adjacent external region, where they are consumed by the reduction reaction. Crevice corrosion can be prevented by using welded instead of riveted or bolted joints, frequently removing the accumulated deposits, designing containment to avoid stagnant areas and ensure complete drainage of fluids [19,20].

2.1.4 Pitting Corrosion

Pitting corrosion is a localized form of corrosion which results in small holes or perforations through the material, but with little measurable general metal loss [19,20]. Pitting has the same mechanism as crevice corrosion in stainless steels [20]. Some of the methods used to reduce or prevent pitting corrosion are to use alloys with high content of chromium, molybdenum and dissolved nitrogen. The use of cathodic protection is also effective against pitting.

2.1.5 Intergranular Corrosion

Intergranular corrosion is due to the formation of chromium carbides at high temperatures in the range of 425 to 815°C [19,20]. These form preferentially at the grain boundaries thus reducing the chromium content and resulting in low corrosion resistance around the grains. Materials can be protected by subjecting the sensitized material to high temperature heat treatment to dissolve chromium carbides, to lower the carbon content to 0.03 wt% so that carbide formation is minimal and to alloy with other elements such as niobium or titanium, which has a grater tendency to form carbides than chromium [20]. Hence chromium will remain in solid solution.

2.1.6 Selective Leaching Corrosion

Selective leaching corrosion is found in solid solution alloys and occurs when one active element is preferentially removed as a consequence of the corrosion process [19,20]. De-alloying of brass, known as dezincification, is a common example of selective leaching corrosion. It can be reduced by small additions of phosphorous, arsenic, or antimony [20].

2.1.7 Stress Corrosion Cracking and Corrosion Fatigue

Stress corrosion cracking results from the combined action of applied tensile stress and a corrosive environment. Corrosion fatigue occurs under cyclic stresses in a corrosive environment [19,20]. To reduce or eliminate these types of corrosion, is to lower the magnitude of stress, to use an appropriate heat treatment to remove residual thermal stresses, cathodic protection and control of the environment by lowering the concentration of the oxidizing agents.

2.1.8 Erosion-Corrosion

Erosion-corrosion is the corrosion of a metal which is caused by a combination of corrosive fluid and a high flow velocity [19,20]. It is characterized by surface features with a directional pattern which are a direct result of the flowing fluid. Abrasive particles in suspension or high velocities erode away the film, leaving the exposed metal surfaces which then suffer high rates of corrosion. Some of the best ways to reduce or eliminate erosion-corrosion is to change the design, to eliminate fluid turbulence and impingement effects, to use abrasion resistant coatings and to add inhibitors [20].

There are also other types of corrosion that are widely prevalent in furnaces, petrochemical and chemical industries as a result of hot gases in the form of high temperature corrosion [1,21]. High temperature corrosion of alloys is a fairly complex process that typically involves scale formation and subsurface degradation [22]. It can be classified into different forms such as [1,21]:

- Oxidation
- Sulphidation
- Nitriding
- Carburization

Oxidation is a process whereby oxygen at high temperatures reacts with a metal to form the surface oxide that may protect the underlying metal. At high temperatures some materials are rapidly oxidized and the oxide film may also thicken into a non-protective scale with various defects including cavities, micro-cracks, and porosity [20]. It causes loss of material thickness and also reduces the amount of certain alloying elements in the material that react with oxygen [23]. The oxidation resistance of the high temperature alloys, such as stainless steels is based on a protective chromium oxide layer [20].

Sulphidation involves the formation of sulphides in the metal, through reaction with sulphur, and results in intergranular pitting of the components [23]. The corrosion rate is increased with increasing temperature. Chromium is an important alloying element in resisting sulphidation and addition of nickel generally increase the susceptibility to sulphidation attack, high nickel alloys being particularly susceptible to sulphidation attack.

Nitriding occurs when metals are exposed to nitrogen bearing atmospheres where nitrogen diffuses into the metal, thus precipitating nitrides in the metal matrix and at grain boundaries [23]. Precipitation of nitrides leads to embrittlement of the metal. Iron-based alloys are more

susceptible to nitriding than nickel-based and cobalt-based since the alloy's resistance is enhanced by increasing the nickel content.

The present study is centred on carburization. Carburization is a mechanical property degradation caused by carbon ingress into the alloy and subsequent formation of internal carbides [24-27]. It occurs in carbon bearing atmospheres at temperatures above 400°C and a carbon activity less than one (a_C<1). Metal dusting is a catastrophic form of carburization which occurs in a strongly carburizing atmosphere with a_C>1 at intermediate temperatures of 400 - 900°C. It causes severe pitting or uniform thinning of the affected material. When it occurs, it causes unscheduled process shutdowns which results in a loss of profit. It also increases the maintenance expenditure. Preventing metal dusting in industrial processes is essential to achieve high economic efficiency. Research on metal dusting has been going on for some years but the reaction mechanisms of it are not always clear [28,29]. The literature on metal dusting is not as widely available as other types of corrosion. Alloys that can resist metal dusting are able to form a protective oxide film which blocks the ingress of carbon. The present study evaluates the resistance of commercial alloys to metal dusting.

2.1.9 Commercial Alloys Currently Used in Petrochemical and Chemical Industries

This section gives a brief description of the high temperature resistant alloys that are commonly used in the chemical and petrochemical industries. The nominal compositions of all the alloys discussed below are shown in Table 2.1.

HAYNES® 214™ alloy (alloy 214) is a nickel–chromium-aluminium–iron alloy and is produced in the solution heat-treated condition [30]. It is used for high temperature applications, for instance, at 955°C and above. It is said to exhibit outstanding resistance to oxidation due to the

formation of an Al_2O_3 scale which forms in preference to a Cr_2O_3 scale at high temperatures. Alloy 214 is also said to exhibit excellent resistance to carburization, nitridring, and corrosion in chlorine-bearing oxidizing environments. It is used in the heating industry as a refractory anchor, furnace flame hoods, and rotary calciners for processing chloride compounds.

HAYNES® HR-120™ alloy (HR 120) is a solid-solution-strengthened heat resistant alloy that exhibits excellent strength at high temperatures [30]. It is said to exhibit very good resistance to carburizing and sulphurdizing environments. It also exhibits good resistance to oxidizing environments up to 1205°C. HR 120 is manufactured in the solution annealed condition. It is used in corrugated boxes for carburizing furnaces, used to carburize large gears for ships at commercial heat treatment operations.

HAYNES® HR-160™ alloy (HR 160) is a nickel-cobalt-chromium-silicon alloy and solid–solution-strengthened alloy [30]. It is said to be a high temperature corrosion resistant alloy that provides excellent resistance to sulphidation and chloride attack in both a reducing and oxidizing environments. It has exceptional good resistance to oxidation, carburization, metal dusting and nitriding. It is used in petroleum refinery processes and nuclear waste incinerators.

INCONEL® alloy 230 (Alloy 230) is a carbide strengthened nickel-chromium-tungsten-molybdenum alloy with an exceptional combination of strength, stability, and resistance to corrosion at very high temperatures [31]. It has good resistance to oxidation at temperatures greater than 980°C and also offers good resistance to carburization and nitriding. It can be used in the petrochemical processing, heat treating and metal refining industries.

Table 2.1: Nominal compositions of various alloys used in the petrochemical industries [30-33].

Alloys	Ni	Fe	Cr	Si	Al	Mo	Mn	W	Co	Ti	Other
Alloy 214	75$^{\beta}$	3	16	0.2$^{\xi}$	4.5	-	0.5$^{\xi}$	-	-	-	Y,B, Zr,C
HR 120	37	33$^{\beta}$	25	0.6	0.1	2.5$^{\xi}$	0.7	2.5$^{\xi}$	3$^{\xi}$	-	Cb,N, B,C
HR 160	37$^{\beta}$	2$^{\xi}$	28	2.75	-	1$^{\xi}$	0.5	1$^{\xi}$	29	0.5	Cb, C
253MA	10-12	β	20-22	1.10-2.0	-	-	0.8$^{\xi}$	-	-	-	S,Ce, N,P,C
Alloy 230	β	3$^{\xi}$	20-24	0.25-0.75	0.20-0.50	1.0-3.0	0.3-1.0	13-15	5$^{\xi}$	-	P,S, La,B
GR 309	12-15	β	22-24	1$^{\xi}$	-	-	2$^{\xi}$	-	-	-	P
Alloy 600	72	6-10	14-17	0.5$^{\xi}$	-	-	1$^{\xi}$	-	-	-	Cu, S
Alloy 601	58-63	β	21-25	0.5$^{\xi}$	1.0-1.7	-	1$^{\xi}$	-	-	-	Cu
Alloy 693	β	2.5-6.0	27-31	0.5$^{\xi}$	2.5-4.0	-	1$^{\xi}$	-	-	1$^{\xi}$	Cu,S, Nb
Alloy 690	58$^{\delta}$	7-11	27-31	0.5$^{\xi}$	-	-	0.5$^{\xi}$	-	-	-	S.Cu
Alloy 800HT	30-35	39.5$^{\delta}$	19-23	-	0.25-0.60	-	-	-	-	-	Ti + Al=0.8-1.2

(β) As Balance, **(ξ)** maximum and **(δ)** minimum

INCONEL® alloy 600 (Alloy 600) is a nickel-chromium-iron solid-solution alloy [31]. It has good resistance to oxidation, carburization, and

sulphidation at moderate temperatures, but is subject to sulphidation in high temperature sulphur containing environments. It is used extensively in the chemical and heat treating industries. Its application includes heaters and nuclear reactors.

INCONEL® alloy 601 (Alloy 601) is a nickel–chromium-iron solid-solution alloy [31]. It exhibits outstanding resistance to oxidation and is also resistant to carburization, sulphidation and nitriding. It is used in petrochemical processing as a catalyst generator and air pre-heater in the manufacturing of high density polyethylene.

INCONEL® alloy 693 (Alloy 693) is a nickel-chromium-iron-aluminium solid-solution single-phase alloy [31]. It is a newly developed alloy from Special Metals in the United Kingdom. It has better resistance to metal dusting in chemical and petrochemical processing environments than the conventional alloys currently manufactured. Alloy 693 is said to offer excellent resistance to oxidation, carburization and sulphidation. It is used in petrochemical industries, thermal processing, and burner nozzles, and high temperature fuel cell reformers. It is used as reformer tubes, tube ferrules, baffle plates and valve components.

INCONEL® alloy 690 (Alloy 690) is a high chromium-nickel solid-solution alloy [31]. It is resistant to oxidizing atmospheres and has good resistance to sulphidation and carburization. It is used in coal-gasification units, burner and ducts for processing sulphuric acid and furnaces for petrochemical processing.

INCOLOY® alloy 800HT (Alloy 800HT) is a nickel-iron-chromium solid solution alloy [31]. It is said to exhibit excellent resistance to oxidation and good resistance to carburizing atmospheres at 925°C to 980°C. It also has good resistance to many sulphur-bearing atmospheres at high temperatures and nitriding atmospheres. It is used in the hydrocarbon processing industry, hydrocarbon reforming for catalyst tubing, convection

tubing, pigtails and high temperature heat exchangers in gas-cooled nuclear reactors.

253 MA is a fairly low nickel content alloy that has good resistance to oxidation and excellent resistance to sigma phase precipitation [32]. It also exhibits good resistance to sulphur-bearing gases in an oxidizing atmosphere. It is used in furnace components including burners, radiant tubes, refractory anchors, and petrochemical and refinery tube hangers.

GR 309 is a highly alloyed austenitic stainless steel used for its excellent oxidation resistance, high temperature strength and creep resistance. A low nickel content ensures more resistance to sulphidation [33].

2.2 CARBURIZATION

Carburization is an increase in carbon content on the surface of alloys due to interaction with a carbon rich environment at elevated temperatures. Carbon monoxide and carbon dioxide can penetrate resistant oxides like chromia (Cr_2O_3) through pores, micro-cracks and other defects and subsequently carbon dissolves in the alloy until it reaches sufficient activity to precipitate carbides [20]. Carburization has a significant influence on the corrosion behaviour of alloys since carbon form internal carbides such as $Cr_{23}C_6$, Cr_3C_2 and/or Cr_7C_3, depleting the alloy matrix locally of chromium [34]. The formation of internal carbides leads to a volume increase and additional local stresses that affect the mechanical properties of the carburized alloy [35-37].

Carburization is often enhanced in high temperature oxygen deficient atmospheres containing water vapour, CO_2, and/or CO [20]. In reforming processes, natural gas reacts with steam to form CO, H_2, CO_2 and a H_2O gas mixture, which are strongly carburizing and slightly oxidizing to the alloy components. Hence metal dusting which is a severe form of

carburization is prevalent in reforming plants. Under highly carburizing environments ($a_C>1$), the alloys are subjected to metal dusting. Carburization processes are largely affected by the alloy composition, temperature and composition of the atmosphere [20]. These parameters determine the type of chemical reaction that occurs at the surface which results in carbon diffusion into the alloy [35].

2.2.1 Mechanism of Carburization

Austenitic alloys with higher solubility for carbon are more susceptible, and the ferritic stainless steels are often recommended for resistance to carburization [38]. Carburization is a high temperature corrosion phenomenon caused by carbon diffusion from the atmosphere into a metal or alloy component leading to internal carbide precipitation within the temperature range of 450 – 1000°C. It can proceed by the following reactions when the environment contains CH_4, CO, CO_2 and H_2:

$$CO + H_2 = H_2O + C \qquad (2.1)$$

$$2CO = CO_2 + C \qquad (2.2)$$

$$CH_4 = 2H_2 + C \qquad (2.3)$$

$$M + CO_2 = CO + MO \qquad (2.4)$$

where M = Metal.

From these equations carbon diffuses into an alloy until it reaches sufficient activity to form the internal carbides. Carburization involves the following steps:

1. C/CO transport to the surface of the alloy
2. C diffuse into the surface of the alloy
3. Solid state reaction with Fe in the alloy or steel, $Fe + C = Fe_3C$, resulting in carbide formation [39].

2.2.3 Kinetics of Carbon Diffusion

Factors that influence the diffusion of carbon into the alloy are temperature and the microstructure of the alloy. The diffusion rate increases very rapidly with increasing temperature. At low temperature diffusion is faster in polycrystalline than in single crystal materials, because of the accelerated diffusion along the grain boundaries and dislocations. Diffusion is faster in alloys with fine grains than alloys with coarse grains. Often it is necessary to know how fast diffusion occurs or the rate of mass transfer. This rate is expressed as a diffusion flux (J).

$$J = -D\frac{dC}{dx} \qquad \textbf{(Kg/m}^2\textbf{.s)} \qquad (2.5)$$

where, D is the diffusion coefficient (m^2/s) and is a temperature dependent diffusion coefficient related to temperature according to [19]

$$D = D_0 \exp\left(-\frac{Q_d}{RT}\right) \qquad (2.6)$$

where,

$\frac{dC}{dx}$ = concentration gradient (Kg/m^4)

D_0 = a temperature independent pre-exponential (m^2/s)

Q_d = the activation energy for diffusion (J/mol)

R = the gas constant, 8.314 J/mol.K

T = absolute temperature (K)

The minus sign in the equation means that the diffusion is down the concentration gradient, from a high to a low concentration. The driving force for diffusion in equation (2.5) is the concentration gradient.

2.3 METAL DUSTING

Metal dusting is a high temperature corrosion phenomenon that leads to the disintegration of engineering metals and alloys into dust consisting of

fine metal particles or alloy, carbon and carbides [40]. The corrosion products are carbonaceous deposits known as "coke". It occurs in a strongly carburising atmosphere with a carbon activity greater than one (a_c >1) at intermediate temperatures, 400–800°C. Metal dusting is prevalent in atmospheres containing carbon dioxide, carbon monoxide, natural gas and hydrocarbons.

Metal dusting causes pitting or uniform thinning of metals and alloys. Examples of alloys attacked by metal dusting are shown in Figure 2.1 and Figure 2.2 below [41]. Metal dusting is of concern within petrochemical industries and results in unscheduled process unit shut downs and loss of production. It is also a concern in steel industries, internal combustion engines, waste heat boilers, carbon dioxide cooled nuclear reactors, coal-gasification components, in methanol production, in hydrocarbons and ammonia synthesis and syngas generation [5,34,42,43].

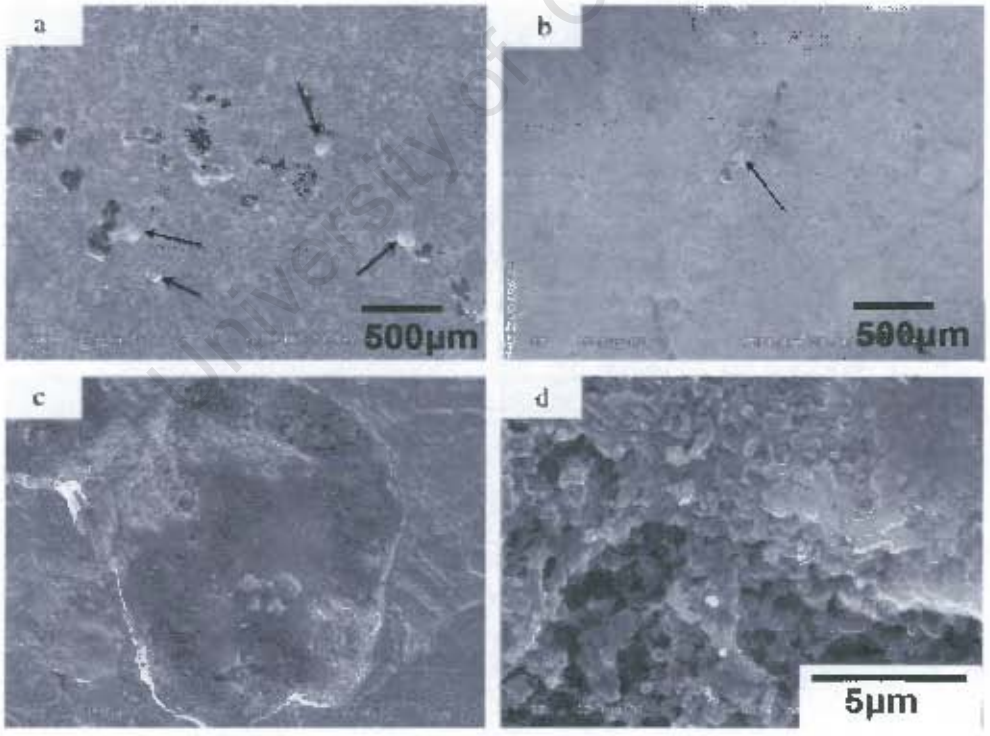

Figure 2.1: SEM photographs showing pits left by growing coke protrusions on alloy 803 (34% Ni-27% Cr-37.21% Fe) with (a) large grain size and (b) small grain size after 370 hours, (c) the bottom of a pit and (d) graphite filaments at the pit bottom [41].

Figure 2.2: Alloy 800 (32% Ni-20% Cr-38% Fe) attacked by metal dusting. Pits are evident towards the right. It was exposed to syngas at 780°C.

2.3.1 Mechanism of Metal Dusting

Metal dusting occurs as a result of carbon diffusion from a carbonaceous atmosphere into the alloy or metal. Carbon can diffuse into the alloy or metal by one of the following reactions if present in the carburizing atmosphere:

$$CO + H_2 - H_2O + C \qquad (2.1)$$

$$2CO = CO_2 + C \qquad (2.2)$$

$$CH_4 - 2H_2 + C \qquad (2.3)$$

Nickel and nickel-based alloys, iron and iron-based alloys are the most common metals and alloys used for high temperature applications. The mechanism of metal dusting for pure iron and iron-based alloys are well understood but, for nickel and its alloys, the mechanism is not as clear as that of iron and its alloys. Metal dusting of iron and iron-based alloys was found to be slightly different from nickel and nickel-based alloys

[6,17,25]. Szakalos *et al* has proposed that there are three main metal dusting mechanisms operating depending on the alloy composition denoted Type I, Type II and Type III [28]. Type I involves the formation and decomposition of metastable carbides; Type II involves graphite formation into and inside the Ni-containing matrix and disintegration of the matrix and Type III involves an active corrosion with carbon and oxygen.

2.3.2 Mechanism of Metal Dusting of Iron and Iron-based Alloys

The following metal dusting mechanism is classified as the Type I mechanism [28]. Carbon diffuses into the metal and reacts with Fe to form cementite, Fe_3C. The following reaction sequence occurs on Fe and low alloy steels [8,17,39,40,44]:

I. Transfer of carbon into the metal phase and super saturation of the metal with dissolved carbon;
II. Precipitation of Fe_3C at the surface and at the grain boundaries;
III. Deposition of graphite from the gas atmosphere onto the Fe_3C, which is at the surface;
IV. The start of Fe_3C decomposition under formation of graphite and metal particles and;
V. Further graphite deposition, catalyzed by the metal particles.

This mechanism is depicted schematically in Figure 2.3 [17]. When the carbon activity is greater than one, carbon diffuses into the metal and form cementite. The formation of cementite acts as a barrier to further carbon ingress, hence, the carbon activity at the surface rises and graphite nucleates. Nucleation of graphite decreases the carbon activity to one (a_c=1) as depicted in Figure 2.3a and thus Fe_3C becomes unstable. The cementite decomposes to graphite and iron by growth of graphite into cementite [17].

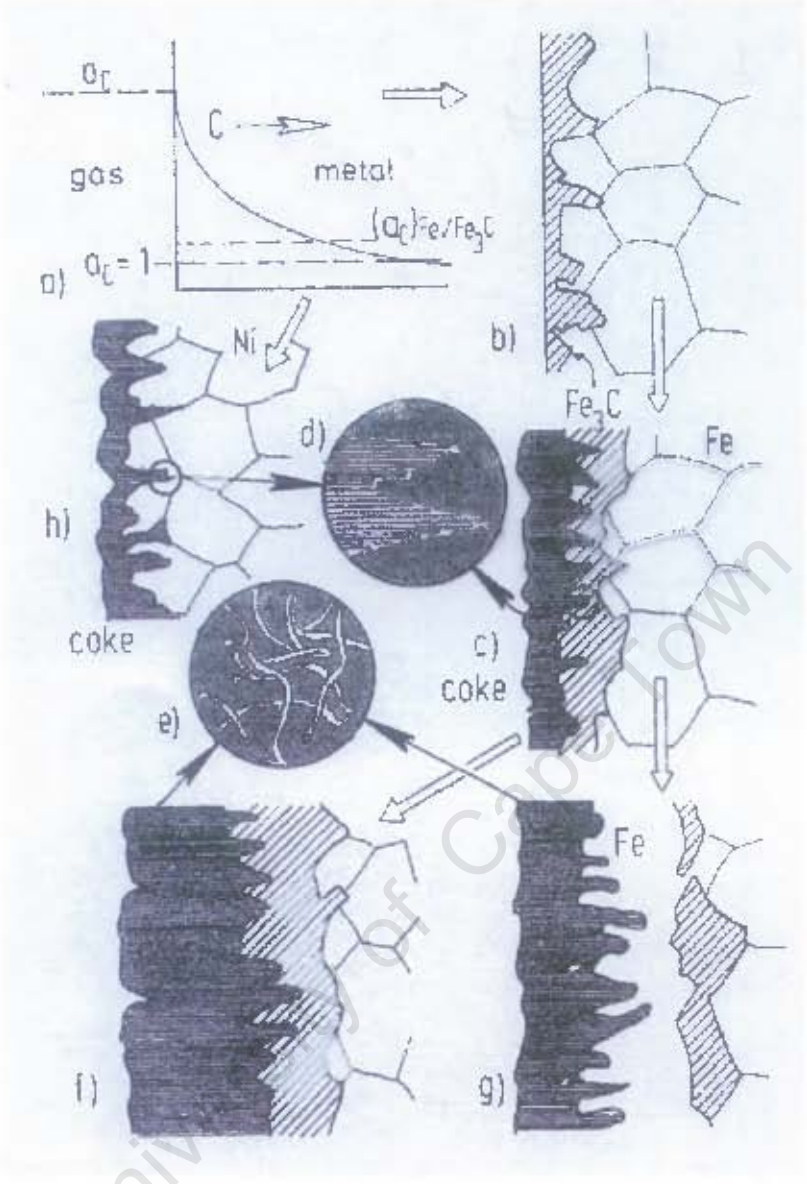

Figure 2.3: Schematic illustration of metal dusting mechanism of Fe, low alloy steels and Ni, (a) Carbon transfer into the metal and over saturation, (b) Nucleation and growth of Fe_3C in Fe and low alloy steels, (c) and (d) Nucleation and growth of graphite into Fe_3C by C atoms attaching to the lattice plane of graphite, (e) Carbon filaments with metal particles at the tip after disintegration, (f) Steady state metal dusting of Fe and low alloy steels at temperature less than 600 °C, inward growth of Fe_3C which disintegrates outward under coke formation, (g) Steady state metal dusting of Fe and low alloy steels at temperatures greater than 700 °C, formation Fe layer between Fe_3C and coke, carbon diffusion through this layer and final disappearance of Fe_3C [17].

2.3.3 Metal Dusting of Nickel and Nickel-based Alloys

The reactions occurring for nickel and nickel-alloys are almost the same as for iron and iron-alloys, but different with only one step. For nickel and nickel-based alloys, there is no formation of intermediate metastable carbides [17]. After saturation of the matrix by carbon, the saturated matrix directly decomposes into metal particles and graphite. Pippel *et al* showed that alloying of iron with nickel changed the mode of disintegration [45]

When a nickel concentration of about 10 wt% is present in iron, the alloy will disintegrate directly as in nickel and nickel-based alloys [45]. Muller-Lorenz *et al* have also observed that HK40 (a 53.9% Fe, 25.6% Cr and 20.5% Ni alloy) disintegrated directly without forming cementite layers. This type of mode is normally observed in nickel and nickel-based alloys [46]. Szakalos *et al* observed that Type II and III may occur simultaneously in austenitic stainless steels and Type III in nickel-based alloys and high alloyed steels [28,47]. The Type II metal dusting mechanism involves graphite formation inside the carbon supersaturated alloy matrix; consequently the matrix disintegrates into small metal particles.

The particles continue to disintegrate until they are too small to nucleate graphite and this leads to the formation of nano-particles of Type IV. Type IV is a continuous disintegration of small particles. Type III is an active corrosion by carbon and oxygen. Carbon diffuses into the alloy and carbides are formed. The carbides that are formed are selectively oxidized by free oxygen from the dissociation of CO or H_2O. Consequently, free carbon is released which forms carbides and graphite again. The process is repeated over and over again until the alloy is consumed. Type II, III, and IV are depicted in Figure 2.4.

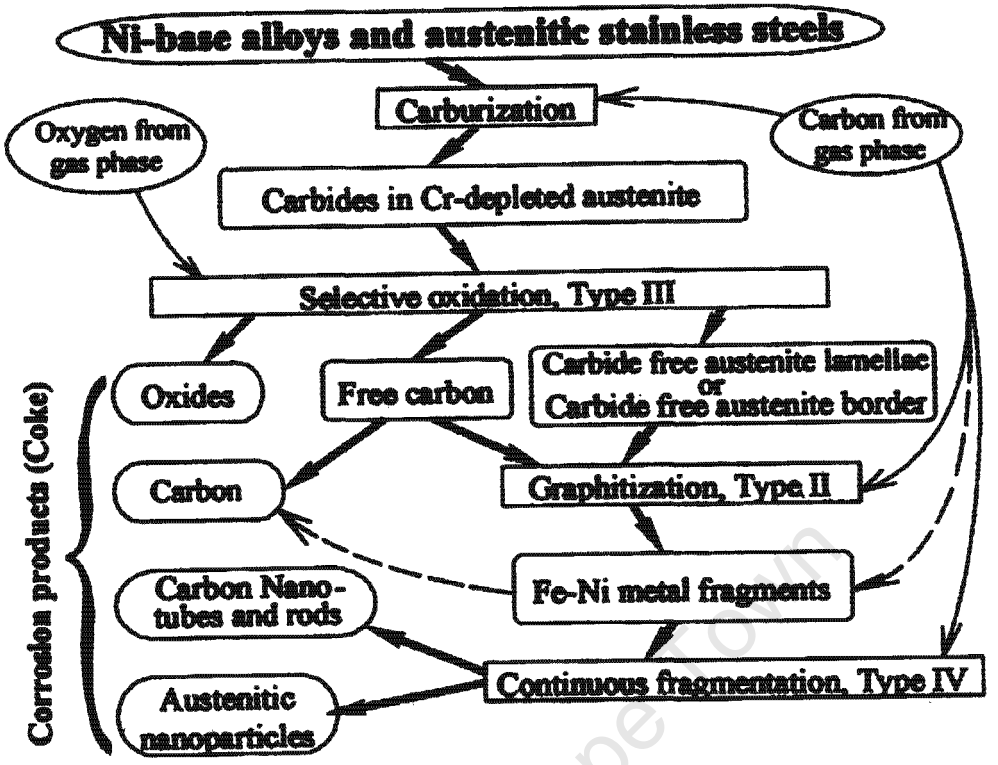

Figure 2.4: Schematic metal dusting mechanism chart for nickel-based alloys and austenitic stainless steels. Dashed arrows denotes a catalytic carbon reaction, which is not primarily included in the metal dusting process [47].

2.3.4 Metal Dusting of High Alloyed Steels

Basically the mechanisms here are the same for nickel or iron, but some additional steps are considered, as depicted by the diagram in Figure 2.5 [17]:

I. The protective oxide scale fails at some weak point in the surface and a virgin material is exposed to the environment;
II. Carbon diffuses into the metal and reacts with carbide forming elements in the alloy to form stable carbides, $M_{23}C_6$ and M_7C_3 with Cr as the main component and MC with M = Ti, Zr, V, Nb, W and Mo_2C. A zone with internal carbide precipitates is formed (Figure 2.5b) and this region is oversaturated with dissolved carbon;

III. After saturation the remaining iron or iron-nickel matrix disintegrate by one of the mechanisms described in sections 2.3.2 and 2.3.3, and fine metal particles are formed;

IV. The fine metal particles act as a catalyst for further carbon deposition and outgrowth of coke from the pit which is starting to grow from the "weak point" (Figure 2.5e). If the oxide scales have inclusions or cracks and are thick, flat pits are formed. If the oxide scales are strong and stable, pits are likely to be hemispherical. Figure 2.6 illustrates the formation of a hemispherical region which will lead to hemispherical pit formation [48];

V. When the metal matrix is subjected to disintegration by metal dusting; simultaneously the carbides $M_{23}C_3$, M_7C_3 and MC are oxidized and spinels are also formed such as $(Mn,Fe)Cr_2O_4$. The spinel oxides spalled off during the metal dusting process are retained in the carbon deposit

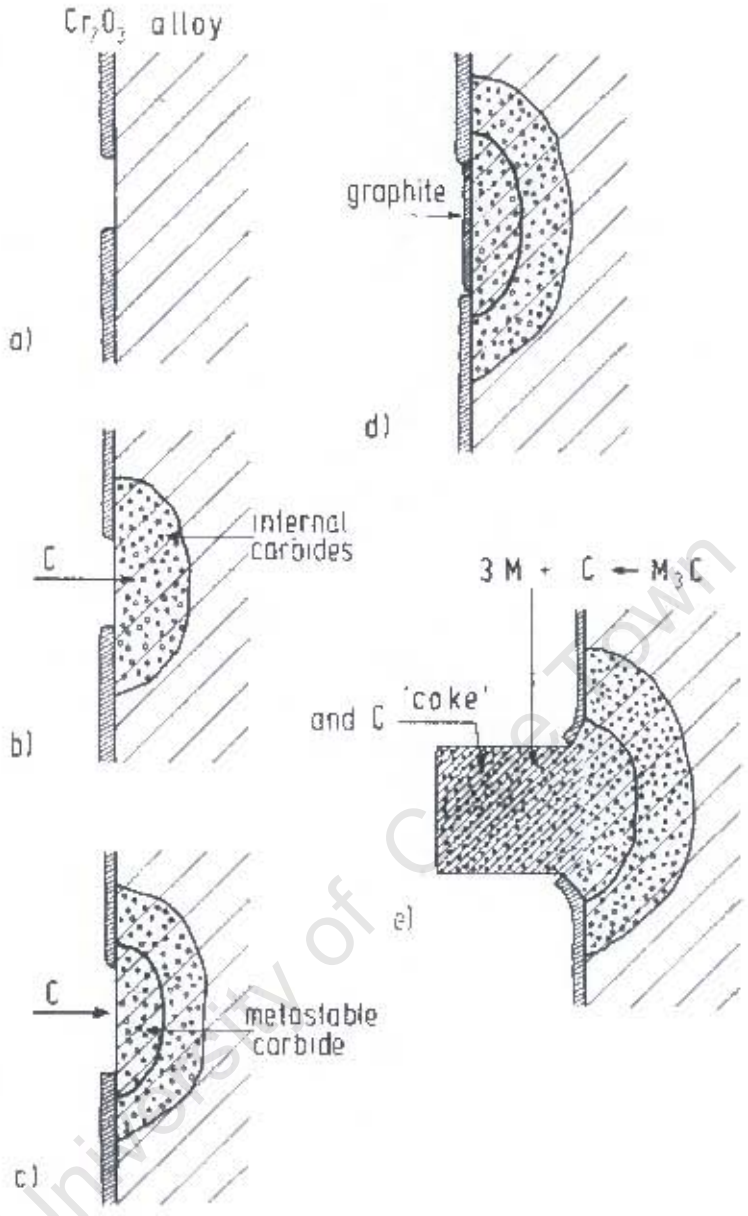

Figure 2.5: Schematic of the metal dusting mechanism in high-alloy steels. The additional steps are: (a) Occurrence of a defect in the oxide scale and (b) internal carbide formation, (c) formation of a metastable intermediate carbide, (d) decomposition of the now unstable carbide to carbon and metal particles, and (e) outgrowth of coke by graphite deposition on metal particles [8].

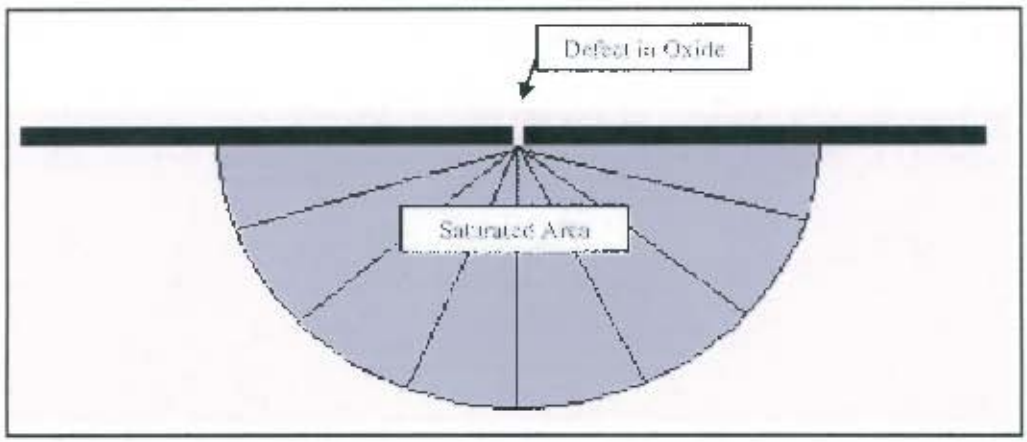

Figure 2.6: Illustration of the equidistant diffusion of carbon from a localized defect in the protective oxide scale that results in the saturation of a hemispherical region with carbon [48].

2.3.5 Characteristics of Coke

Carbon deposition from environments onto alloys leads to the disintegration of alloys into a powdery mixture consisting of fine metal particles of the base alloy, graphite, and sometimes carbides and oxides [17,49]. These corrosion products are known as "coke" [8,50] Coke is removed by flowing gases in plants leaving pits and grooves in the affected metal surface [17]. In the laboratory simulation of metal dusting, coke can be retained and analyzed. Han *et al* have observed that the amount of coke protrusion was large on alloys with bigger grains when compared to alloys with small grains [41].

A SEM micrograph of coke protrusion is shown below in Figure 2.7 [41]. The coke protrusion consisted of graphite filaments, particles of metals and oxides.

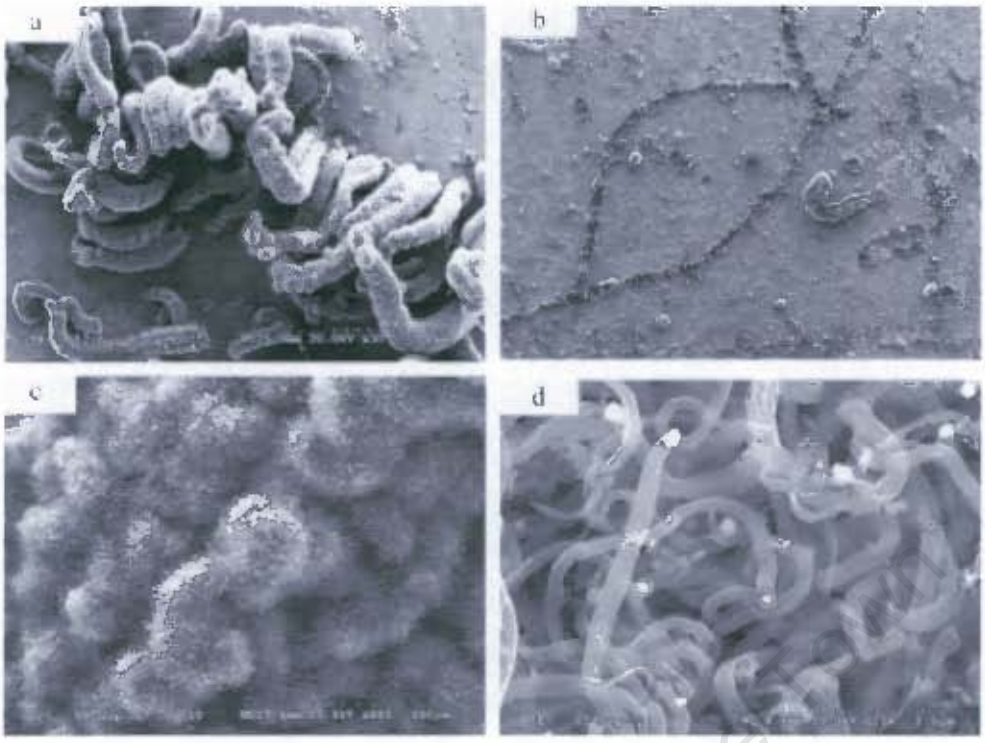

Figure 2.7: (a) and (b) Coke growing from alloy 803 (34% Ni-27% Cr-37.21% Fe), (c) filamentous graphite and (d) metal particles at tip of graphite filaments [41].

The morphology of graphite in the coke is categorized into three types [51,52]. The first type is porous graphite clusters with embedded iron-containing particles, the second type is compact bulk graphite with a uniform thickness and a columnar layered structure, and the third type is filamentous carbon with iron-containing phases at the tip. The gas composition affects the morphology of the graphite. Figure 2.8 shows the morphology of graphite on the samples with different composition of the gas mixture. For gas mixtures with low CO content (1-5%), porous graphite clusters were observed. With high CO contents, two layers of graphite were observed [51,52]. The inner parts consist of a mixture of porous graphite clusters and inter-woven graphitic filaments. The outer part consists of a uniform thickness and a columnar dense layer.

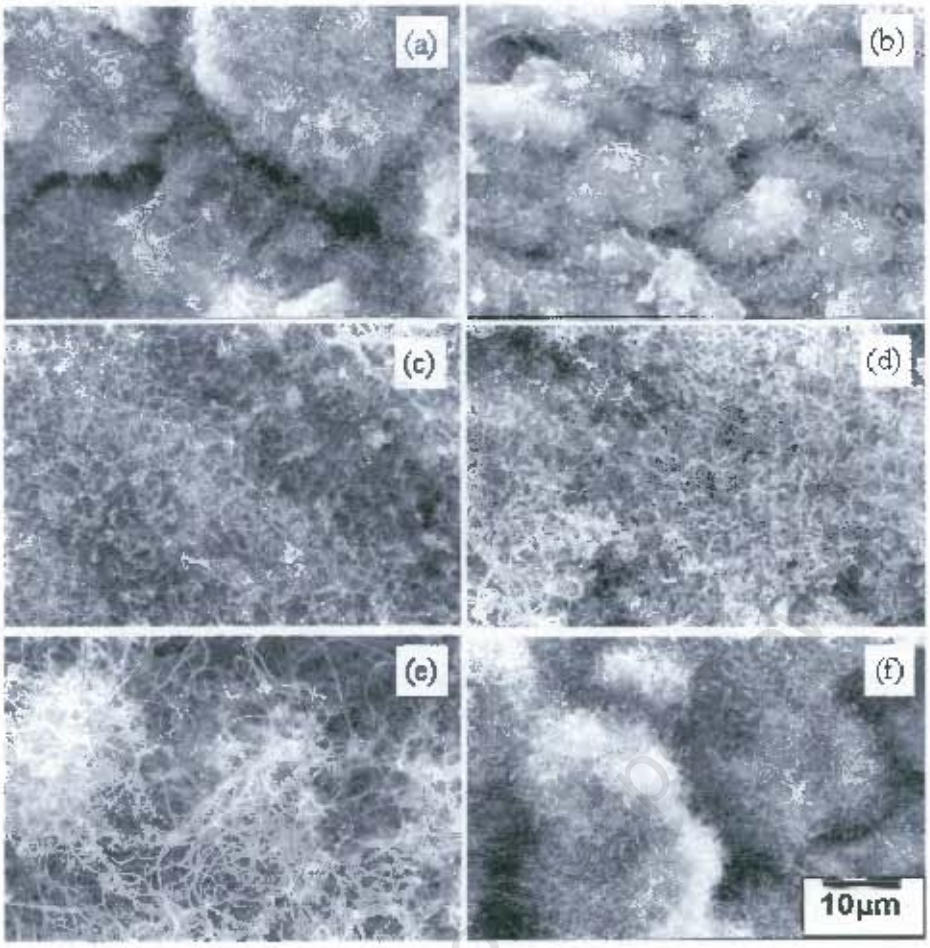

Figure 2.8: SEM observation of the graphite morphologies of iron samples after carburization for (a) 21.5 hours with 1% CO, (b) 5 hours with 5% CO, (c) 4 hours with 30% CO, (d) 2 hours with 50% CO, (e) 2 hours with 75% CO and (f) 2 hours with 95% CO in CO-H-0.2% H_2O [52].

2.3.6 Thermodynamics of Metal Dusting

Carbon activity is a thermodynamic driving force for metal dusting and increases with a decreasing temperature. Metal dusting occurs when the carbon activity of the environment is greater than one at elevated temperatures [44]. The carbon activity or chemical potential of carbon can be used to measure the susceptibility to metal dusting. When the carbon activity of the gaseous atmosphere is much greater than one ($a_C >> 1$), metal dusting have a propensity to be more severe. Natural gas reacts with steam to form a CO, CO_2, H_2 and H_2O gas mixture in syngas

reformer plants [53]. These products are robustly carburizing and somewhat oxidizing to the structural materials. Carbon can be deposited onto the alloy by one of the following reactions [5,17,44]:

$$CO + H_2 = H_2O + C \qquad (2.1)$$

$$2CO = CO_2 + C \qquad (2.2)$$

$$CH_4 = 2H_2 + C \qquad (2.3)$$

$$C_XH_Y = \frac{y}{2}H_2 + xC \qquad (2.7)$$

The carbon activity of each reaction can be calculated as follows [5,8,17]:

$$CO + H_2 = H_2O + C$$

$$a_C = \frac{P_{CO} \times P_{H_2} \times K_3}{P_{H_2O}} \qquad (2.8)$$

$$2CO = CO_2 + C$$

$$a_C = \frac{(P_{CO})^2 \times K_1}{P_{CO2}} \qquad (2.9)$$

$$CH_4 = 2H_2 + C$$

$$a_C = \frac{P_{CH_4} \times K_2}{(P_{H_2})^2} \qquad (2.10)$$

$$C_xH_y = \frac{y}{2}H_2 + xC$$

$$a_C = \left(\frac{P_{C_xH_Y} \times K_4}{(P_{H_2})^{\frac{Y}{2}}} \right)^{\frac{1}{x}} \qquad (2.11)$$

where K is an equilibrium constant of a reaction and P is the partial pressure of the constituent gases.

Increasing the system pressure increases the carbon activity for reaction (2.2) irrespective of the composition [5]. The carbon activity values will be the same for reactions (2.2) and (2.3) if the equilibrium gas phase prevails at high temperatures and/or for a long time since thermodynamically the gas composition will change to give the most stable composition [5]. As the temperature increases the carbon activity decreases while the diffusivity and carbon saturation concentration both increases with increasing temperature [54]. Hence it is not easy to envisage which temperature will have the most severe action on the alloy surface. Dean used the carbon precipitation temperature (CPT), which is the temperature at which the carbon activity is unity, to envisage the metal dusting severity of a syngas [54,55]. The higher the CPT, the more aggressive the syngas will be and metal dusting will occur.

The oxygen partial pressure, P_{O_2}, is an important factor which has an influence on metal dusting resistance since the oxide scale formed act as a barrier for inward diffusion of carbon in the alloy [5,17]. In the laboratory simulation of metal dusting environment, oxygen is available to the alloy by the following reactions:

$$H_2O = H_2 + \tfrac{1}{2}O_2 \qquad (2.12)$$

$$CO_2 = CO + \tfrac{1}{2}O_2 \qquad (2.13)$$

The initiation time for metal dusting to occur is affected by the competition between the oxidation process to form a protective, stable and self repairing oxide scale on the alloy surface and the deposition and diffusion of carbon into the alloy [5]. If the alloy can develop a protective

oxide scale rapidly and early during exposure, subsequent deposition of carbon on top of the oxide scale can delay further ingress of carbon into the alloy and hence the initiation of metal dusting [5,17].

Metal dusting occurs very fast in laboratory simulations since the partial pressure of oxygen is very low [5,17]. In industries, the partial pressure of oxygen P_{O_2} is high enough that chromium rich alloys can be oxidized before carbon deposition and therefore metal dusting in industries take a longer time when compared to laboratory simulation. Metal dusting in laboratory simulation is more aggressive than in actual plants. For actual plants, metal dusting initiation can take months or years whereas in the laboratory, it can take days or even weeks.

2.3.7 Factors Affecting Resistance to Metal Dusting

This section describes possible ways of retarding carburization and metal dusting or minimizing its occurrence.

2.3.7.1 Formation of an oxide film

It is believed that a dense uniform layer of chromia or alumina can prevent carburization on engineering alloys at least for a certain period [17]. Since carburization is the main cause of metal dusting, suppressing carburization therefore suppresses metal dusting for a certain period. The protective oxide film forms an effective barrier to further carbon ingress [15,56,57]. The success of surface oxide films in restraining metal dusting therefore depends on the specific process environment and the influence that it has on the oxide scale stability. It also depends on the ability of a damaged oxide film to repair itself.

The oxidation rate and diffusion of carbon in the alloy will be minimized if the oxide film has a combination of favourable properties that include [20]:

- The film must have good adherence, to prevent flaking and spalling;
- The melting point of the oxide must be high;
- The oxide must have low vapor pressure to resist evaporation;
- The oxide film and the metal must have almost the same thermal expansion coefficient;
- The oxide film must have high temperature plasticity to accommodate differences in specific volumes of the oxide and parent metal, and differences in thermal expansion;
- The oxide film must have low electrical conductivity and low diffusion coefficients for metal ions and oxygen;
- It must have good erosion resistance;
- The scale must have good resistance to impurities such as deposits and ashes.

Impermeability against aggressive components of the environment, such as carbon, nitrogen and sulphur is essential. Carbon penetration into the alloy occurs by diffusion of carbon-containing molecules through the pores of the oxide films or scale. The carbon penetration is enhanced by creep of the materials and/or in the condition causing cracking of the scales. When metal dusting occurs locally at defects on a stable oxide film, damage is manifested as pitting of the base metal at the oxide film defect site [17]. The brittleness of the oxide film makes durability difficult and the oxide film can be damaged by particle abrasion or by internal stresses developed during the transient condition of pressure and temperature. The difference in the thermal expansion between the oxide films and the metal can create stresses that result in cracking or spalling of the oxide film.

2.3.7.2 *Effects of various individual alloying elements*

The resistance of an alloy to metal dusting is strongly dependant on the alloy composition. Nickel in conjunction with chromium improves the high-temperature corrosion resistance in alloys. It also gives improved resistance to thermal cycling during the high-temperature oxidation. Carbon diffusivity and solubility is decreased with increasing nickel content and therefore retards carburization [11,17]. Nickel-based alloys were found to resist metal dusting more than iron-based alloys [53,58]. The alloy composition has a significant effect on the rate of metal dusting and also on the type of metal dusting mechanism that will occur. The kinetics of metal dusting becomes slower depending on the type of mechanism operating in the order I-II-III [28]. Szakalos *et al* has suggested that the alloy composition in Fe-Ni-Cr alloys determines which metal dusting mechanism will occur. A chart of metal dusting mechanism as a function of composition is shown below in Figure 2.9 [28].

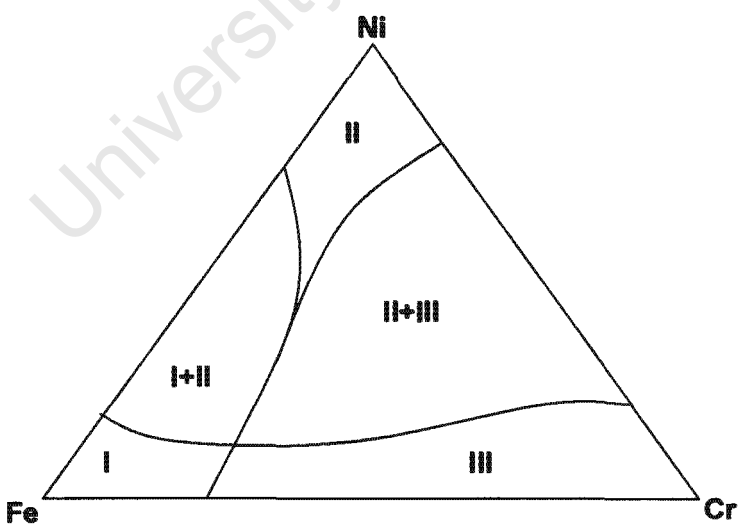

Figure 2.9: Schematic chart of the operating metal dusting mechanism as a function of the alloy composition during metal dusting conditions in a CO-atmosphere at 650°C [28].

An alloy with a higher nickel content, *i.e.*, close to the top corner of the triangle will only suffer from the type II mechanism which is slower than type I. Alloys with higher chromium content will be subjected to a type III mechanism which is slow, hence the incubation period for the initiation of metal dusting is prolonged. Nishiyama *et al* had found that an alloy with more than 30% Cr had high pitting resistance due to a formation of a stable chromium oxide scale [59]. Alloys with less chrome and less nickel contents are attacked within a short period as shown in Figure 2.10 [59].

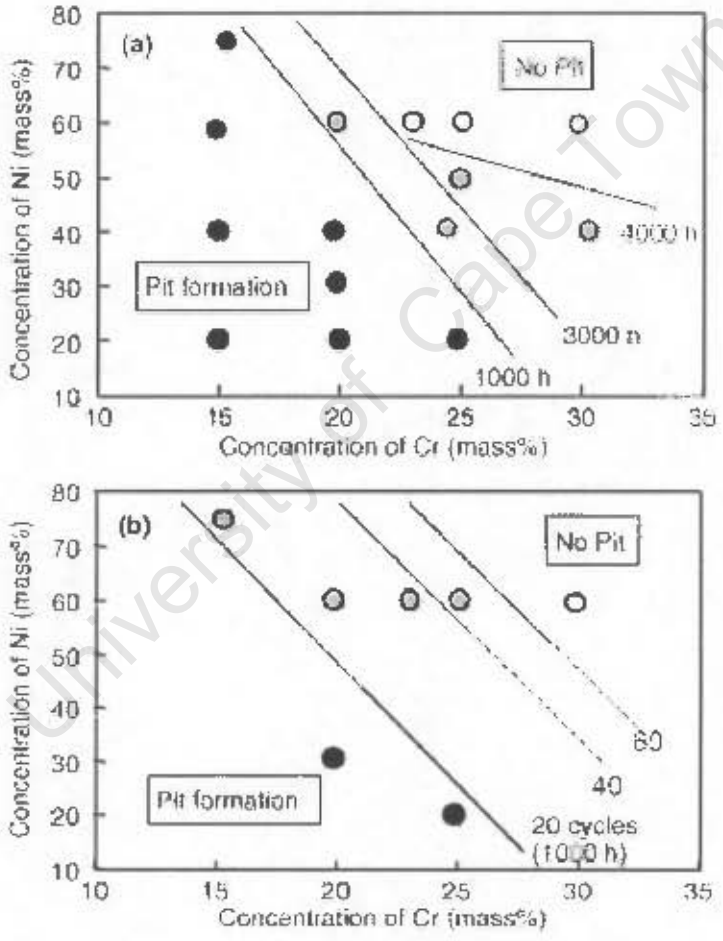

Figure 2.10: Formation of pits on the surface of specimens exposed to a 60% CO-26% H_2-11.5% CO_2-2.5% H_2O gas mixture at 650°C. (a) isothermal, (b) cyclic test. Black dots-pitting after 1000 hours, grey dots-pitting after 3000-4000 hours and white dots-no pitting after 5000 hours [59].

Silicon forms adherent resistance films alone and in conjunction with chromium. It is thought to reduce the solubility and diffusivity of carbon in alloys [15,17]. It is added at 2 to 3% levels to many iron and nickel-based chromium-bearing alloys to improve the corrosion resistance.

Maier *et al* had done investigations on factors affecting metal dusting and found that silicon had a significantly beneficial influence upon the resistance to metal dusting attack [15]. The 12% Cr-2.75% Si alloy behaved in similar manner to that observed for 25% Cr-20% Ni. The 25% Cr-20% Ni alloy resisted metal dusting with little evidence of attack. Aluminium forms protective oxide films, but at a lower rate than chromium. Alumina has been proven to resist carbon diffusion into the metal matrix, but the kinetics of formation of this oxide film are, however, extremely slow at temperatures of 500 -800°C [36,47,60].

Chromium diffusion rates are higher in ferritic steels than in austenitic stainless steel and thus protective oxide films are more likely to heal rapidly at a low temperature in high chromium ferritic steels than in austenitic steels [8].

Baker and Smith have shown that a high chromium and aluminium contents in combination with a high nickel alloy matrix performed better than other alloys in their laboratory test [53]. They also showed that titanium and molybdenum had a significant effect on the resistance to metal dusting because they promote early carbide formation and provide diffusion blocking of carbon flux. Molybdenum, tungsten, niobium and titanium form carbides when they are present in the alloy, so as to reduce the depletion of chromium so that the protective chromia film can be formed [20]. Without these carbides forming elements, only chromium rich carbides $M_{23}C_6$, M_7C_3 or Cr_3C_2 would be formed. Subsequent depletion of chromium due to chromium carbide formation reduces the capability of the alloy to form an adherent, protective, healable oxide film [11,17,53,58].

2.3.7.3 Effects of sulphur

Sulphur can suppress the adsorption of carbon by forming a monolayer on the surface of steel, hence carburization and metal dusting can be prevented [6,8,39,40]. It can be introduced in the gas atmosphere as hydrogen sulphide (H_2S) and will be adsorbed according to the following reaction:

$$H_2S - H_2 + S(ad) \qquad (2.14)$$

where S(ad) is adsorbed sulphur.

The adsorbed sulphur hinders two important steps of the metal dusting mechanism. The first step is the adsorption of carbon and diffusion of it into the steel surface, and the second step is the nucleation of graphite [8,17,39]. Nucleation of graphite is needed for decreasing the carbon activity at the surface to start the decomposition of Fe_3C. H_2S maybe added in some plants if it will not affect the production process since it tends to react with the catalysts in the plants that use catalytic processes [8].

2.3.7.4 Thermal cycling

Oxide films that are ductile at high temperatures are often brittle at lower temperatures. Most have different coefficients of thermal expansion than those of the metals from which they are formed, setting up thermal stresses when the temperature changes. Thus, an oxide formed at high service temperature may lose adherence to the substrate alloy, when cooled to lower temperatures, and become unprotective when cycling or periodic heating and cooling occurs [20]. Cyclic oxidation of Cr_2O_3 forming alloys can lead to spinel formation ($FeCr_2O_4$) and thermal cycling causes damage on the chromia scale. The chromia scale replenishes itself and

these processes recur, and as a result chromium level is lowered in the alloy [3,61].

2.3.7.5 Surface finish

Cold working the alloy by grinding the surface introduces dislocations in an alloy. Large numbers of dislocations serve as fast-diffusion paths for chromium to the surface to form a protective oxide scale [3,15,56]. The affected alloy regions recrystallized, forming a finer grained structure. The increased number of boundaries due to a refined grain structure then provides rapid diffusion pathways for chromium. The oxide scale prevents gas access to the metal and any consequent internal precipitation. Although the oxide scale spalls readily during thermal cycling, it is quickly reformed by relatively fast delivery of chromium along the grain boundaries to the surface [25].

Etching the alloy does not introduce dislocations that assist diffusion. Chemically etched alloys cannot repair their scales as fast as ground alloys because chromium diffusion is slow. Hansel and co-workers had investigated the effects of surface finish [3]. They found that in general, the severity of metal dusting attack was greater for etched alloys than for ground alloys [3]. The results of Hansel *et al* are shown in Figure 2.11. They show weight change kinetics for different reaction temperatures and two surface finishes (ground and etched). The results represent net values from any weight gain due to uptake of carbon and/ or oxygen and weight loss due to spallation of the oxide scale or disintegration of the sample. The weight versus time of exposure provides useful data about the susceptibility of an alloy to metal dusting and carburization.

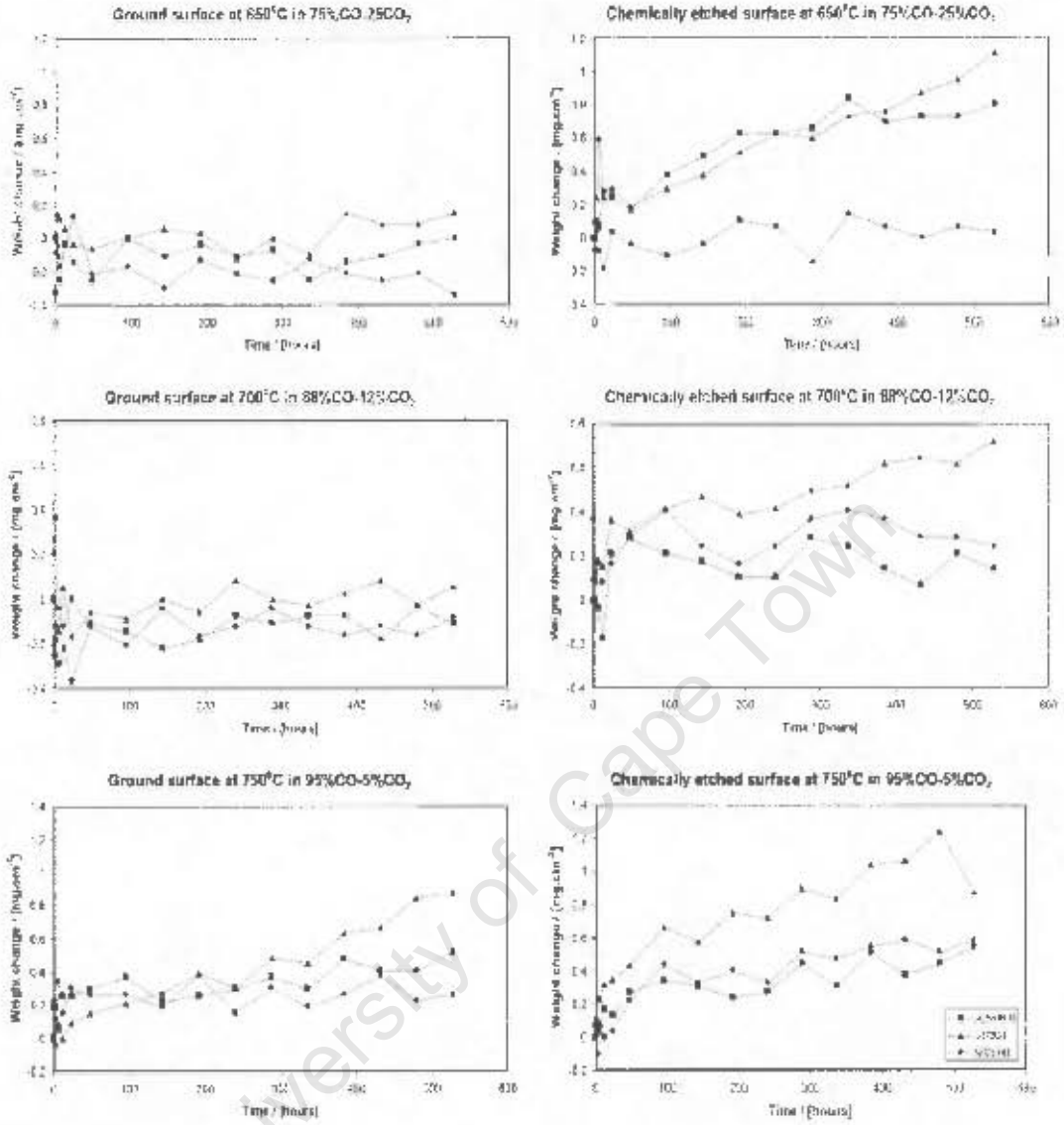

Figure 2.11: Weight change kinetics for different reaction temperatures and two surface finishes (ground and chemically etched alloys) during thermal cycling [3].

Grabke *et al* found that grinding the alloy surface prolonged the protection of an alloy against metal dusting [17,25]. A ferritic structure and a high degree of surface deformation promote chromium diffusion to the surface and these factors favours the rapid formation of a chromium rich protective oxide scale [56,62]. Piehl *et al* had observed that the thickness of the oxide scale had a strong dependence on the surface finish [62]. The more the surface of the material has been deformed, the thicker the

oxide scale and hence, the higher the resulting mass gains, see Figure 2.12. A high degree of surface deformation increases the diffusion coefficient of chromium in alloys as illustrated by Figure 2.13 [62]. Consequently, chromium diffuses rapidly outward to the surface to form a protective oxide layer.

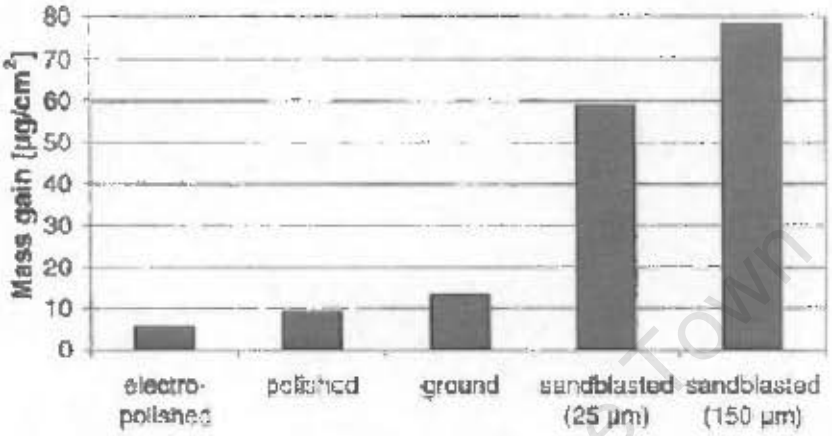

Figure 2.12: The mass gain of a ferritic 12 wt% Cr steel for different surface finishes after 100 hours of oxidation at 599°C in H_2-2.5%H_2O [62].

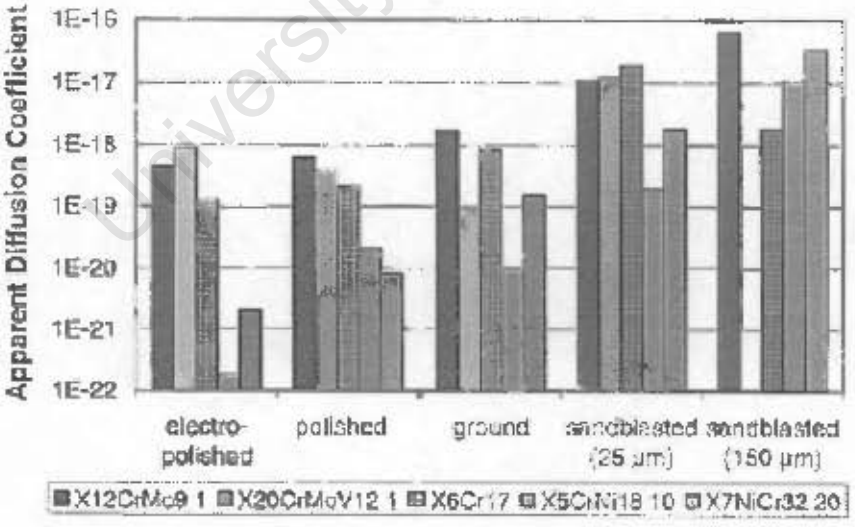

Figure 2.13: Apparent diffusion coefficient (m^2/s) of chromium alloys deduced from samples of alloys with different surface finishes after 10 hours of oxidation time [62].

2.3.7.6 Effects of grain size

Since chromium, aluminium and silicon are substitutional solute atoms, they require vacancies for diffusion [19]. Grain boundaries have regions with high concentration of vacancies. Reducing the grain size of the alloy enhances the resistance to metal dusting [6,17,41]. Alloys with small grain sizes have more grain boundaries than alloys with bigger grains. Reduced grain seize provides fast diffusion paths for scale-forming elements such as silicon, aluminium and chromium to the alloy surface to form a protective oxide scale.

Han *et al* found that the alloy with large grains was severely pitted compared to alloy with small grain size [41]. Perez suggested that the oxidation behaviour of Fe-Cr-Al alloys depends on the grain size of the alloy and showed that a fine grained alloy containing 1 at. % less in chromium and aluminium than the coarse grained alloy reveals a better oxidation resistance [63]. Voisey *et al* also showed that refinement of grain size has a significant positive effect on the diffusion coefficient for Cr in the alloy [64].

2.4 SUMMARY

It is apparent that metal dusting can occur in an environment containing carbon with a carbon activity greater than one. A rather random attack of metal dusting occurring across all types of petrochemical plants makes it difficult to propose a resistant material. Industrial experience shows that the environment places a big role on the propensity for metal dusting. It indicates, for instance, that if Alloy 600 is resistant in a heat exchanger for synthesis, it does not necessarily mean it will be resistant in heat a exchanger of an ammonia plant. The environments are not exactly the same. The laboratory experience on metal dusting only serves as a guide

on material selection since the exact environment on the plant cannot be simulated in the laboratory. The gas mixtures used in the laboratory for a metal dusting corrosion test in the literature gives lower oxygen partial pressures and higher carbon activities than in the actual plants. The laboratory environments are enhanced so that metal dusting can start almost immediately which is not the case in the plants. This enhancement is done so that plant designers can choose the likely resistant material since it would take a long time to get the results if the candidate materials were to be exposed to the plant environment and would also be very costly.

The rather unpredictable behaviour of Alloy 600 and 800 in different plants can be attributed to some change in the operation condition in the plants, repairs or change of the material and sudden ingress of impurities. Impurities such as chlorine, forms chlorides which hinders the formation of protective oxides scales. Some plants may have a high concentration of sulphur and some not, and sulphur is known to suppress metal dusting. In addition, Alloy 800 is a rather large grained alloy as compared to Alloy 600 with fine grains. A fine grained material would form Cr-rich protective oxides rapidly than a coarse grained material, especially at relatively low temperatures. A fine grain microstructure provides fast diffusion paths for the transport of Cr, Al and Si to the surface. In general, the explanation for the apparent anomalies may lie with differences in the process environments that affect the stability of protective oxides films. The experiments carried out in this project were designed to serve as a guide for material selection by exposing different alloys to a specific environment in order to compare the performance of various candidate alloys for the PetroSA plant.

CHAPTER THREE

EXPERIMENTAL METHODS

3.1. MATERIALS

The test materials used consisted of iron and nickel-based alloys. The iron-based alloys are alloy 800HT, GR 309 and 253 MA. The nickel-based alloys are alloys 214, 230, 600, 601, 690, 693, and HR 120 and HR 160. The HR 160 had higher silicon content than the other alloys. Alloy 214 and alloy 693 had higher aluminium contents than the other alloys. Aluminium and silicon have a high affinity for oxygen and can form a protective oxide layer. Table 3.1 shows the nominal composition of the selected alloys. The data was obtained from the suppliers of the alloys.

3.2. METAL DUSTING SIMULATION RIG

An original furnace rig built by Andrew J. L. Vaughan was refurbished and used to accommodate bigger samples [65]. The modified furnace rig consists of an alumina tube 1 (80 mm in diameter), an alumina tube 2 (50 mm in diameter) wounded with a heating wire, a humidifier, quartz glass tube, cooling coils and a sample holder. Alumina tube 2 is inserted into the middle of tube 1. A quartz glass is inserted inside the alumina tube 2 and the samples were placed inside the quartz glass, the reaction chamber, as shown in Figure 3.1. Brass flange caps with O-rings seal closed the ends of the quartz tube. The flange caps provide port fittings for the gas flow and sample holder. Aluminium flange caps with an O-ring seal, closes the ends of the alumina tube 1. The flange caps provide port fittings for the cooling coils system, the power supply and the thermocouple attached to the heating wire. The metal dusting simulation rig is shown in Figure 3.2 and the outlet of the test gas in Figure 3.3.

Table 3.1: Nominal chemical composition of alloys selected for exposure.

Alloys	Ni	Fe	Cr	Si	Al	Mo	Mn	W	Co	Ti	Other
Alloy 214	75^{β}	3	16	0.2^{ξ}	4.5	-	0.5^{ξ}	-	-	-	Y,B, Zr,C
HR 120	37	33^{β}	25	0.6	0.1	2.5^{ξ}	0.7	2.5^{ξ}	3^{ξ}	-	Cb,N, B,C
HR 160	37^{β}	2^{ξ}	28	2.75	-	1^{ξ}	0.5	1^{ξ}	29	0.5	Cb, C
253 MA	10-12	B	20-22	1.10-2.0	-	-	0.8^{ξ}	-	-	-	S,Ce, N,P,C
Alloy 230	β	3^{ξ}	20-24	0.25-0.75	0.20-0.50	1.0-3.0	0.3-1.0	13-15	5^{ξ}	-	P,S, La,B
GR 309	12-15	B	22-24	1^{ξ}	-	-	2^{ξ}	-	-	-	P
Alloy 600	72	6-10	14-17	0.5^{ξ}	-	-	1^{ξ}	-	-	-	Cu, S
Alloy 601	58-63	B	21-25	0.5^{ξ}	1.0-1.7	-	1^{ξ}	-	-	-	Cu
Alloy 693	β	2.5-6.0	27-31	0.5^{ξ}	2.5-4.0	-	1^{ξ}	-	-	1^{ξ}	Cu,S, Nb
Alloy 690	58^{δ}	7-11	27-31	0.5^{ξ}	-	-	0.5^{ξ}	-	-	-	S.Cu
Alloy 800HT	30-35	39.5^{δ}	19-23	-	0.25-0.60	-	-	-	-	-	Ti + Al=0.8-1.2

(β) As balance, **(ξ)** maximum and **(δ)** minimum.

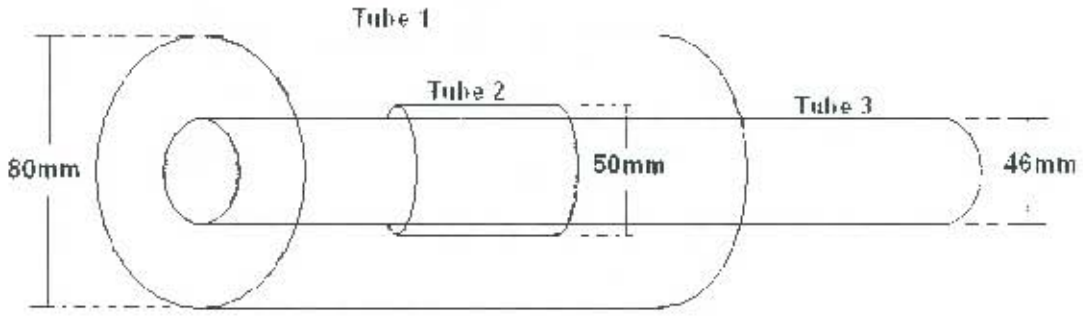

Figure 3.1: Diagram showing the construction of the tubes for a metal dusting rig; Tube 1 - alumina tube, Tube 2 - alumina tube wounded with a resistive heating wire inside Tube 2 and Tube 3, a quartz tube, is inserted in Tube 2.

Figure 3.2: Metal dusting simulation rig covered with a meshed wire for protection. Samples are slide in and out of the reaction chamber by a sample holder attached to the rails shown. The arrow shows a sample holder.

Alumina Tube (Tube 2)

A heating wire was wound around the alumina tube and a K-type thermocouple was attached between the wire the alumina to monitor the temperature of the tube wall. Ceramic cement was used to cover the wires so that they cannot move around. The maximum operating temperature is 650°C at a pressure of one bar for an uninterrupted period of one week.

Figure 3.3: The extraction system. The gas flows through the reaction chamber and flows out via the outlet into the metallic tube sheet and into the ventilation system. The arrow shows a gas outlet.

Humidifier

It consists of a Perspex tube, 50 mm in diameter and 300 mm in height and filled with distilled water, see Figure 3.4. The test gas enters the water through a diffuser. The diffuser breaks down the gas into small bubbles to ensure faster transfer of water vapour to the gas. The water in the humidifier is held at a temperature of 20°C. The gas mixture enters the humidifier as CO-H_2 and leaves the humidifiers as a 74%CO - 24%H_2 - 2%H_2O gas mixture [65]. Equilibrium was assumed to have been achieved inside the humidifier. The CO-H_2-H_2O gas mixture is then directed into the reaction chamber.

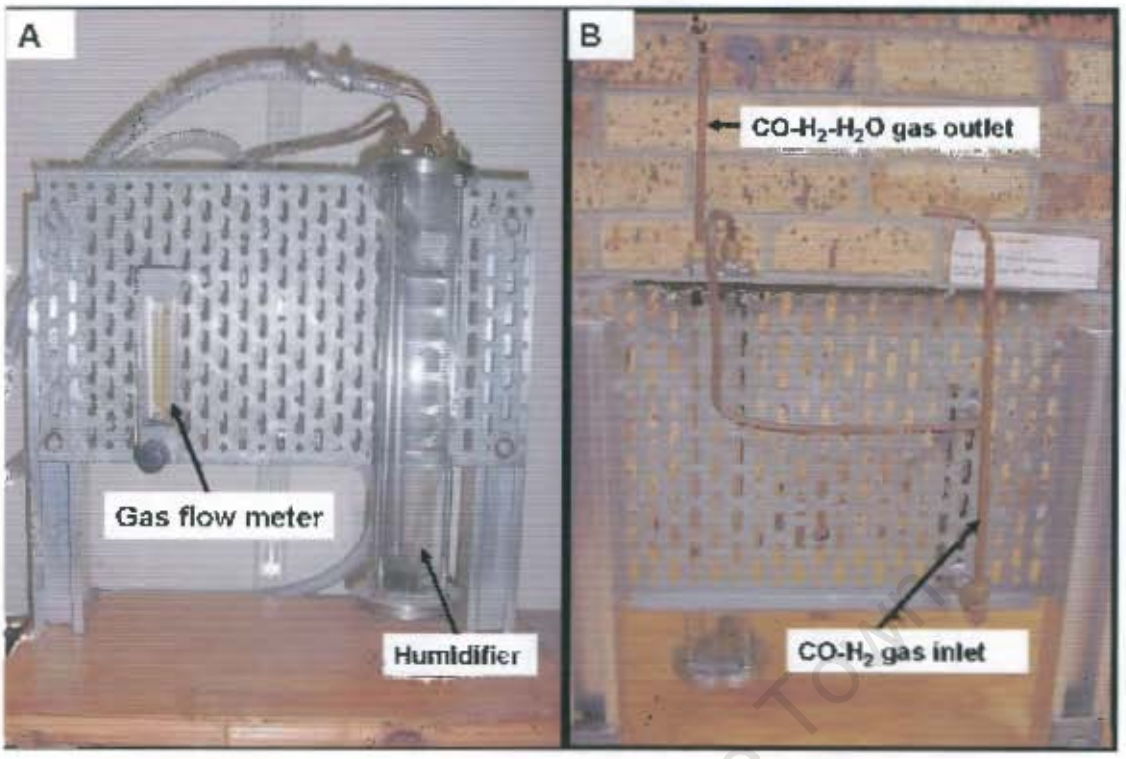

Figure 3.4: Components of the humidifier, A - front view, B – rear view the humidifier.

Sample Holder

It consists of a K-type thermocouple covered with a ceramic sheath to protect it from the carburizing gas. This thermocouple is used to measure the temperature of the samples. Ten alumina rods with a diameter of 1.8 mm are attached on top, along the length of the thermocouple, as shown in Figure 3.5.

3.3. ALLOY SAMPLE PREPARATION

Two samples of about 3 X 13 X 20 mm from each alloy were drilled with a 2 mm hole near the top edge. The hole drilled on the samples was used to hang the samples on the alumina rods attached to the sample holder, as shown in Figure 3.5. The black covering over the alumina rods is ceramic cement.

For the first exposure at 650°C for 500 hours, one sample was ground with 800 grit SiC paper and denoted "GRD". The other sample was not ground and was denoted "ARD" (as-received).The samples were cut from a cold rolled plate. Each sample was given a unique identification by stamping a letter on its surface. For the second exposure at 500°C for 268 hours, the same preparation performed for the first exposure at 650°C was carried out. For the third exposure at 500°C for 268 hours, one sample was heat treated at 850°C for an hour in an inert atmosphere and was denoted "HT" (heat treated). The other sample was not heat treated and was denoted "ARD". After the sample preparations, all samples were cleaned with acetone and weighed before exposure.

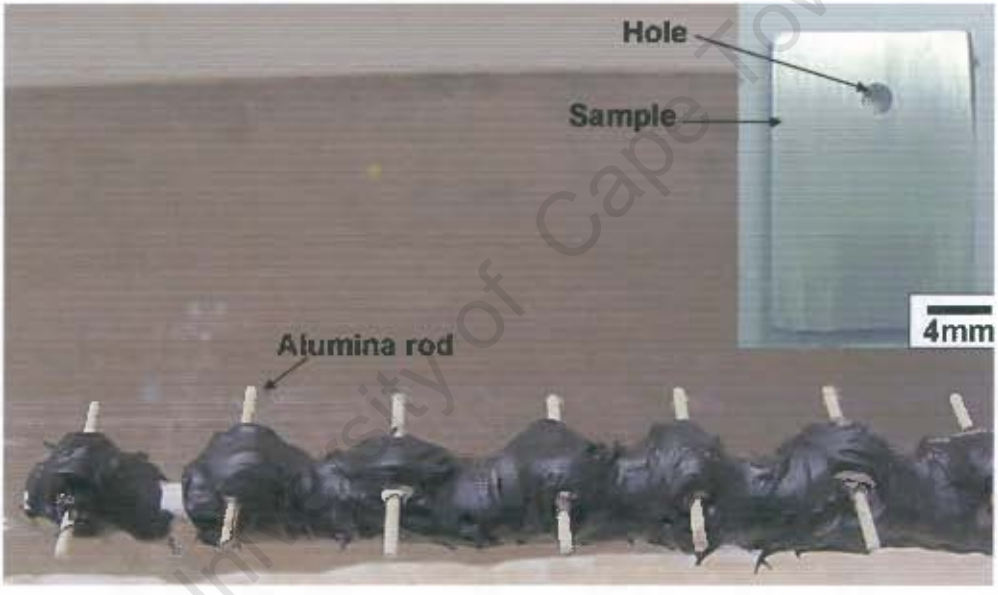

Figure 3.5: Specimen holder with a thermocouple at the tip and alumina rods attached on it. The dark covering over the alumina rods is a ceramic cement. Samples are hanged on the rods.

3.4. TEST ENVIRONMENT

The exposure of commercial alloys was conducted in a flowing $CO-H_2-H_2O$ gas mixture at temperature of 650°C and at pressure of about 1.2 atm. The gas used was purchased as pre-mixed and was a binary H_2-CO mixture, composed of 75 vol. % H_2 and 25 vol. % CO. Prior to passing

the gas into the reaction chamber, water vapour was introduced by bubbling the H_2–CO mixture at a rate of 6 litres per hour through a humidification system held at a constant temperature of 20°C to give a 2 vol. % H_2O. Upon entry into the reaction chamber, the carburizing gas composition was 74% H_2, 24% CO and 2% H_2O. The atmosphere is strongly carburizing and slightly oxidizing. The carbon activity of the test gas was calculated from the following reaction and equation [11]:

$$CO + H_2 - H_2O + C \qquad (3.1)$$

$$a_C = \frac{P_{CO} \times P_{H_2} \times K_3}{P_{H_2O}} \qquad (3.2)$$

whereby the equilibrium constant, K, is given by the following equation

$$\log K = {}^{7100}/_{T} - 7.496 \qquad (3.3)$$

The equilibrium oxygen partial pressure was calculated from the following reaction and equation:

$$H_2O = H_2 + {}^{1}/_{2}O_2 \qquad (3.4)$$

$$\Delta G^0 \quad - RT \ln K = -RT \ln\left(\frac{P_{H_2} \cdot P_{O_2}{}^{1/2}}{P_{H_2O}}\right) \qquad (3.5)$$

ΔG^0 is standard Gibbs free energy change for the above reaction and is given by [66]:

$$\Delta G^0 = 246400 \quad 54.8T \qquad (3.6)$$

where T is the absolute temperature, R is the universal gas constant and P_i's are the partial pressures of the constituent gases [66].

3.5. TEST PROCEDURE AND ANALYSIS

The samples were introduced into the reaction chamber and purged with argon at room temperature for an hour. After that, the samples were heated until the test temperature (650 and 500°C) was reached. Argon was replaced by a carburizing and slightly oxidizing test gas mixture of CO-H_2-H_2O under a pressure of 1.2 atm. The flow rate was 6 litres per hour at standard temperature and pressure. After each period of exposure, the test gas was replaced by argon and the reaction chamber was let to cool to room temperature.

Samples were taken out and their visual appearance noted. The mass change of the samples was measured after each period of exposure. Each sample was weighed after removing the coke deposit by a soft brush and by ultrasonic cleaning in acetone.

The pits on the sample surface were analyzed with a stereo-microscope and scanning electron microscope (SEM) equipped with energy dispersive spectroscopy (EDS) for chemical analysis. The microstructures of the samples were studied by optical microscopy. The micro-hardness of the samples was measured with a Highwood (HWDM-3) Vickers's micro-hardness tester machine with a load of 100 gf before exposure and after exposure to check the effects of any precipitation hardening process that might occur. Prior to exposure, the composition of the selected alloys were analysed by spark emission spectroscopy and scanning electron microscope with energy dispersive spectroscopy.

3.6. PLAN OF TESTING

Three series of tests were carried out. The first exposure was conducted at 650°C (Experiment A) for a total of 500 hours. The main aim of the first exposure was to evaluate the effects of surface finish to metal dusting resistance. Six alloys in the table were exposed, see Table 3.2.

Table 3.2: The selected alloys exposed at 650°C and 500°C for a total of 500 hours and 268 hours, respectively.

Alloys	Surface Finish	
Alloy 600	Ground	As-received
HR 160	Ground	As-received
253 MA	Ground	As-received
GR 309	Ground	As-received
Alloy 230	Ground	As-received
Alloy 214	Ground	As-received

The second exposure was conducted at 500°C (Experiment B) for 268 hours. The main aim of this exposure was to evaluate the effects of surface finish and effects of temperature and carbon activity of the environment. The effects on temperature and carbon activity of the environment were achieved by comparing the metal wastage of the first exposure at 650°C and the second exposure at 500°C. The same types of alloys used in the first exposure were used for this exposure. The third exposure was conducted at 500°C (Experiment C) for 268 hours. The aim was to evaluate the effect of heat treatment prior to metal dusting exposure. Five different alloys were exposed. The alloys selected are shown in Table 3.3.

Table 3.3: Selected alloys exposed at 500°C for 268 hours.

Alloys	Heat Treatment (HT)	
Alloy 601	HT	As-received
Alloy 690	HT	As-received
Alloy 693	HT	As-received
Alloy 800HT	HT	As-received
HR 120	HT	As-received

CHAPTER FOUR

RESULTS

4.1 CHEMICAL ANALYSIS

The composition of the alloys analyzed by SEM was different to the nominal composition shown in section 3.1. The difference between the nominal composition, spark emission spectroscopy composition and composition obtained from SEM could be attributed to the different techniques that are used to analyze chemical composition of metals. Spark emission spectroscopy used was specifically programmed to analyse stainless steels and low and high carbon steels, hence the newly developed alloys cannot be analysed accurately. In addition, to analyse the metal by spark emission spectroscope one has to select the type of the alloy in the programmed menu of the spectroscopy and most of the alloys were not in the programmed menu. Thus there exists a large discrepancy between SEM and spark emission spectroscopy in the alloys that were not in the programme. The nominal composition serves as a guide for the composition of an alloy and not the exact composition.

The chemical composition obtained by SEM will be used to explain the different behaviour observed in the exposed alloys. The chemical compositions of the alloys are shown in Table 4.1a and Table 4.1b.

Table 4.1a: Chemical composition of alloys selected for exposure.

Alloys	Ni	Fe	Cr	Si	Al	Mo	Mn	W	Co	Ti	Source
Alloy 214	75[β]	3	16	0.2[ξ]	4.5		0.5[ξ]				Nominal
	72.99	5.59	15.23	0.23	5.96						SEM
	70.7	5.7	19.29		3.8	0.038	0.158		0.027		Spark
HR 120	37	33[β]	25	0.6	0.1	2.5[ξ]	0.7	2.5[ξ]	3[ξ]		Nominal
	42.64	36.77	19.63	0.19				0.57	0.2	0.19	SEM
	72.8	3.58	20.8		0.943	0.712	0.583		0.199		Spark
HR 160	37[β]	2[ξ]	28	2.75		1[ξ]	0.5	1[ξ]	29	0.5	Nominal
	42.66	0.5	22.09	1.32				0.61	32.6	0.21	SEM
											Spark
253 MA	10-12	β	20-22	1.10-2.0			0.8[ξ]				Nominal
	11.21	66.03	21.24	0.9			0.62				SEM
	11.03	65.2	20.5	1.69	0.013	0.212	0.615		0.243	0.009	Spark
Alloy 230	β	3[ξ]	20-24	0.25-0.75	0.20-0.50	1.0-3.0	0.3-1.0	13-15	5[ξ]		Nominal
	65.43	1.91	13.7	0.29	1.14			17.23	0.3		SEM
	72.5	3.53	20.8		0.918	0.724	0.579		0.192		Spark
GR 309	12-15	β	22-24	1[ξ]			2[ξ]				Nominal
	12.43	67.59	18.08	0.82			1.09				SEM
	11.75	65.2	19.09	1.79	0.009	0.192	1.391		0.119	0.006	Spark

Table 4.1b: Chemical composition of alloys selected for exposure.

Alloys	Ni	Fe	Cr	Si	Al	Mo	Mn	W	Co	Ti	Source
Alloy 600	72	6-10	14-17	0.5[ξ]			1[ξ]				Nominal
	75.38	8.54	14.7	1.11			0.28				SEM
	69.3	9.64	18.6		0.224	0.039	0.241		0.052	0.140	Spark
Alloy 601	58-63	β	21-25	0.5[ξ]	1.0-1.7		1[ξ]				Nominal
	62	17.55	16.14	0.29	4.02						SEM
											Spark
Alloy 693	β	2.5-6.0	27-31	0.5[ξ]	2.5-4.0		1[ξ]			1[ξ]	Nominal
	64.13	4.13	29.68	0.1	1.45					0.52	SEM
	64.8	1.44	30.06		1.78	0.025	0.042		0.015	0.095	Spark
Alloy 690	58[δ]	7-11	27-31	0.5[ξ]			0.5[ξ]				Nominal
	68.9	12.3	17.19	0.22	1.39						SEM
											Spark
Alloy 800HT	30-35	39.5[δ]	19-23		0.25-0.60						Nominal
	33.39	48.57	16.86		0.77					0.41	SEM
	32.23	45.69	18.94	0.42	0.58	0.255	0.9		0.171	0.487	Spark

4.2 MASS CHANGE AS A FUNCTION OF TIME

This section shows the mass change over time of all alloys during the experiments for two surface finishes *viz.* as received (ARD) and ground (GRD). For these purpose three types of investigations was carried out. The results represents the average mass change (mg/cm^2) resulting from any mass gain due to uptake of carbon and/or oxygen, and mass loss due to spallation of the oxide surface layer or disintegration of the alloy (see again section 3.6)

4.2.1 Alloy Exposure at 650°C for 500 hours (Experiment A)

The main aim of the first exposure was to measure the corrosion rates and evaluate the effects of surface finish to metal dusting resistance at high temperature. All solid lines indicate as-received, whereas dashed lines indicate ground alloys.

Figure 4.1a and Figure 4.1b shows the metal wastage of the various alloys with exposure time for the as-received and ground conditions, respectively. From these two plots, in general, it can be seen that there was neither significant mass loss nor gain after about 250 hours. The onset of metal dusting of alloys in the as-received conditions was observed after 300 hours and the rate of mass loss seemed to be much faster for the as-received alloys than the ground alloys. The behaviour of 253 MA was rather unexpected since it seemed that 253 MA (ARD) performed better than 253 MA (GRD).

After a total exposure of 500 hours, the most resistant (Figure 4.2) to metal dusting alloys in both the as-received and ground conditions were Alloys 230 and HR 160. The better resistance of these two alloys to metal dusting can be attributed to their high nickel, high chromium and very low iron content. The presence of high contents of tungsten and cobalt is also beneficial as they are carbide forming elements.

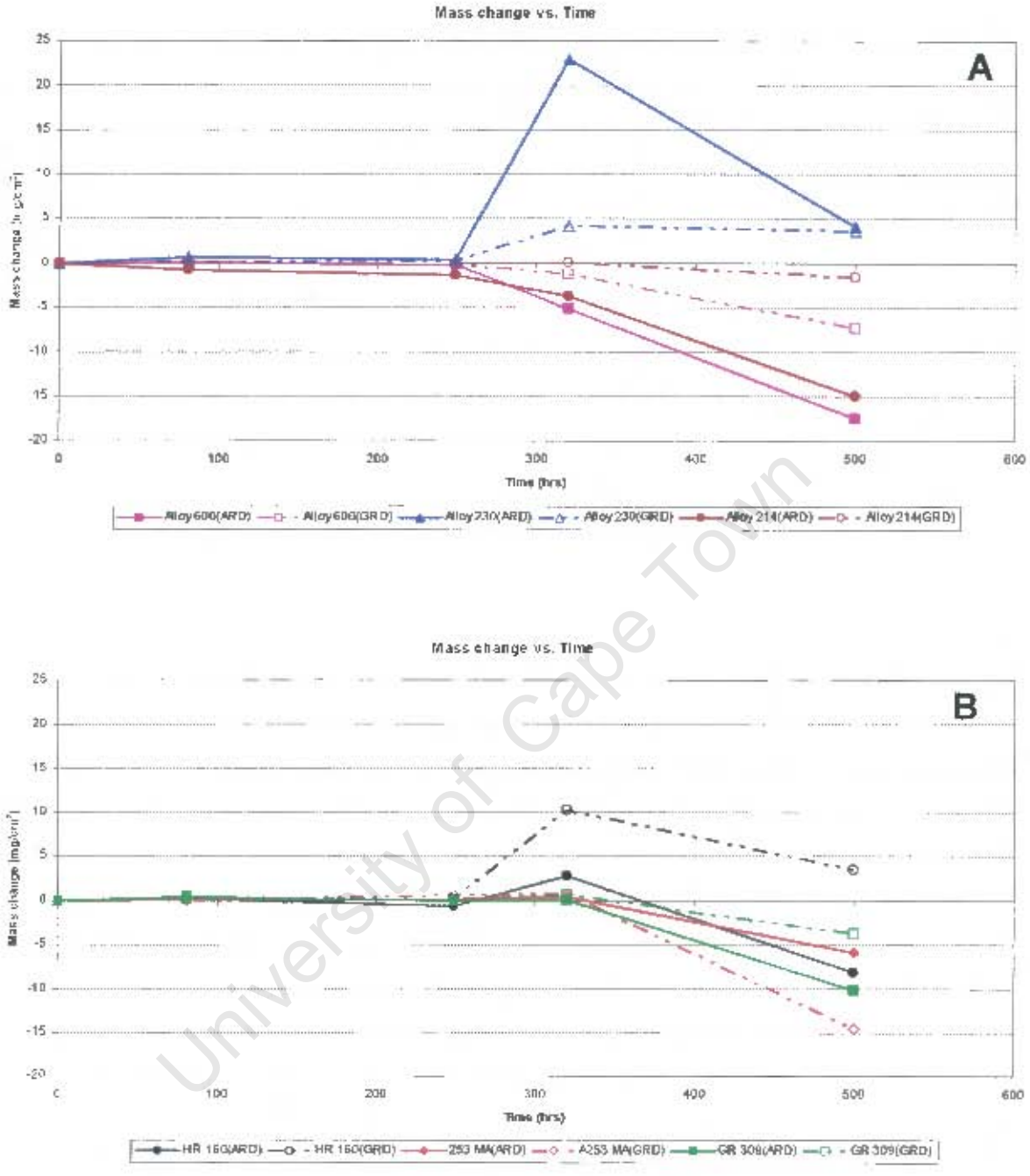

Figure 4.1: Mass change vs. time curves for the exposed alloys at 650°C with different surface finishes.

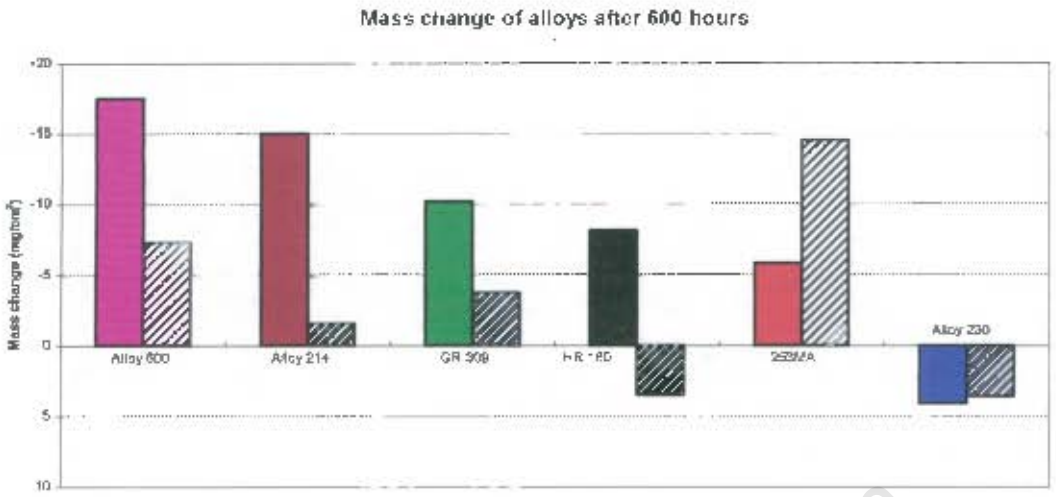

Figure 4.2: Mass change of selected alloys after a total exposure at 650°C for 500 hours. Solid bars = as-received; striped bars = ground alloys.

4.2.2 Alloy Exposure at 500°C for 268 hours (Experiment B)

The main aim of this exposure was to evaluate the effects of surface finish and effects of temperature and carbon activity of the environment. The effects on temperature and carbon activity of the environment were achieved by comparing the initiation and severity of metal dusting of the alloy in the first exposure at 650°C and the second exposure at 500°C.

Figure 4.3a and Figure 4.3b shows the metal wastage of various alloys with exposure time for the as-received and ground conditions, respectively. From these two plots, in general, it can be seen that the onset of metal dusting occurred earlier for both the as-received and ground conditions when compared to exposure at 650°C for all the alloys. For the as-received condition the onset now occurs after 100 hours, whereas for the ground surfaces the onset of metal dusting appears to occur at 200 hours. It would also appear that the as-received alloy, alloy 214 (ARD) starts to show metal dusting after only 1 day of exposure. The behaviour of 253 MA is still an anomaly with the ground material

performing worse than in the as-received condition. Also, alloy GR 309 now shows very high rates of corrosion in both the as-received and ground conditions (Figure 4.4).

After the total exposure of 268 hours, the most resistant alloys in the as-received conditions were again Alloys 230 (ARD) and HR 160 (ARD), as shown in Figure 4.4. The onset of metal dusting in Experiment A occurred between 250 and 300 hours whereas the onset of metal dusting in Experiment B occurred after 100 hours. Nishiyama *et al* suggested that carbon activity can be considered as an index to represent metal dusting propensity [16]. The earlier onset of metal dusting of alloys in Experiment B can be attributed to the higher carbon activity of 500 at 500°C as compared to 15 at 650°C for Experiment A. Thus the environment in Experiment A was more aggressive than in Experiment B. A much higher carbon activity ensures early carbon deposition and hence early onset of metal dusting as compared to a lower carbon activity.

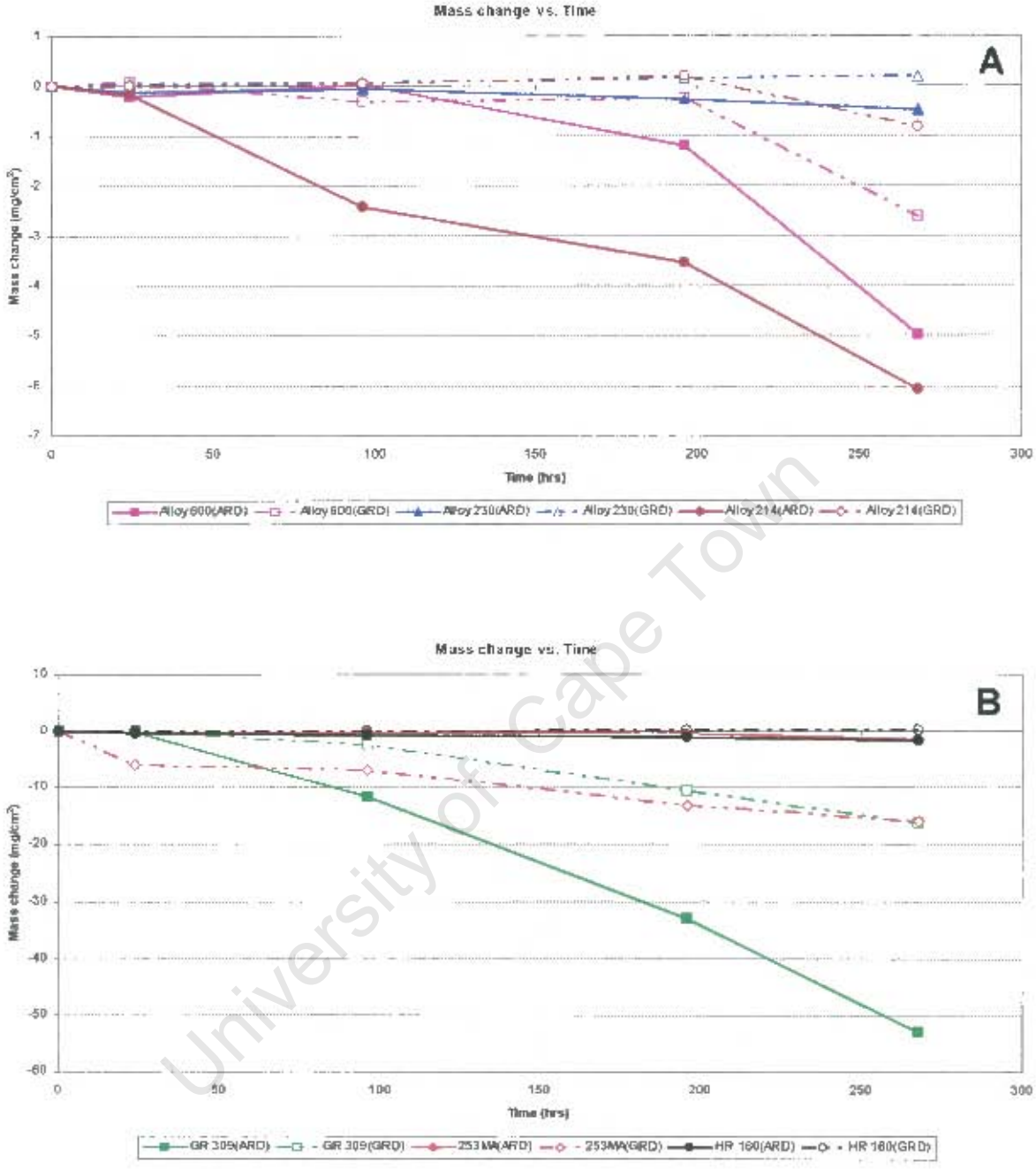

Figure 4.3 : Mass change vs. time curves for exposed alloys at 500°C with different surface finishes.

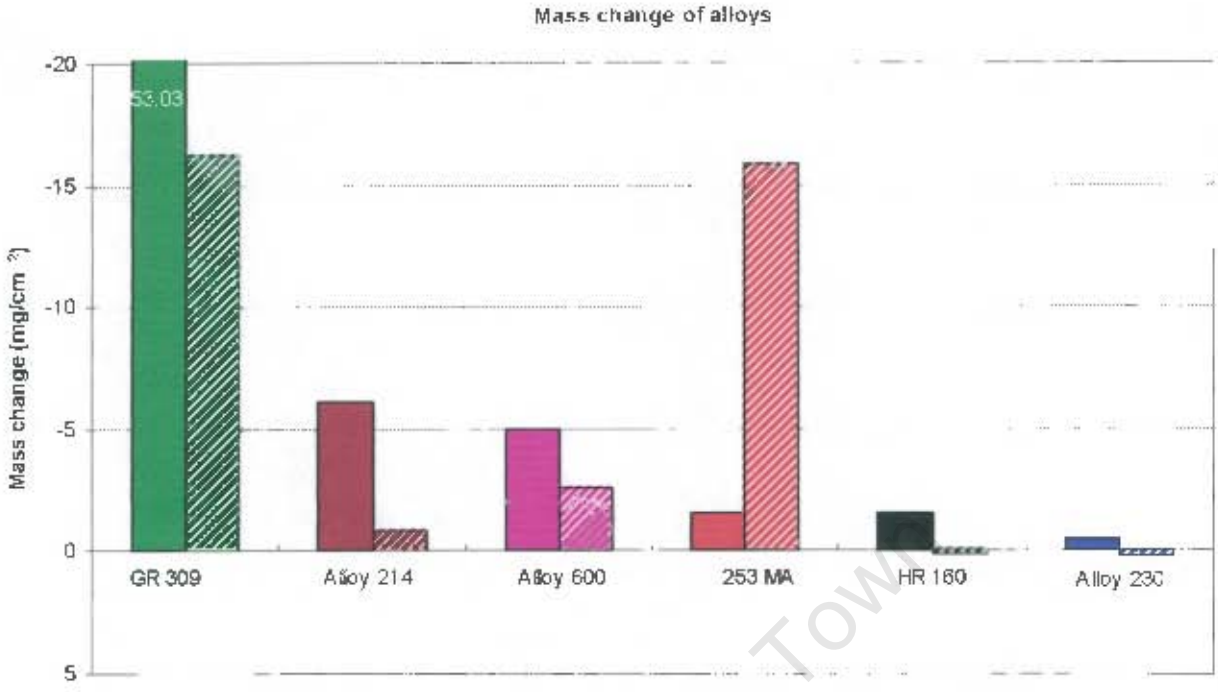

Figure 4.4: Mass change of alloys after a total exposure at 500°C for 268 hours. Solid bars = as-received; striped bars = ground alloys.

4.2.3 Alloy Exposure at 500°C for 268 hours (Experiment C)

The aim of this exposure was to evaluate the effect of heat treatment prior to metal dusting exposure. The heat treatment was conducted in a vacuum furnace filled with argon. After the heat treatment, the surfaces of the alloys were a bit dull in colour and that may be attributed to the heat treatment and reactions within the alloy since the atmosphere was inert. Figure 4.5 shows the metal wastage of various alloys with exposure time for the as-received and heat-treated conditions, respectively. From these plots, in general, it can be seen that the onset of metal dusting occurred after one day of exposure for Alloy 800HT (HT), Alloy 800HT (ARD) and HR 120 (HT). Alloy 601 (ARD) starts to show metal dusting after 100 hours (4 days) whereas Alloy 601 (HT) showed metal dusting after 200 hours (8 days). The early onset of metal dusting can be attributed to their high iron content and low chromium content. The high resistance of Alloy 693 and Alloy 690 in either condition can be attributed

to its high nickel content and high chromium content. The effect of heat-treatment prior to exposure seemed not to be obvious since the behaviour is not following any pattern. The microstructures of the alloys after heat-treatment and before heat-treatment did not show any discernible difference. In addition, the micro-hardness before heat-treatment and after heat-treatment was also the same (see section 4.5). The mass loss difference between the as-received alloys and heat-treated alloys, as shown in Figure 4.6, may be due to experimental error. The final value of mass loss of Alloy 800HT (HT) is an estimated value as the sample was not placed back in the furnace due to excessive coking having occurred. It is interesting to note that Alloy 693 and Alloy 690 in both conditions were much more resistant than the other alloys to metal dusting, despite having lost more mass than Alloy 601 (see in Figure 4.6). The higher mass loss of Alloy 690 and 693 may be attributed to rapid oxidation and oxide spallation. In addition, Alloy 601 (HT) and Alloy 601 (ARD) were both attacked by metal dusting.

Comparing the alloy performance in the as-received condition in Experiment B and Experiment C after 268 hours, all alloys showed severe pitting and hence they were attacked by metal dusting except Alloy 693 and Alloy 690. The combination of rapid oxide spallation and disintegration of the alloys can be attributed to the mass loss observed, as shown in Figure 4.7. The mass gain can be due to carbon ingress and oxidation.

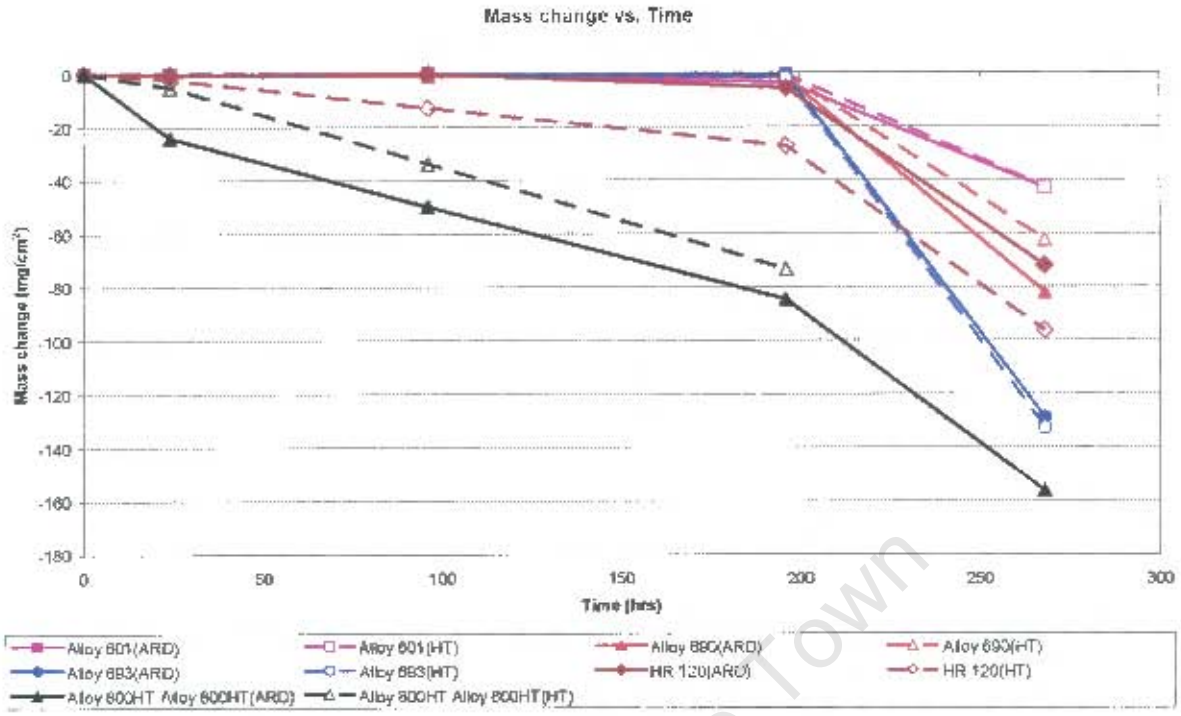

Figure 4.5: Mass change vs. time curves for exposed alloys at 500°C.

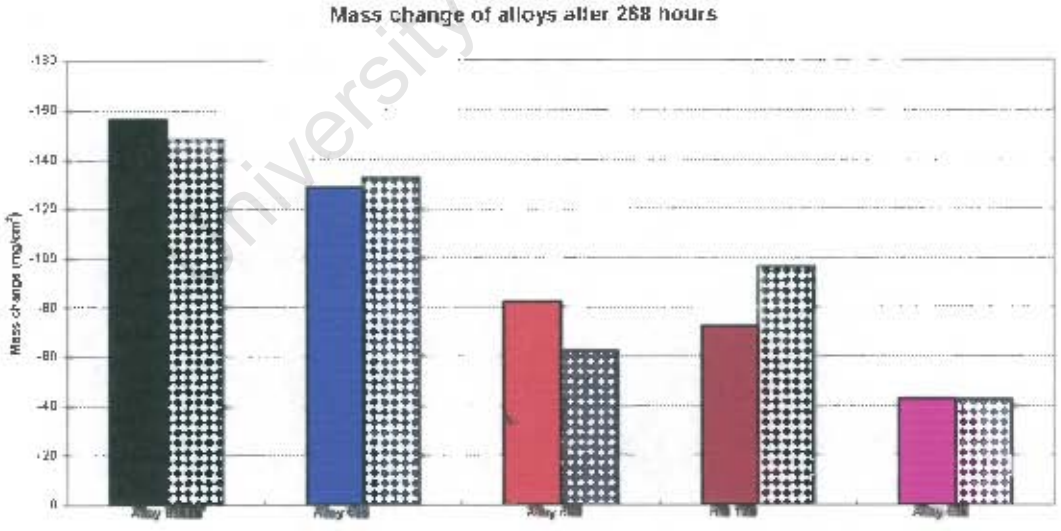

Figure 4.6: Mass change of alloys after a total exposure of 268 hours at 500°C. Solid bars = as-received; striped bars = ground alloys

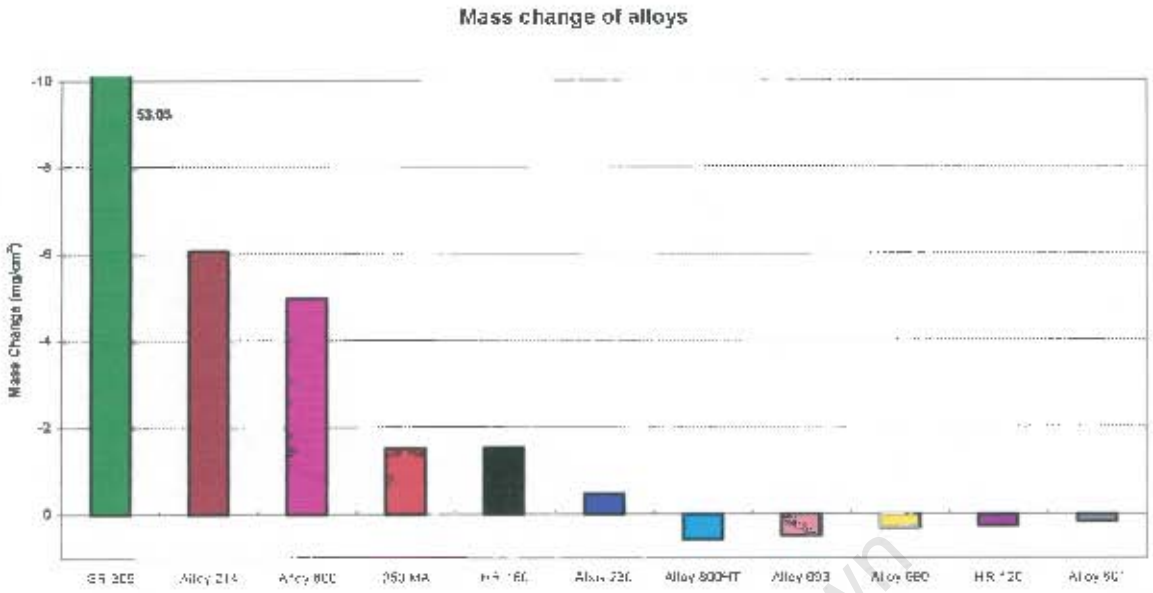

Figure 4.7: Mass change of different alloys after a total exposure to CO-H_2-H_2O gas mixture at 500°C for 268 hours. All alloys are as-received.

4.3 SURFACE AND MICROSTRUCTURAL ANALYSIS

This section shows the effects of metal dusting corrosion on the surfaces and on the microstructures of all the exposed alloys. It is divided into three categories, *viz*, severe metal dusting, mild metal dusting and no metal dusting (absence of metal dusting). Severe metal dusting is when a sample surface shows uniform wastage and / or wide localized or irregular pits covering almost the entire surface of the sample. Mild metal dusting is when a sample surface has few pits whereas the absence of metal dusting is when the sample surface shows no discernible pitting or wastage.

4.3.1 Severe Metal Dusting Corrosion

Table 4.2 shows all alloys that suffered severe metal dusting corrosion in experiments A, B and C. Experiment A was conducted at 650°C for 500 hours and experiment B and C were both conducted at 500°C for 268 hours.

Alloys that have suffered severe metal dusting corrosion (Table 4.2) showed similar features as Alloy 600 (ARD) shown below in Figure 4.8, and most of the pits have coalesced, giving an appearance of a uniform wastage. In addition, some showed erratic pitting. Severe metal dusting occurred in both the ground (GRD) and as-received (ARD) conditions. Figure 4.8 shows pitting on the sample surface for alloy GR 309 (GRD) and uniform wastage on Alloy 600 (ARD) in experiment B. The dark areas are pits and bright or light areas are the unaffected areas.

Table 4.2: Alloys that showed severe metal dusting for experiments A, B, and C, in different conditions.

Alloys	Experiment A	Experiment B	Experiment C
Alloy 600	• As-received • Ground	• As-received • Ground	No test
GR 309	• As-received • Ground	• As-received	No test
253 MA	• Ground	• Ground	No test
Alloy 214	• As-received	• As-received • Ground	No test
HR 160	No test	• As-received	No test
Alloy 230	No test	• As-received	No test
Alloy 601	No test	No test	• As-received
Alloy 800HT	No test	No test	• As-received • Heat-treated
HR 120	No test	No test	• As-received • Heat-treated

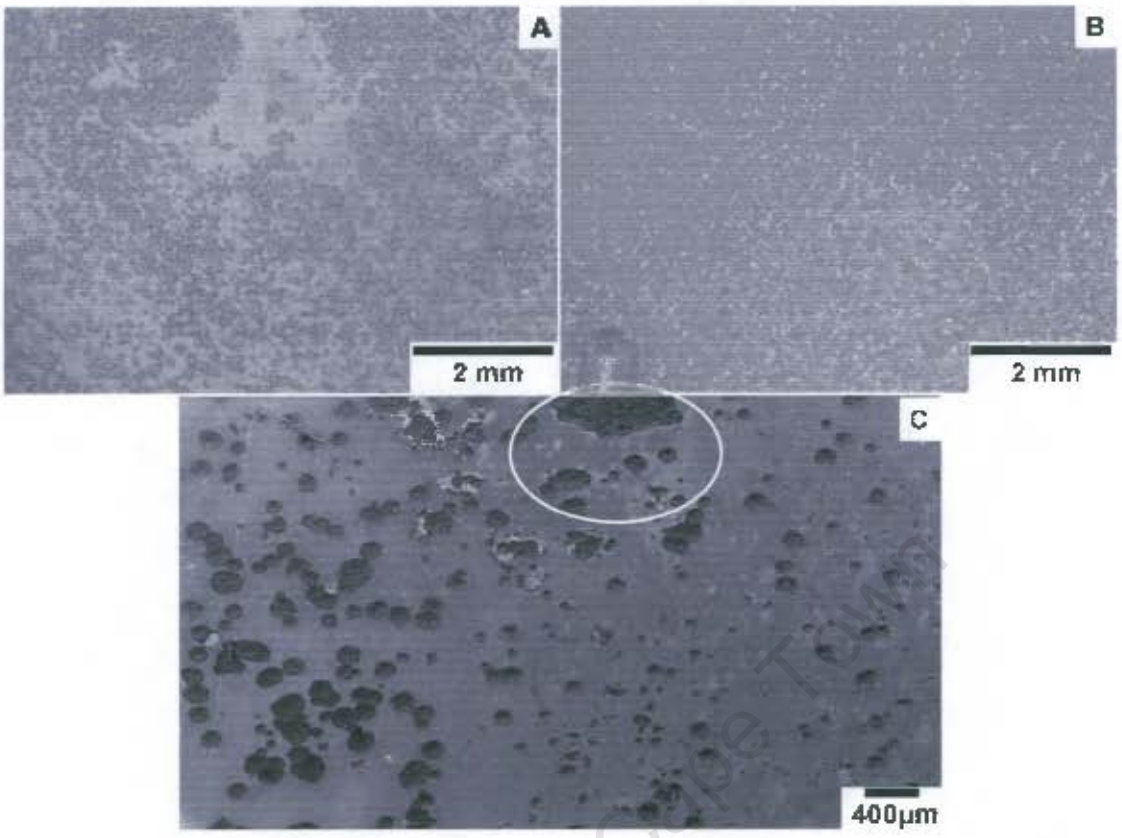

Figure 4.8: Pitting and uniform wastage of GR 309 (ARD) and Alloy 600 (ARD) after 268 hours (11 days) of exposure at 500°C, respectively. a) GR 309(ARD), b) Alloy 600 (ARD) and c) Alloy 600 (GRD), all showing severe pitting.

Alloy 600 (ARD) from experiment B showed erratic pitting after eleven days as shown in Figure 4.8c. The pits marked by a circle are shown at higher magnification in Figure 4.9. Since oxide film is believed to provide protection for the alloy against metals dusting, it seems that where pits had not developed there was a protective oxide film. However, it appears that the pits had developed where there was less protection from the oxide film and the pits coalesced to form wider pits. The metal particles at the bottom of the pits acted as catalysts for further carbon deposition which led to the continuation of metal dusting in the pit area as shown in Figure 4.9 and Figure 4.10. Thus the bottoms of the pits were uneven.

A quantitative analysis with EDS was done on the unaffected area marked "U" and inside the pit (Figure 4.9) to show that there is micro-segregation

of elements taken place during the metal dusting process which leaves certain regions in the metal depleted of other elements. It is not clear how segregation of these elements took place during the metal dusting process.. It was found that the unaffected surface was composed of 17.55 wt% Cr, 8.12 wt% Fe and 73.79 wt% Ni. In contrast, the pit shown by the arrow was composed of 28.34 wt% Cr, 8.61 wt% Fe and 58.89 wt% Ni. It is evident that the surface had a higher content of nickel and lower content of chromium when compared to the pits. The same phenomenon was observed for Alloy 600 (ARD) *i.e.* in the as-received state, whereby the unaffected areas had higher contents of nickel and lower chromium contents.

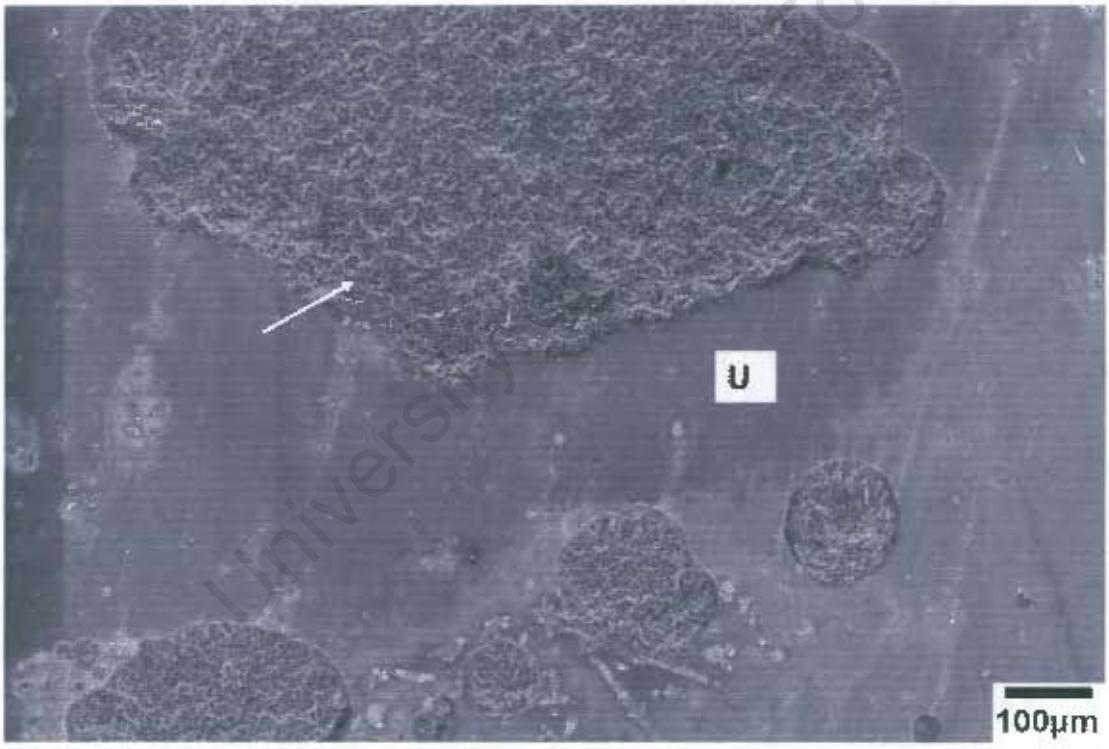

Figure 4.9: Alloy 600 (GRD) with tiny and big pits. The bottoms of the pits are uneven suggesting a continuation of metal dusting within the pits.

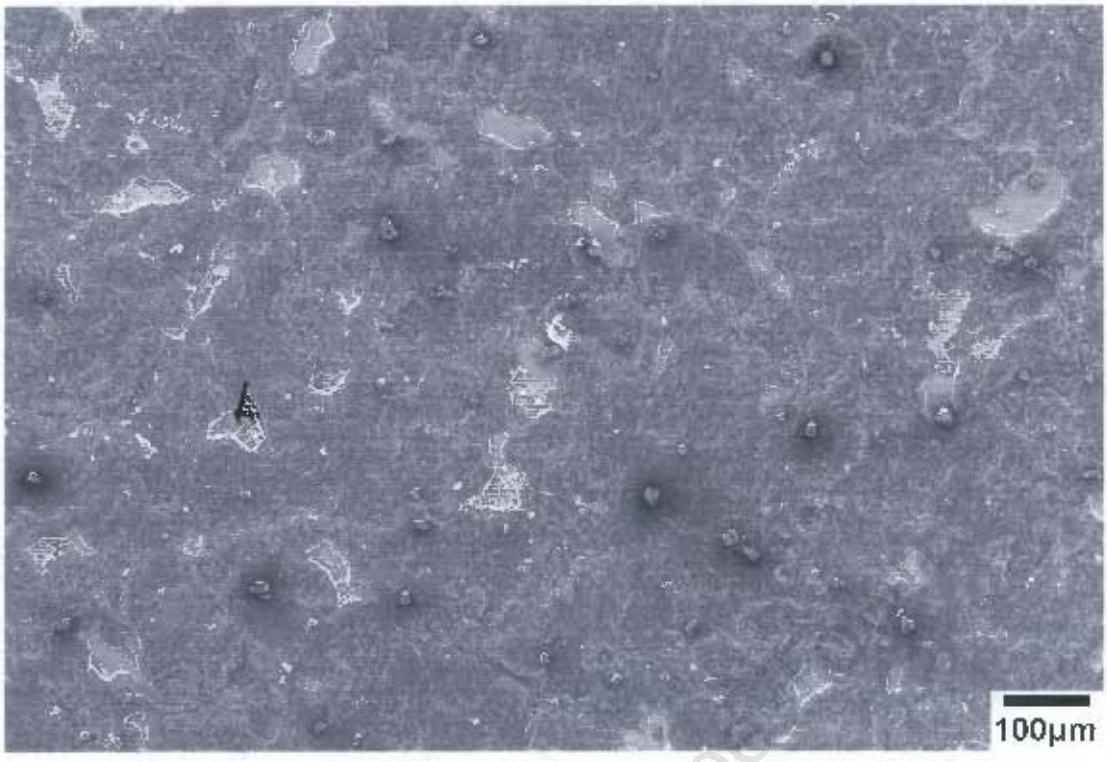

Figure 4.10: Pits had coalesced to give an appearance of a uniform wastage on Alloy 600 (ARD). The bright areas shown by the arrow are the unaffected area and the dark areas are pits.

253 MA, GR 309 and Alloy 600 all suffered severe metal dusting in both the as-received and ground conditions exposed at 650°C for 500 hours (20 days). 253 MA (ARD) was badly affected, as shown in Figure 4.11a, 4.11b and 4.11c, respectively. In Figure 4.11a and 4.11b, 253 MA (ARD) and GR 309 (ARD), respectively, had pits which have coalesced with the neighbouring pits to form wide irregular pits. Loose particles can be seen at the base of bigger pits suggesting a continuation of metal dusting in the pit area. Furthermore, Figure 4.11c shows secondary pits within the primary pits. The secondary pits are white or bright areas and the primary pits are dark areas, shown by arrows and the unaffected area is marked by a letter "U".

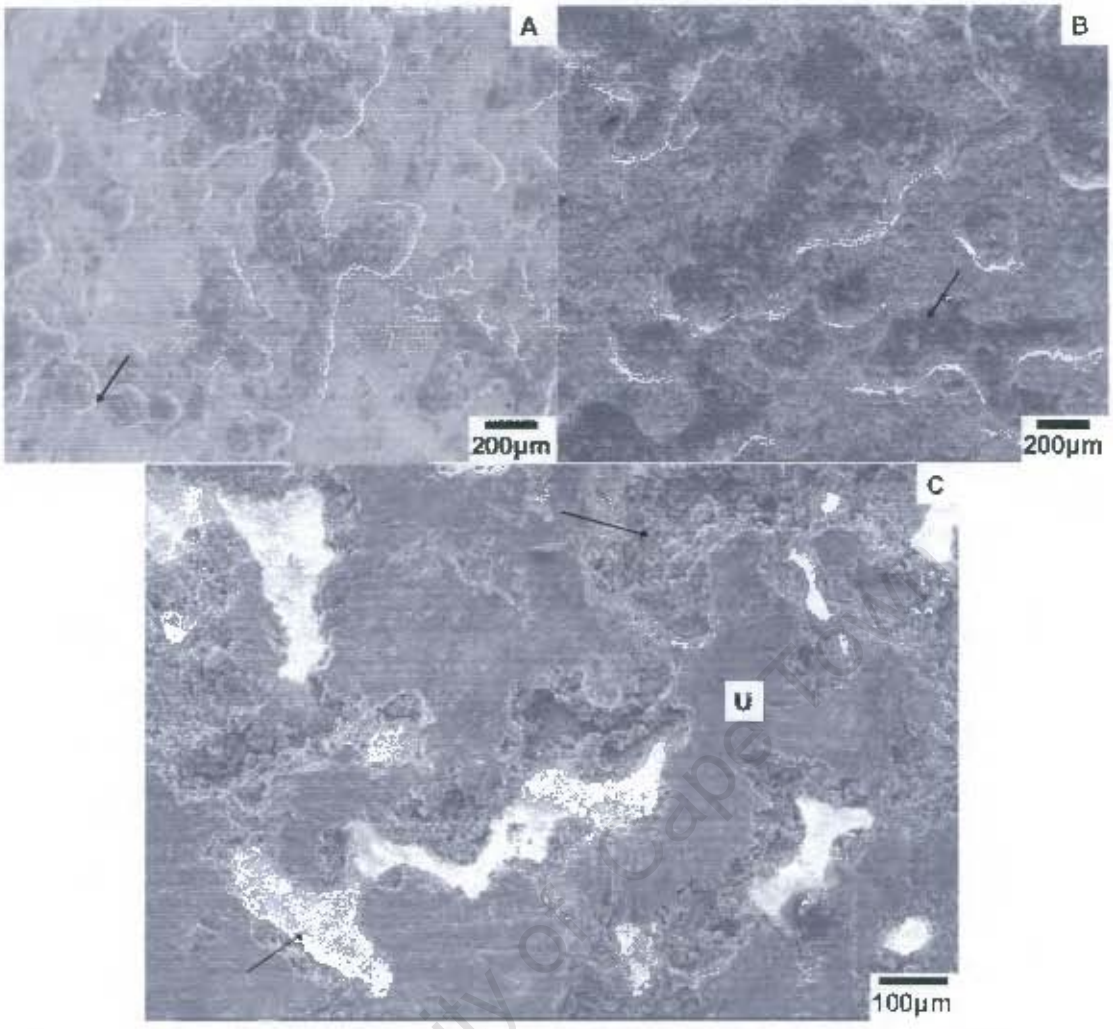

Figure 4.11: Pitting of a) 253 MA (ARD), b) GR 309 (ARD) and c) Alloy 600 (ARD) after exposure of 500 hours (20 days) at 650°C in a CO-H_2-H_2O gas mixture.

At 500°C, 253 MA and GR 309 in the as-received condition, suffered severe metal dusting as compared to the same alloys in the ground state. The attack was so severe that there was no longer unity between the grains as shown in Figure 4.12a and 4.12b. Some of grains had been detached and dislodged during the metal dusting process. The grain boundary attack is more profound in 253 MA (ARD) than in GR 309 (ARD). The dark or black areas correspond to the missing grains as shown by arrows. A quantitative EDS analysis revealed that there was a higher chromium content (35.49 wt%) in the grains than within the pits (20.99 wt%). GR 309 (GRD) and 253 MA (GRD) showed no discernible grain boundary attack.

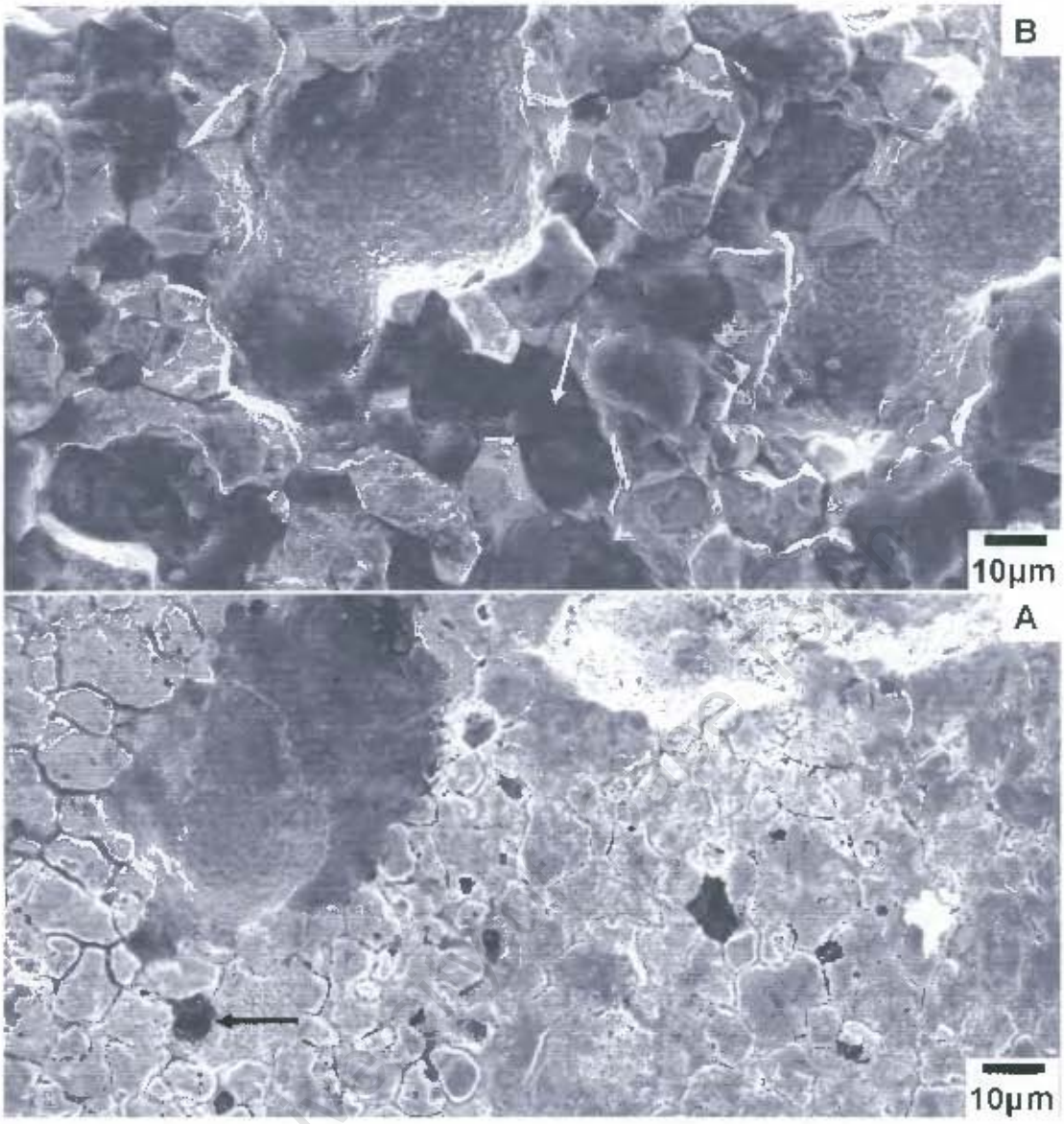

Figure 4.12: Severe grain boundary attack in a) 253 MA (ARD) and b) GR 309 (ARD) after 20 days of exposure at 500°C.

Alloy 214 suffered severe metal dusting in the as-received condition at 650°C for 500 hours and mild corrosion in the ground condition. At 500°C, Alloy 214 in both the as-received and ground conditions suffered severe metal dusting. Both Alloy 214 (ARD) and 214 (GRD) showed intensive carbide precipitation within the grains and along the grains boundaries, as shown in Figure 4.13a. The bright area in Figure 4.13a is a carburized zone and it looks grey at higher magnification as shown in Figure 4.13b. In chromium steels and alloys, a typical carburised zone (zone with internal carbides) appears grey or black after metallographic etching since

the tiny particles formed at low temperatures are not discernible by optical microscopy [17]. A carburized zone ranging from 45 to 65 μm wide was observed in both Alloy 214 (ARD) and 214 (GRD). A jagged surface, marked by a circle, can be seen in Figure 4.13b at the top edge of the surface of Alloy 214 (ARD) corresponding to the disintegration of the alloy. This region is shown at higher magnification in Figure 4.13c. It shows small particles embedded in the coke, shown by arrows. These particles were separated from the parent material during the metal dusting process.

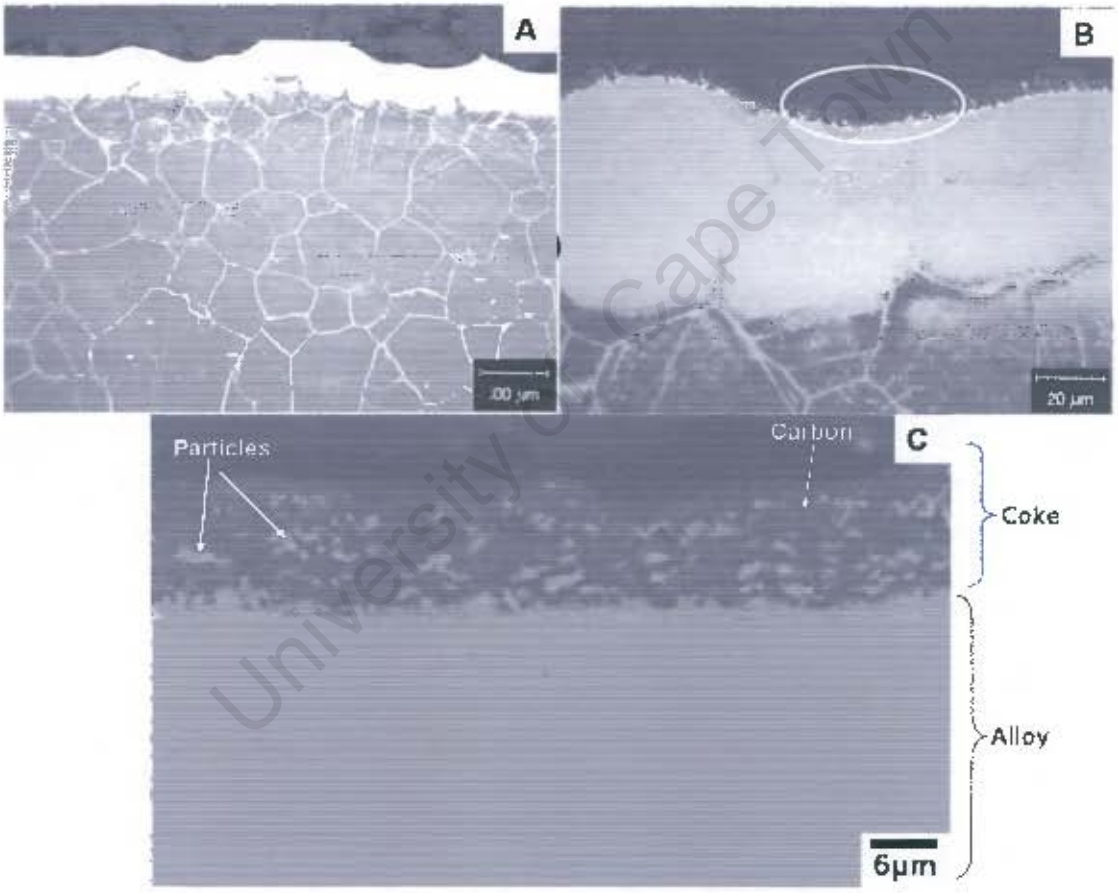

Figure 4.13: Metallographic cross-section of Alloy 214 (ARD) after 500 hours at 650: a) and b) optical microscope photos showing internal carbide precipitation and a carburized zone (bright area) and c) Backscattered electron diffraction image of the cross-section showing coke deposits. Alloys were electro-etched in an oxalic acid.

The carburized zone was not observed for 253 MA (ARD) and was observed for 253 MA (GRD). The carburized zone in Figure 4.14a, was about 20 μm in depth below the surface. Carbide precipitation was observed, largely along the grain boundaries within and near the carburized zone. Alloy 601, 800HT and HR 120 showed a carburized zone in both conditions. A carburized zone was not observed where no pits developed, as shown in Figure 4.14b. A heavily carburized zone and intensive carbide precipitation along the grain boundaries and just below the carburized zone was evident in the heat treated samples in Figures 4.14c-d.

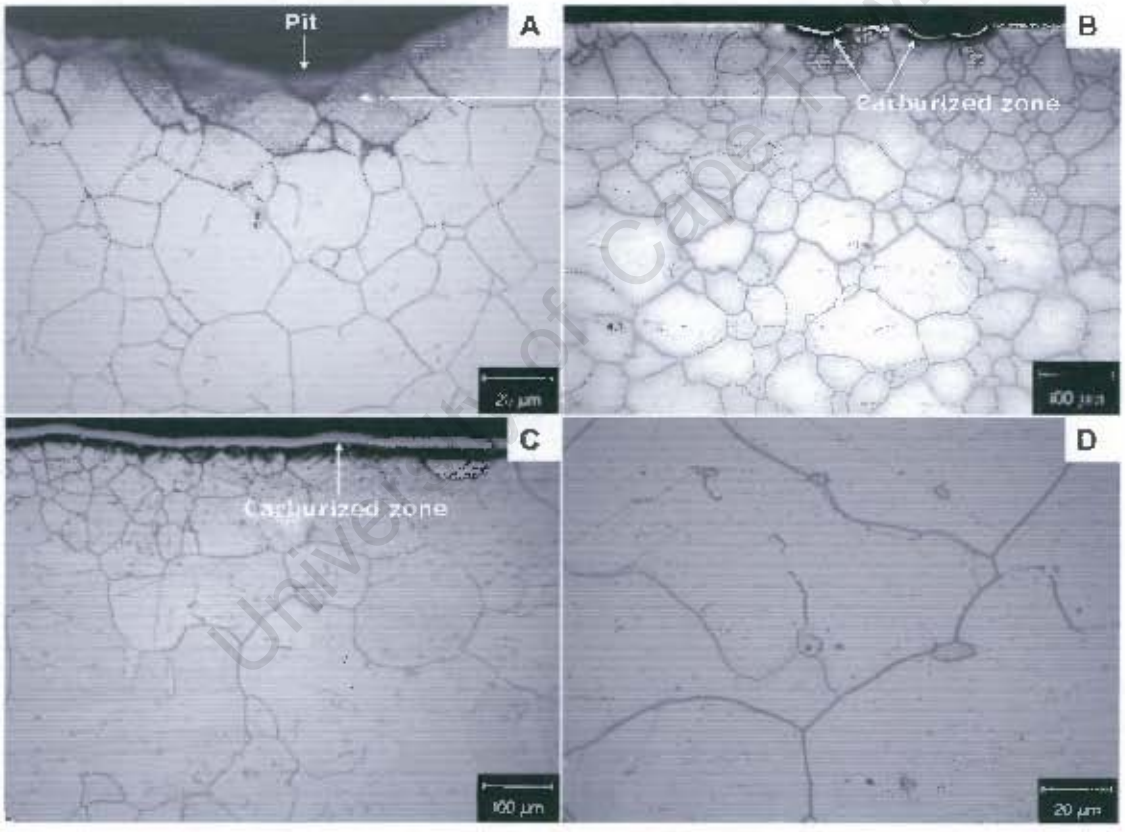

Figure 4.14: Microstructures showing a carburized zone and internal carburization: a) GR 309 (GRD), b) Alloy 601 (HT) and c-d) HR 120 (HT). The samples were electro-etched in oxalic acid which attacks carbides.

Precipitation of carbides occurs mainly along the grain boundaries and tends to take the shape of the grain boundaries whereas inclusions are often small dots or round shape. Thus it would not be difficult to differentiate between an inclusions and carbides.

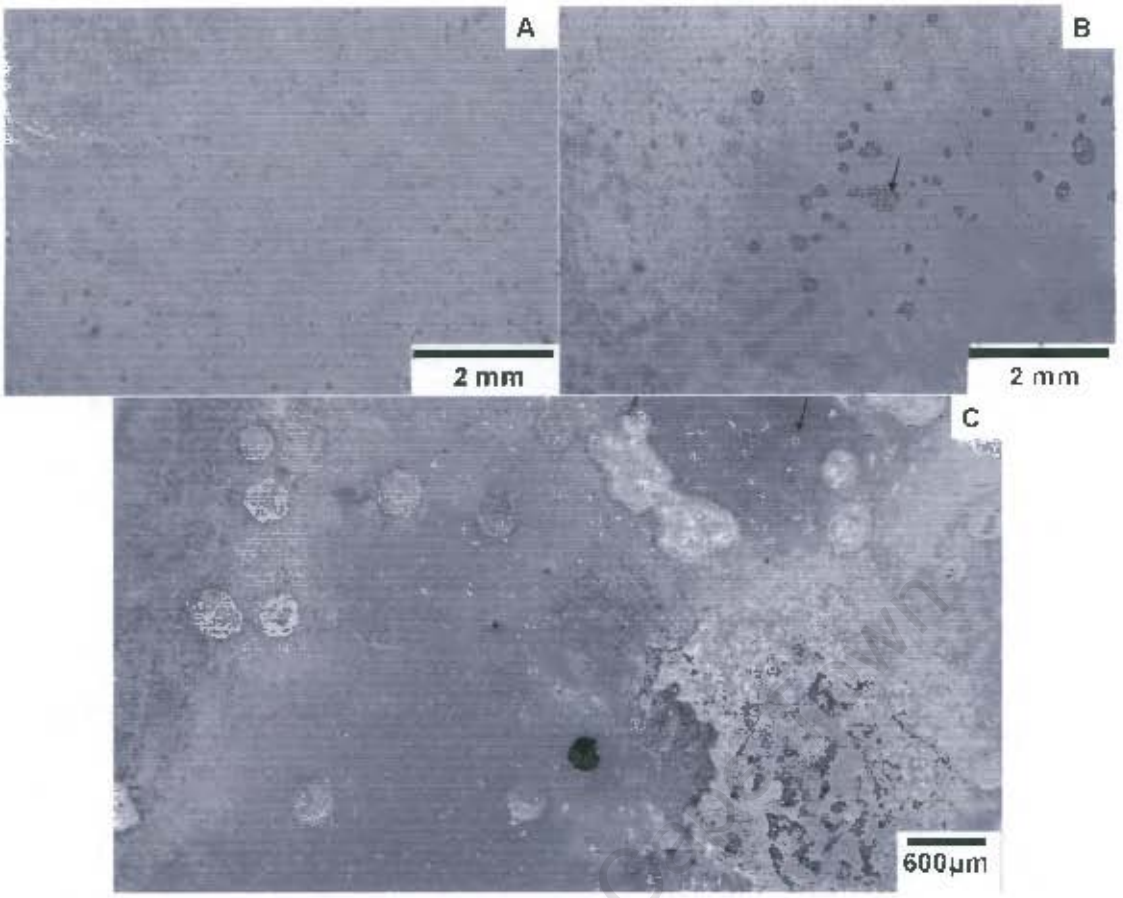

Figure 4.15: Pits on the surface of HR 160 (GRD) and GR 309 (GRD) after 268 hours of exposure at 500°C and Alloy 214 (GRD) after 500 hours at 650°C: a) HR 160 (GRD), b) GR 309 (GRD) and c) Alloy 214 (GRD).

Alloy 690 (ARD) suffered mild metal dusting since few pits were observed on its surface as shown in Figure 4.17a. The pits were very small. The pit marked by a circle is shown at a higher magnification. Secondary pits can be seen within primary pits as shown by an arrow in Figure 4.17b. EDS analysis inside the pits revealed that the pits had a higher chromium content (50.47 wt% Cr) compared to the sample surface (29.22 wt% Cr).

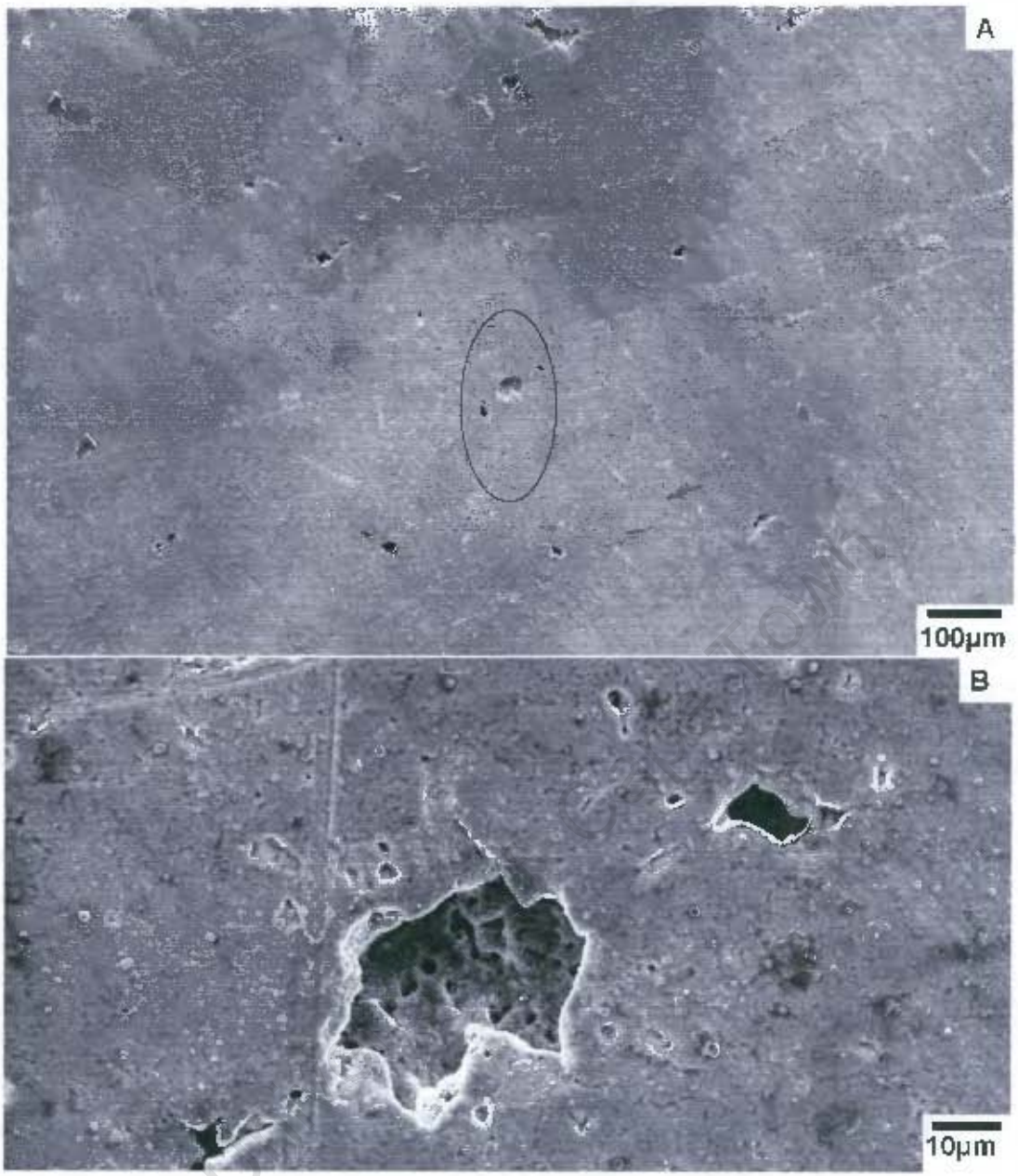

Figure 4.17: Local pitting of Alloy 690 (ARD) after 268 hours (11 days) at 500°C. Secondary pits within primary are evident.

Figure 4.18 shows the microstructure of HR 160 and Alloy 230 before exposure to metal dusting. The alloys were electro-etched in oxalic acid. The etchant attacks the carbides. HR 160 and Alloy 230 are austenitic structures with twin boundaries. . Alloy 230 has secondary intra-granular carbides. After exposure the grain boundaries were attacked and these micrographs have similar features with micrographs that were observed by other researchers in the literature who analysed the type of carbides

observed inside and along the grain boundaries in their samples. Hence these features were assumed to be carbides.

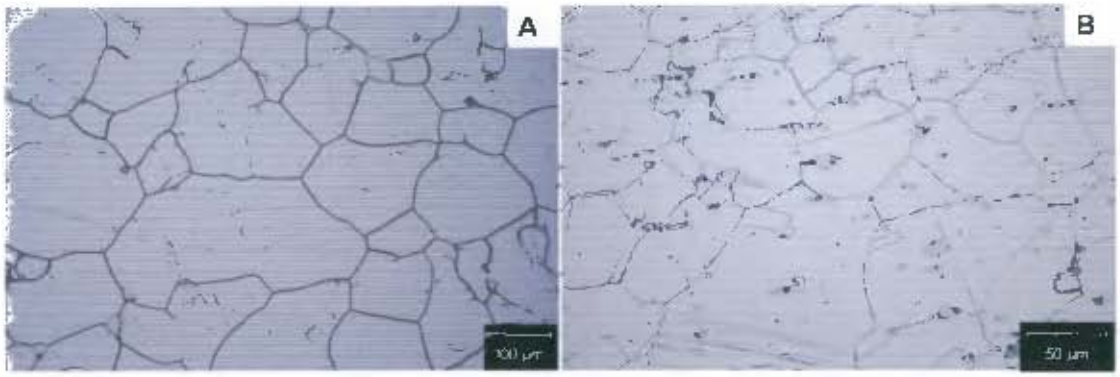

Figure 4.18: Microstructures of HR 160 and Alloy 230 before exposure to metal dusting: a) HR 160 and b) Alloy 230.

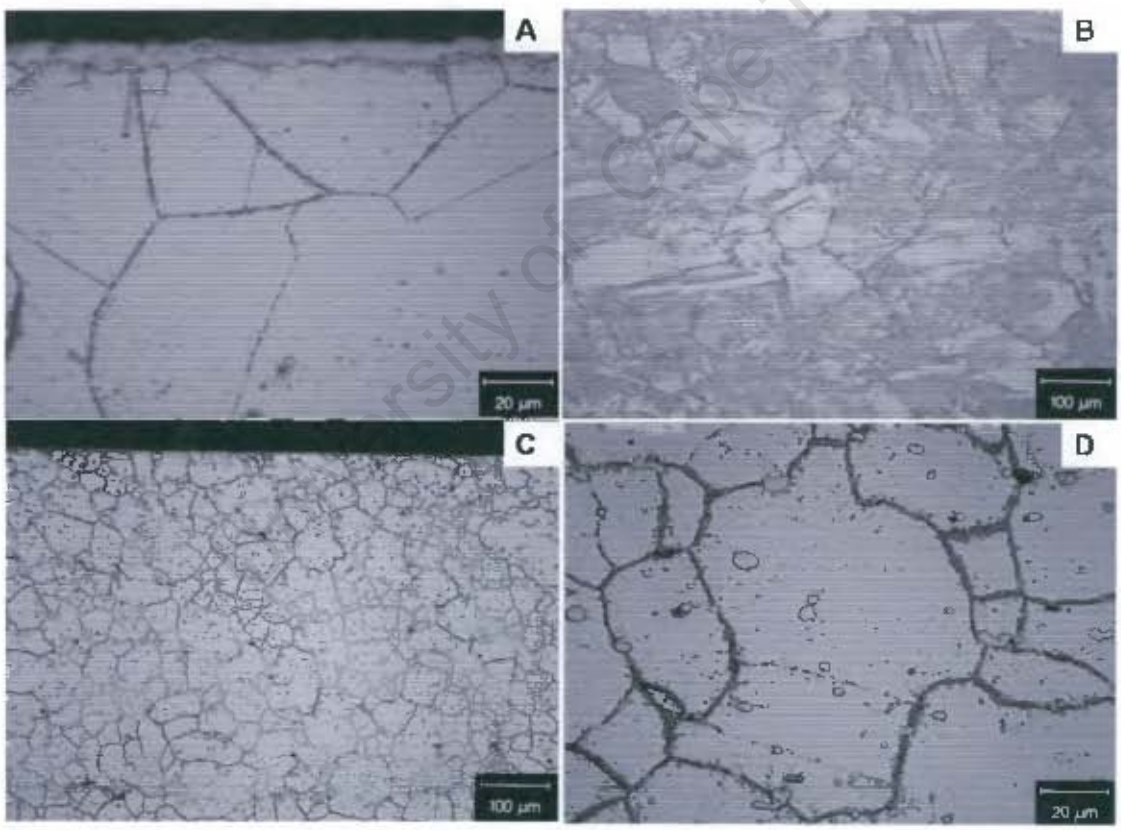

Figure 4.19: Microstructures of HR 160 (GRD) and Alloy 230 (GRD) shows no evidence of a carburized zone after 268 hours of exposure at 500°C. Intensive carbide precipitation: a) and b) HR 160 (GRD) and c) and d) Alloy 230 (GRD).

Figure 4.19 shows no evidence of carburized zone in both HR 160 (GRD) and Alloy 230 (GRD). Intensive carbide precipitation within the grains can be seen in HR 160 (GRD) as shown in Figures 4.19a-b. Intensive carbide precipitation within the grains and along the grains can be seen in Alloy 230 (GRD).

4.3.3 Absence of Metal Dusting Corrosion

HR 160 and Alloy 230 in both the as-received and ground conditions did not show any discernible metal dusting corrosion after 500 hours exposure to the gas CO-H_2-H_2O mixture at 650°C. Alloy 693 in both the as-received and heat-treated conditions also did not show any discernible metal dusting corrosion after 268 hours at 500°C, as shown Figure 4.20. In addition, Alloy 230 (GRD) and Alloy 690 (HT) showed no metal dusting after 268 hours at 500°C.

EDS analysis on the surface of Alloy 693 (ARD) revealed that the alloy surface had a nickel content of 54.7 wt% and a chromium content of 35.5 wt%. In contrast, Alloy 693 (HT) had a nickel content of 47.63 wt% and a chromium content of 40.6 wt%. The high chromium content on the surface of Alloy 693 suggests that a Cr_2O_3 film had been formed, since no metal dusting had been observed and in addition, it is believed Cr_2O_3 provides protection against metal dusting [6,11,17]. Furthermore, the microstructures also show little or no evidence of carburization since internal carburization and the carburized zone is absent as shown in Figures 4.20c-d.

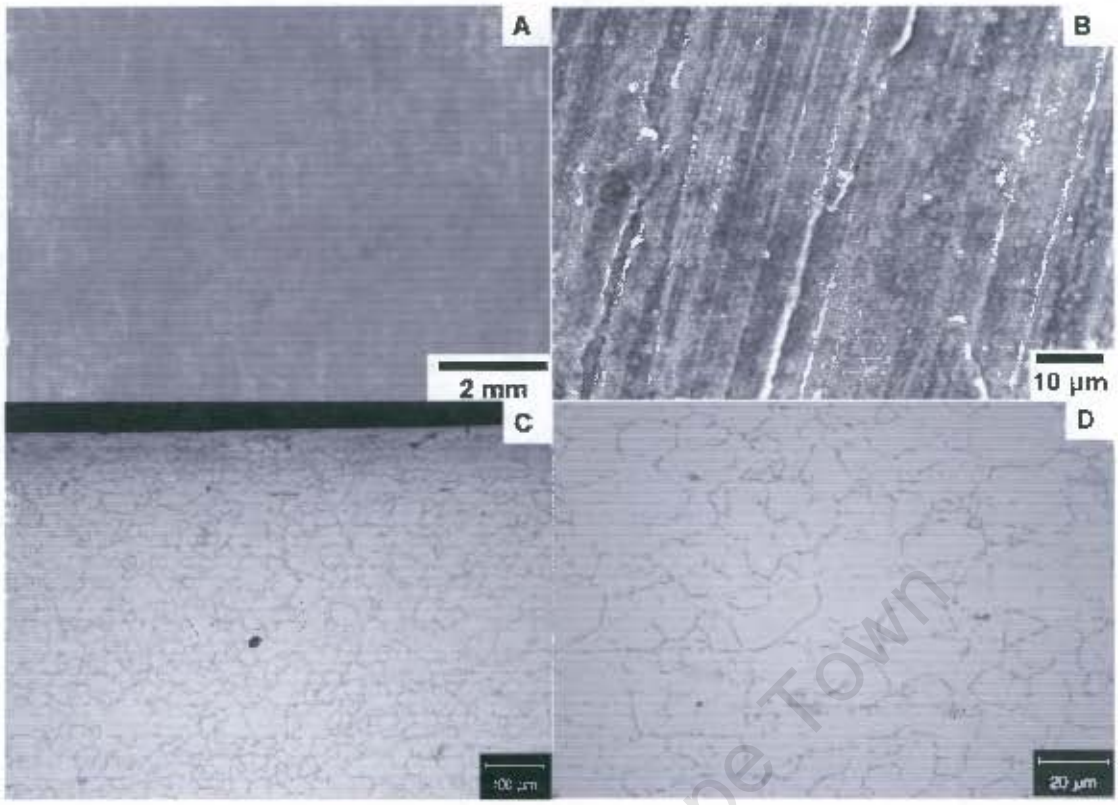

Figure 4.20: Alloy 693 showing no evidence of metal dusting after 268 hours exposure to the CO-H_2-H_2O gas mixture at 500°C: a) visual inspection, b) SEM surface , c) and d) microstructures of Alloy 693 (HT).

4.4 CHARACTERISTICS OF COKE DEPOSITS

Throughout the experiments, the characteristics of coke deposition did not differ that much. The most observed forms of coke were coke nodules, coke protrusions (cones) and carbon plates. The type of coke formed is not peculiar to a particular type of alloy. Coke protrusions were observed on 253 MA in both conditions when exposed at 500°C. The characteristics of coke protrusions are shown in Figure 4.21. They grew from the alloy surface and tend to bend as they grow. The longest length observed was about 2 mm. The protrusions tend to intertwine as they grew longer. After removal of the coke protrusions, deep localised pits were often observed. In contrast, after removal of coke plates, uniform wastage was often observed on the alloy surface.

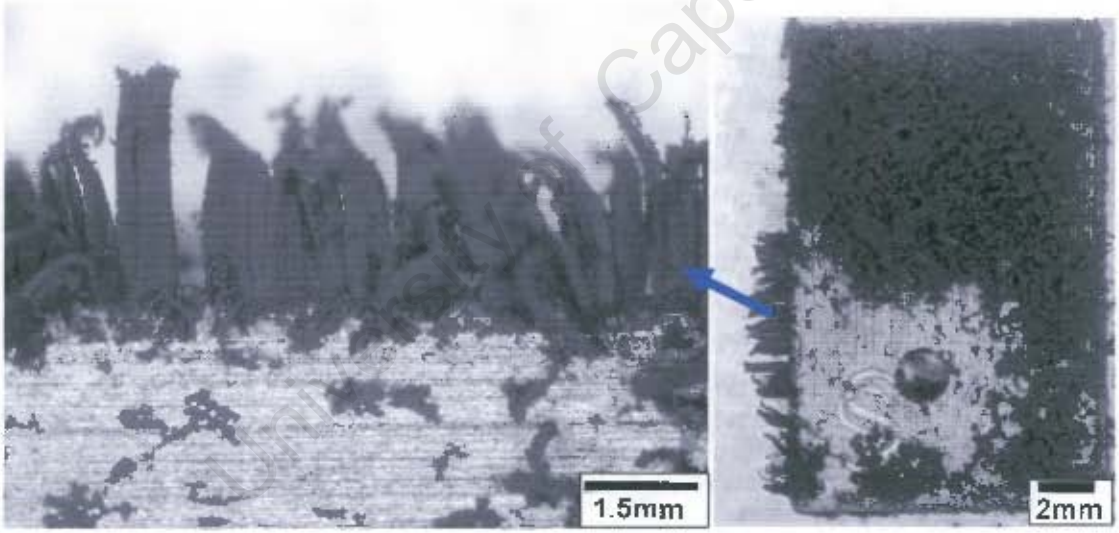

Figure 4.21: Growing coke protrusions on the sample surface of 253 MA at 500°C after 196 hours of exposure. The arrow points to the protrusions at higher magnification.

Coke nodules were observed on the surface of the ground Alloy 600 after exposure at 500°C for 72 hours, whereas carbon plates and protrusions are observed on this alloy in the as-received state. The nodules were randomly dispersed on the alloy surface as shown in Figure 4.22. After removal of the coke nodules, localised pits were often observed.

Generally, the amount of coke deposit on grounded alloys was small when compared to the as-received alloys. A multiplicity of carbon plates were observed mostly on the as-received alloys.

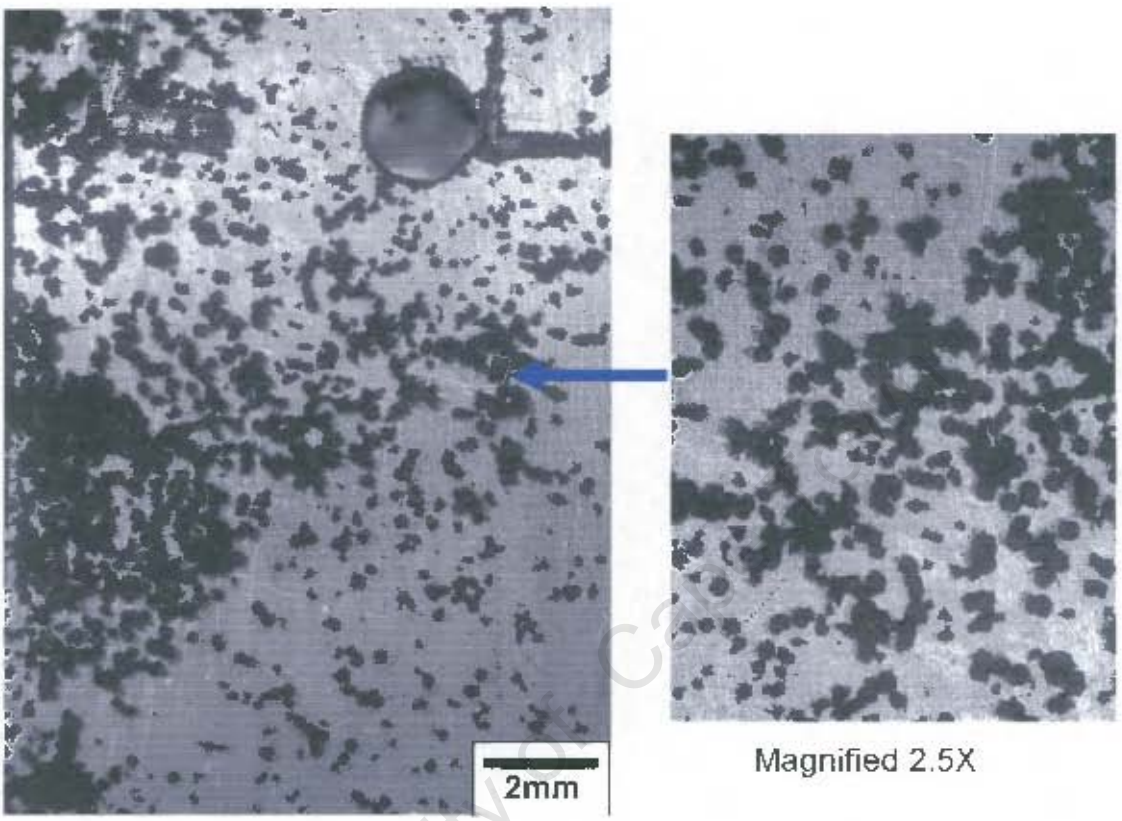

Figure 4.22: Coke nodules on the sample surface of Alloy 600 after exposure at 500°C for 72 hours.

Carbon plates seemed to form more often and rapidly at 500°C than at 650°C. Carbon plates observed on the sample surface of alloys GR 309 at 500°C after 196 hours, are shown in Figure 4.23. The measured thickness of these plates was in the range of 3 to 6 mm. The carbon plates consisted of graphite filaments and metal particles. The formation of metal particles in the coke resulted from the disintegration of the alloys due to metal dusting. The coke deposits were examined by SEM and were found to consist of tangled graphite filaments. A typical metal dusting coke consists of graphite and metallic particles. EDS analysis of coke revealed that it consists of 97.5-99.4 wt% C and other elements depending on the alloy composition, as shown in Figure 4.24.

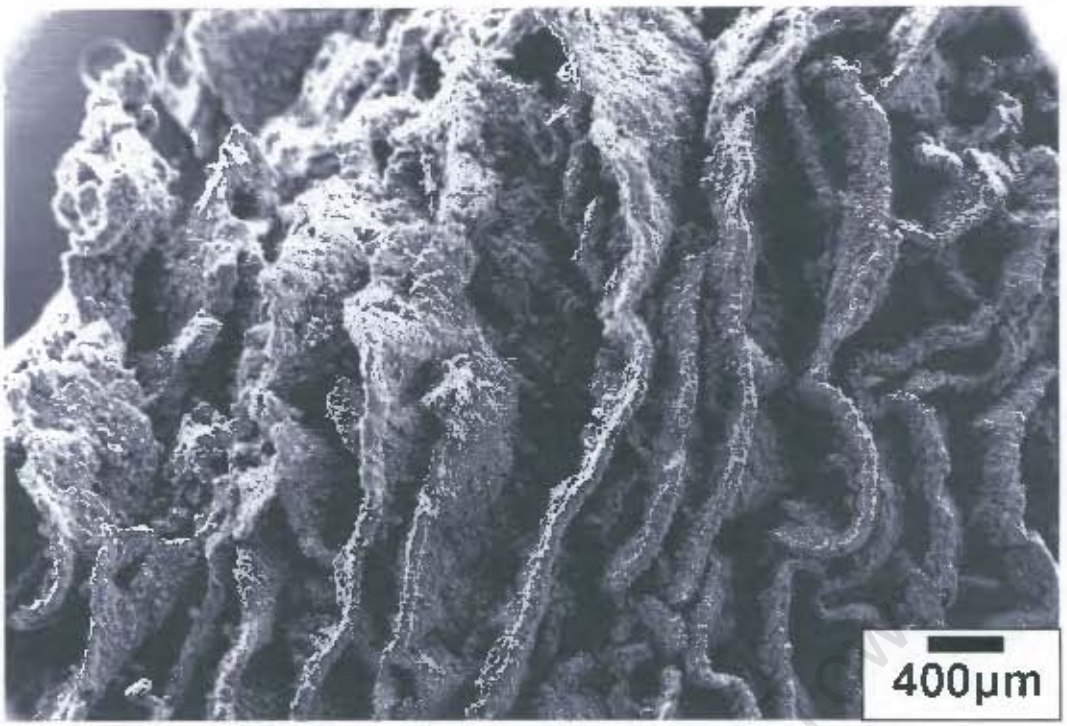

Figure 4.23: Carbon plates observed on GR 309 (ARD) after 196 hours exposure at 500°C in a CO-H_2-H_2O atmosphere.

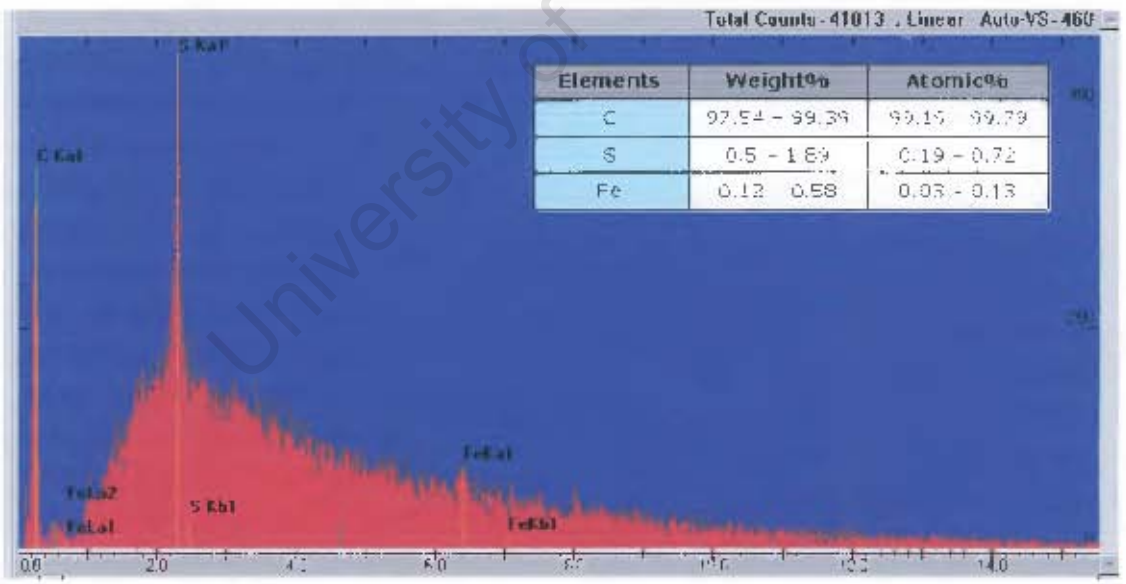

Figure 4.24: Typical EDS analysis of metal dusting coke. The table inset shows the range of elements found in the coke. Elements below 1% are deemed not accurate and hence sulphur and iron detection within the coke is not accurate.

The carbon plates were observed on most of the alloys with high iron content. Carbon plates grew on the surface of the high iron content HR 120 (HT). The carbon plates observed on HR 120 (HT) are shown in Figure 4.25. The plates (Figure 4.25a) are made up of tangled graphite filaments as shown in Figure 4.25b-c. Metallic particles can be seen at the tip and along the length of the filaments (Figure 4.25c). The small amount and size of the metallic particles in the coke limit the accuracy of the detection for elemental analysis due to the overwhelming coke matrix effect. However, the chemical composition of the particles embedded at the tip of graphite filaments were analysed by EDS attached to SEM. The particles are shown in Figure 4.25d. EDS spot analysis revealed that the particles were composed of 84.71 wt% C, 2.09 wt% Ni, and 12.59 wt% Fe, as shown in Figure 4.26.

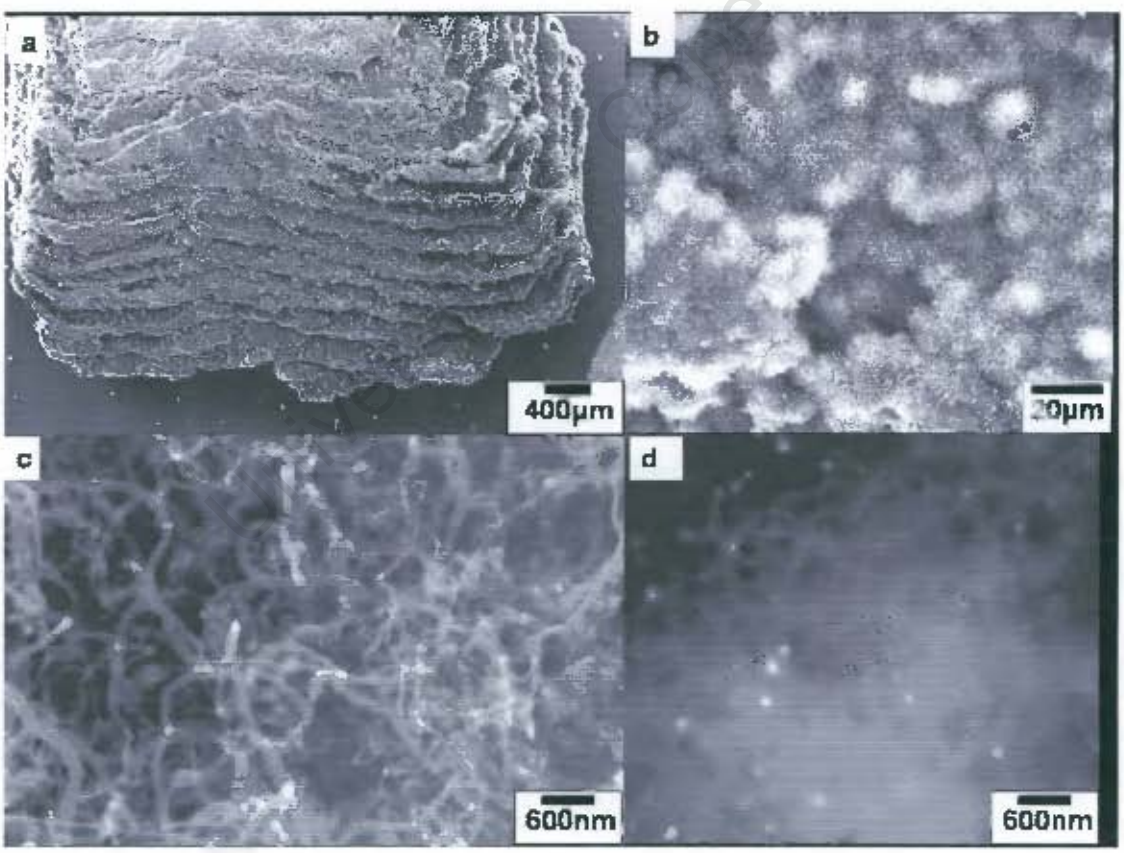

Figure 4.25: Carbon plates: a) multiple layers of carbon plates, b) filamentous graphite, c) filamentous graphite at higher magnification, and d) metal particles at the end of graphite filaments (Backscattered diffraction Images).

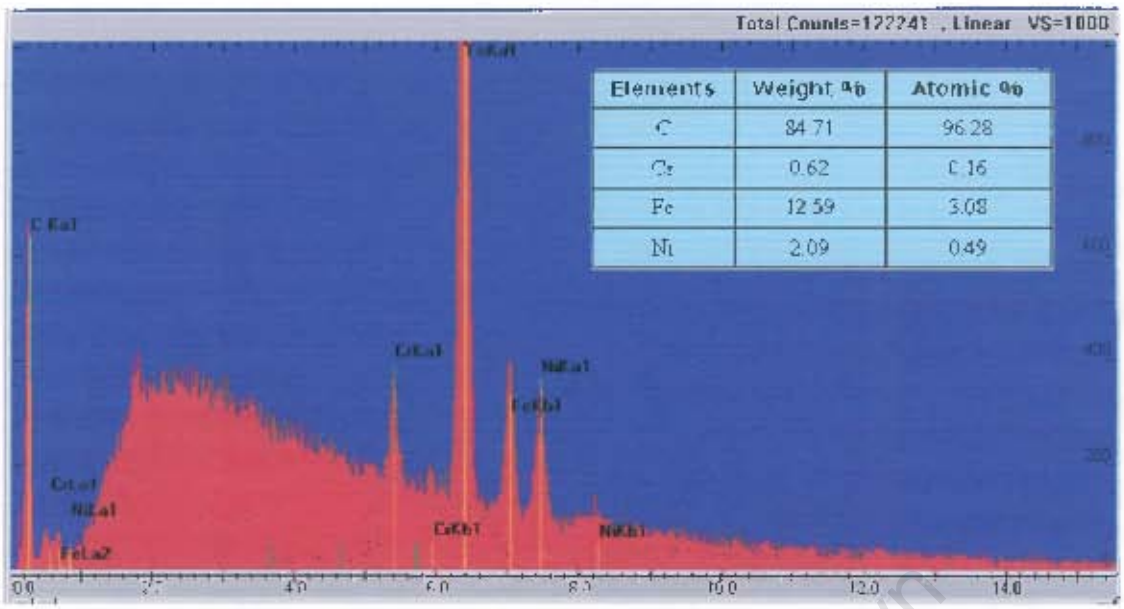

Figure 4.26: EDS spot analysis of metallic particles obtained from HR 120 (HT) coke. Elements below 1% are deemed not accurate and hence Cr detection within the coke is not accurate. The main elements are C, Fe and Ni.

4.5 HARDNESS MEASUREMENTS

The micro-hardness after exposure to a carburizing atmosphere was expected to be higher at the surface that in the bulk material. A typical micro-hardness profile after metal dusting exposure is shown in Figure 4.27a. The micro-hardness of the 253 MA before exposure and after exposure in both the as-received and ground conditions was plotted on the same graph. The load used was 100gf and the average value of between 6 to 9 indentations was recorded. The error bars indicate the scatter of values around the average value. In Figure 4.27, it can be seen that the micro-hardness value near the surface is higher for both the exposed as-received and ground conditions when compared to the unexposed 253 MA sample. In addition, the hardness is also higher near the surface as compared to the bulk material at about 2.5 mm from the surface.

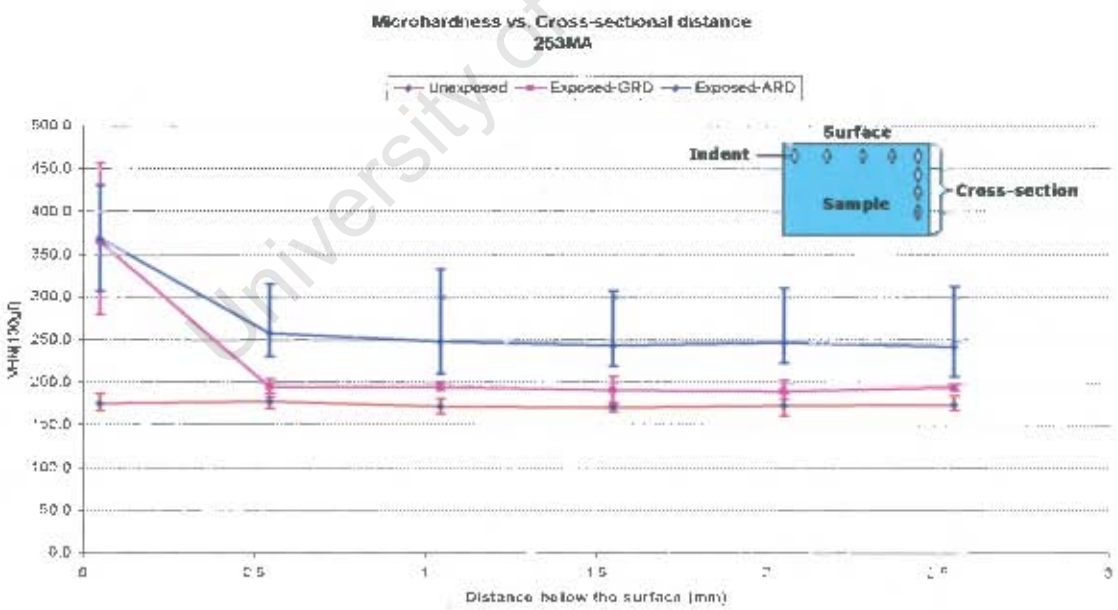

Figure 4.27a: Plots of measured hardness profile on the cross-section of exposed and unexposed Alloy 253 MA.

Since all other alloys showed similar micro-hardness profile patterns, only the micro-hardness near the surface (at a depth of about 45 μm) and in the bulk material (about 2.5 mm) are compared and presented. The density of carbide precipitation increases near the surface and then decreases with increasing distance below the surface. Most of the alloys that showed severe metal dusting at 650°C had the highest hardness near the surface due to carbide precipitation, dissolved carbon and a carburized zone near the surface (Figure 4.28). HR 160 and Alloy 230, which showed no metal dusting, had similar hardness values in the unexposed and exposed ground conditions. Similar hardness values were recorded for alloys 253MA, GR 309 and alloys 214 after exposure in both the as-received and ground conditions. In the bulk, the micro-hardness of alloys 253 MA, GR 309 and alloy 230 are higher after exposure than in the corresponding unexposed alloys (Figure 4.29). These alloys showed severe metal dusting or extensive carbide precipitation.

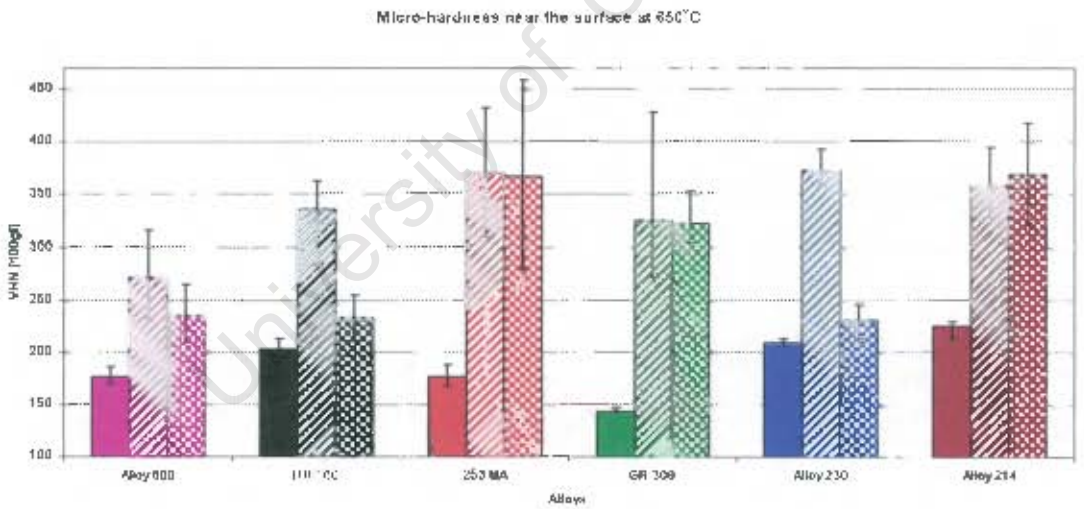

Figure 4.28: Vickers hardness near the surace for all exposed alloys at 650°C for 500 hours near the surface. Error bars represent the maximum and minimum values. Legend: solid = unexposed; stripes = as-received; chequered = ground surface.

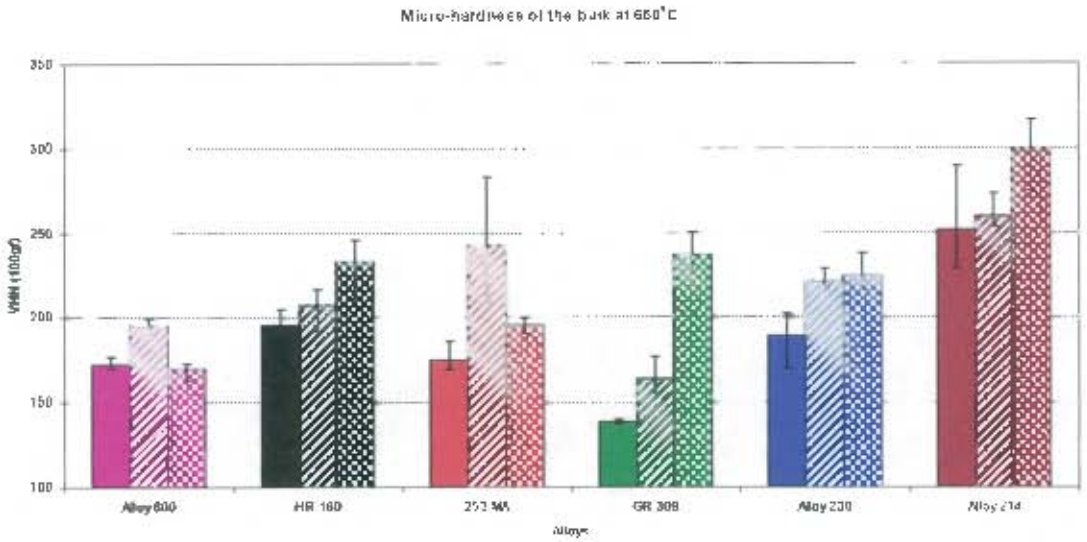

Figure 4.29: The bulk Vickers hardness for alloys exposed at 650°C for 500 hours. Legend: solid = unexposed; stripes = as-received; chequered = ground surface.

For the exposure experiments carried out at 500°C, all the alloys showed lower hardness values in both the as-received and with a ground surface when exposed to a CO-H_2-H_2O gas when compared to the tests performed at 650°C, for hardness indents taken near the surface and in the bulk (see Figures 4.30 and 4.31). The only exception appeared to be alloy 600, which had similar hardness values in the bulk after exposure for all three conditions as shown in Figure 4.31. Furthermore, whereas the hardness values in the near surface areas increased for all the alloys at 650°C, at 500°C the results showed that the alloys either increased, decreased or remained the same for the ground and as-received cases. These phenomena will be discussed on an individual alloy basis and depends on alloy content and test temperature. A closer examination of the data in Figure 4.30 reveals the hardness values were the same for alloys 600, 230 and HR 160. Alloys 253 MA and alloy 214 showed an increase in hardness of the exposed samples. Alloy GR 309 was somewhat of an anomaly because the as-received sample was much harder than the ground sample after exposure (Figure 4.30). The hardness values for all the alloys were either similar or lower in the bulk when compared to the near surface, at 500°C. If we examine the data in Figure 4.31 closely, it is

observed that the hardness values in the bulk at a depth of 2.5 mm are similar for the three different conditions. It does appear though that there are two anomalies. In alloy HR 160, the ground sample was lower than the unexposed sample, whereas the opposite was true for GR 309.

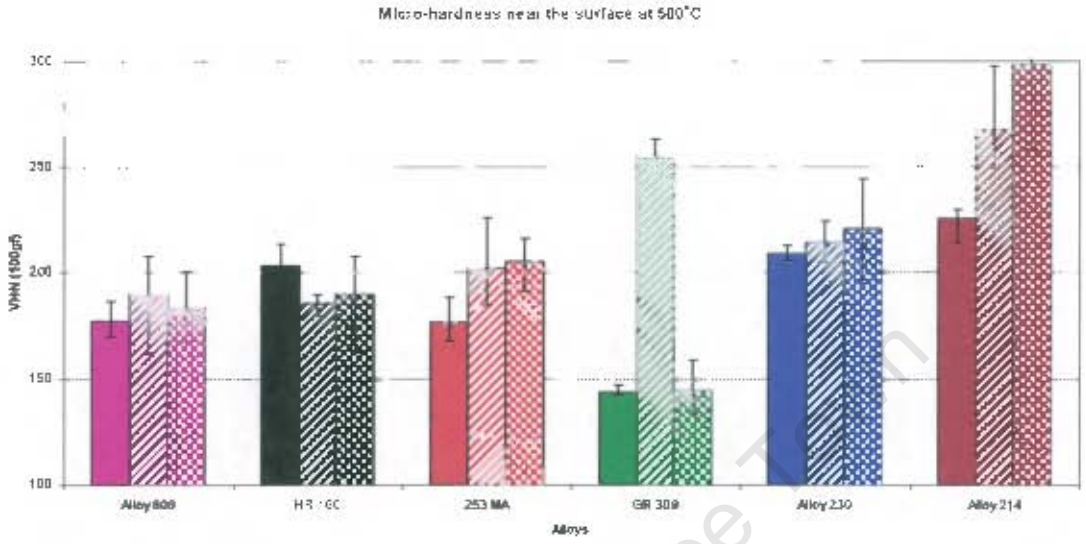

Figure 4.30: Vickers hardness near the surface for all exposed alloys at 500°C for 268 hours in the near the surface. Legend: solid = unexposed; stripes = as-received; chequered = ground surface.

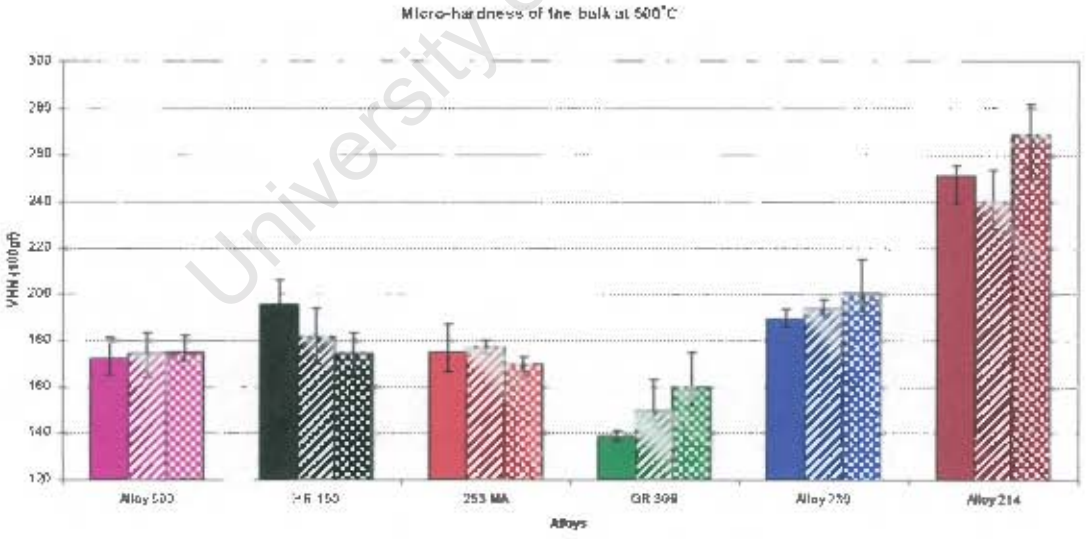

Figure 4.31: Vickers hardness in the bulk for all exposed alloys at 500°C for 268 hours in the bulk. Legend: solid = unexposed; stripes = as-received; chequered = ground surface.

In the exposure experiment C at 500°C, the hardness values for all the exposed alloys near the surface and in the bulk in both the as-received and heat-treated conditions were the same when compared to the corresponding unexposed alloys (Figures 4.32 and 4.33). Furthermore, the hardness for all the exposed alloys in as-received and heat-treated conditions near the surface showed higher or at least similar hardness values when compared to the bulk at a depth of 2.5 mm.

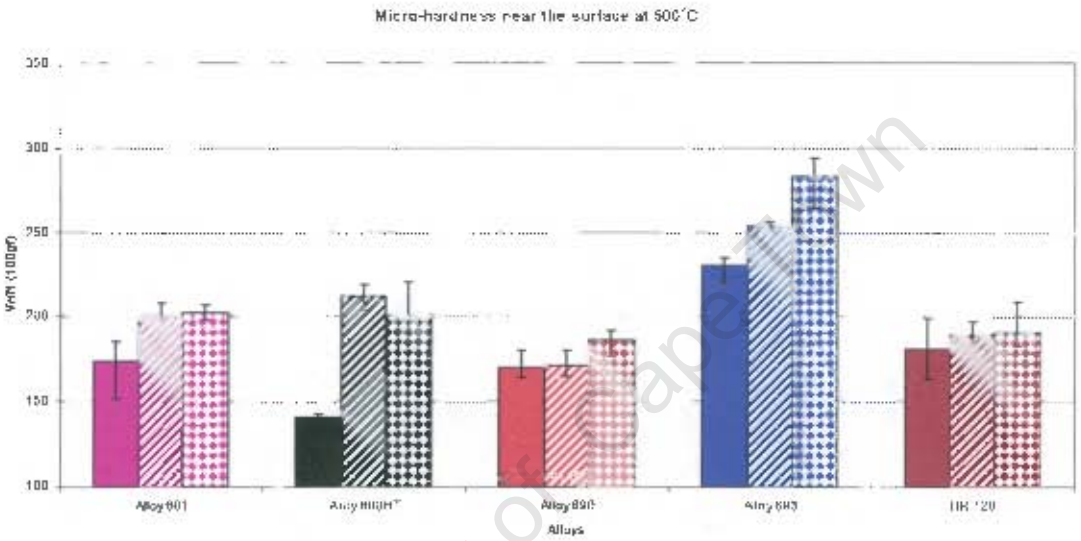

Figure 4.32: Vickers hardness near the surface for all exposed alloys at 500°C for 268 hours near the surface. Legend: solid = unexposed; stripes = as-received; diamonds = heat-treated.

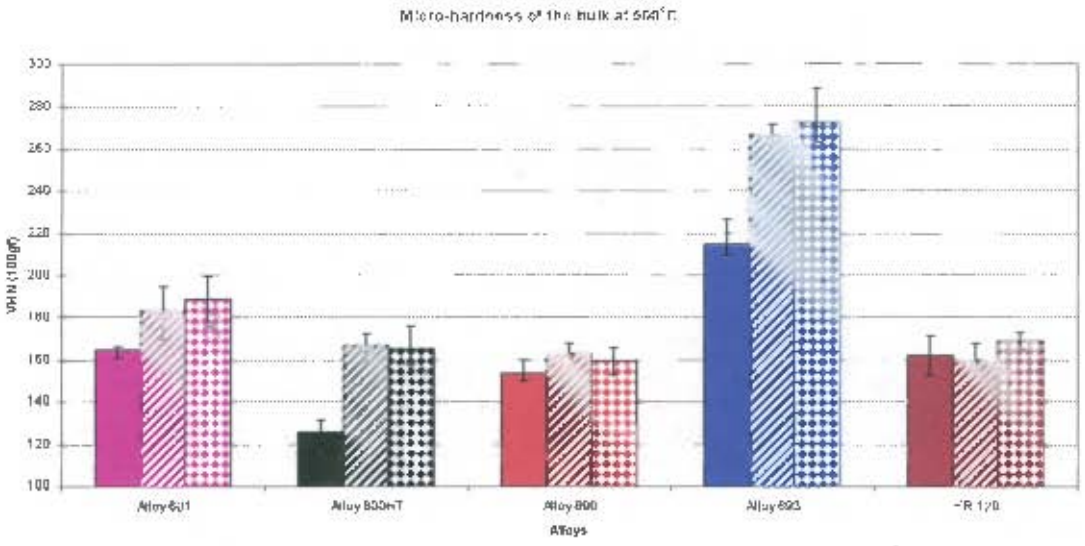

Figure 4.33: Vickers hardness in the bulk for all exposed alloys at 500°C for 268 hours in the bulk. Legend: solid = unexposed; stripes = as-received; diamonds = heat-treated.

4.6 REPRODUCIBITY TESTING

Reproducibility tests were conducted on three alloys and the results superimposed on the original tests for comparison as shown in Figure 4.34 and Figure 4.35. The duration of the reproducibility tests was taken for 196 hours. The shapes of the reproducibility graphs were similar to that of the original test for each of the three alloys that were examined. The measured percentage errors of mass loss after 196 hours for all selected alloys are shown in Table 4.4. The percentage errors for the reproducibility in Table 4.4 were found to be lower than 0.5%. Thus the experiments were deemed to be reproducible.

The samples were placed in specific positions inside the reaction chamber for the original tests at 500°C. The reproducibility tests were only conducted at 500°C. In this test the sample were placed in different positions. Since the results were then found to be similar, the position of the samples inside the reaction chamber did not affect the deposition of carbon.

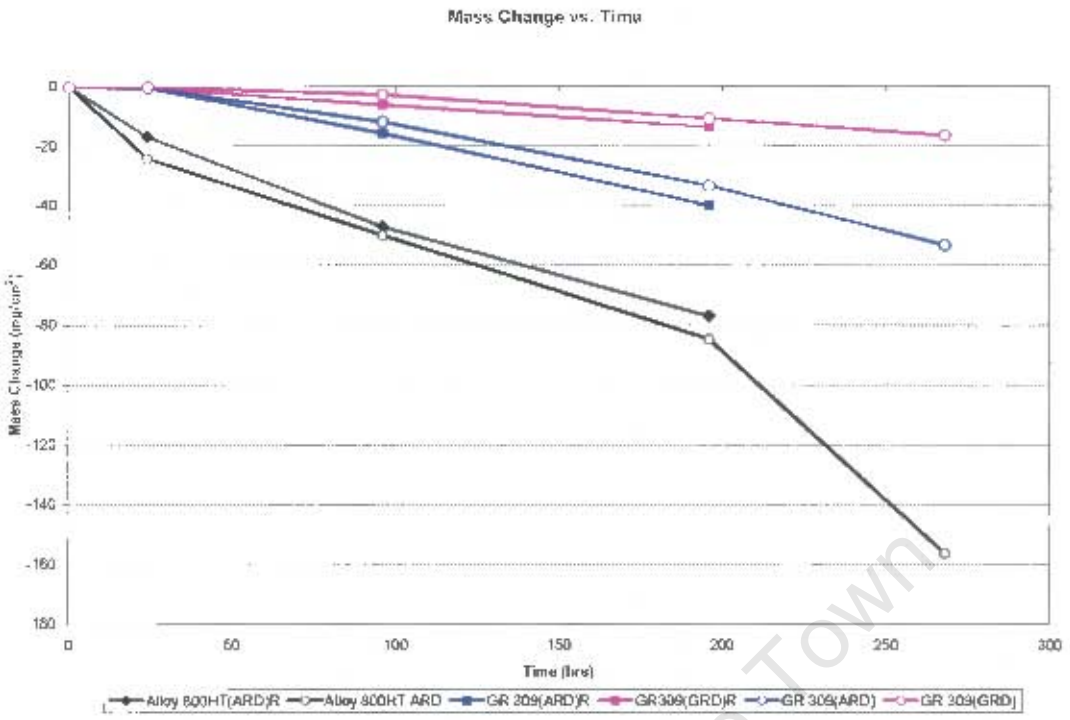

Figure 4.34: Mass change vs. time for reproducibility of selected alloys imposed on the first test at 500°C for 196 hours. Square points = Reproducibility test and Open circle = First test.

Figure 4.35 : Mass change vs. time for reproducibility of selected alloys imposed on the first test at 500°C for 196 hours. Square points = Reproducibility test and Open circle = First test.

Table 4.2: Percentage error of the selected alloys after 196 hours of exposure in CO-H_2O-H_2 environment at 500°C.

Alloys	First Test % mass loss after 196hrs	Reproducibility % mass loss after 196hrs	Δ%
800HT(ARD)	4.4	4.0	0.4
HR 120(ARD)	0.2	0.3	0.1
HR 120(HT)	0.9	1.2	0.3
GR 309(ARD)	1.7	2.0	0.3
GR309(GRD)	0.5	0.7	0.2

CHAPTER FIVE

DISCUSSION

From the results presented, it is apparent that the resistance of the alloys to metal dusting depends on the alloy's ability to form a protective chromium scale and to replenish it continuously. Metal dusting, which is the disintegration of the substrate into fine particles of carbon and metal, was induced on a selection of alloys containing various levels of chrome, iron and nickel at temperatures of between 500°C and 650°C in a flowing CO-H_2-H_2O atmosphere. The resistance of alloys to metal dusting is affected by the alloy composition, its surface properties, the temperature and the carbon activity of the environment [11, 13, 33, 37, 41, 54]. The results presented here, compares well with work done by other researchers on iron and nickel-based alloys. It was shown that metal dusting can successfully be simulated in the laboratory in a rig that was refurbished as part of this project. In addition, the rate of the sample mass loss of each alloy type was consistent and the corrosion products "coke" further attest that the rig is able to produce a consistent severe metal dusting environment. The rig is capable of operating uninterrupted for a week of simulation.

5.1 EFFECT OF INDIVIDUAL ALLOYING ELEMENTS AND SURFACE FINISH

The competition between the oxidation process to form a protective continuous oxide scale such as aluminium dioxide (Al_2O_3), silicon dioxide (SiO_2), and chromium oxide (Cr_2O_3) on a given alloy surface and carburization will determine the onset for metal dusting attack. In order

for the oxidation to prevail, the selective oxidation oxide forming elements and formation of an oxide scale should be enhanced. The formation of an oxide scale is affected by the level of the oxide forming elements and the diffusion path available. In principle, chromia should be selectively oxidized from the alloy to form a Cr_2O_3 external scale to prevent the ingress of carbon into the alloy and subsequent internal precipitation of carbides and super saturation of the alloy matrix by carbon. The growth of the Cr_2O_3 scale was enhanced by fast diffusion paths that were introduced by grinding the alloy surfaces. However, whether metal dusting is going to occur, depends on defects in the oxide scale and whether the oxide scale is repaired before nucleation of graphite. The repair of the oxide scale depends on the level of the oxide forming elements. These factors are discussed below in relation to the metal dusting tests carried out between temperatures of 500°C and 650°C.

5.1.1 Alloy Exposures at 650°C (Experiment A)

Most of the alloys in as-received (ARD) condition showed severe metal dusting and rapid and significant mass loss during the exposure period. The high nickel content alloys, Alloy 600 and Alloy 214, in particular, were strongly attacked. These alloys had high nickel contents of above 70%. An alloy containing a high nickel content is said to provide better resistance to carburization since the carbon solubility and diffusivity decreases with increasing Ni-content [6]. Their poor behaviour is attributed to the fact that they had relatively low chrome levels of about 15%. The Cr content of these alloys was considered to be too low to form a protective continuous oxide scale. The Cr:Ni ratio increased from about 0.24 to 0.48 (*i.e.* doubled) from the bulk to within the pits, indicating the level of migration of chrome during the exposure time. Alloying additions of aluminium and silicon is said to enhance the resistance to metal dusting. It is interesting to note that even though Alloy 214 had a relatively high aluminium content of about 6 wt %, and thus the ability to form an Al_2O_3 scale, it still suffered severe attack.

A lack of elements such as tungsten and molybdenum in both Alloy 600 and Alloy 214 resulted in the Cr being tied up in chromium rich carbides such as $M_{23}C_6$, M_3C_2, and M_7C_3. Hence the formed chromium rich carbides lead to the depletion of Cr in the alloy matrix. The depletion of Cr reduced the capability of the alloy to form a protective oxide scale to suppress the diffusion of carbon into the alloy. Tungsten and molybdenum are strong carbides formers and would form carbides with carbon instead of only Cr forming carbides. The improved resistance of the ground *vs.* the as-received alloys can be attributed fact that surface grinding of these alloys increases the diffusion paths in the alloys for Cr to form a protective oxide scale.

Alloys 253 MA and GR 309 have nickel contents of about 11-12%. These two alloys also exhibited severe metal dusting in both the as-received and ground conditions. This poor resistance can be attributed to their high iron contents of about 65% which increased the solubility and diffusivity of carbon. These two alloys did, however, perform better than the two high nickel-content alloys discussed above, and this can attributed to their higher Cr contents of about 18% and 21% for 253 MA and GR 309, respectively. Previous research has found that high Cr ferritic steels are very resistant whereas ferritic steels with 12-13% Cr were less resistant [11]. These alloys are austenitic steels which have lower diffusivities than ferritic steels and thus are expected to have low Cr diffusion rates [8].

HR 160 and Alloy 230 showed much greater resistance to metal dusting especially when they were ground. This resistance can be attributed to the high levels of nickel and chrome coupled with a low iron content ($\approx$ 2%). The better resistance of the ground alloys is due to an increased density of dislocations in the alloy subsurface regions. This enhanced the Cr diffusion and hence the formation of a continuous Cr_2O_3 scale. Since the iron content was very low, the diffusion rate of carbon was significantly reduced and unstable cementite was not going to be formed. The presence of Si (1.32 wt %) and high Co (32.6 wt %) as carbide formers in HR 160 improved the metal dusting resistance. Cr in

conjunction with Si formed a protective oxide scale to protect the alloy. Consequently Cr was not tied up in $M_{23}C_6$, M_3C_2, and M_7C_3 carbides. The excellent resistance of Alloy 230 can be attributed to the presence of a strong carbide former, tungsten. It had a high W (17.23 wt %) content which formed carbides with carbon and Cr was spared. Without this element, only Cr-rich carbides would form. Cr_2O_3 was formed otherwise the alloy could have suffered metal dusting attack. In addition, it had a very low Fe (1.91 wt %) content. Hence carbon solubility and diffusivity was reduced. Generally, the rate of mass loss or wastage was high for all alloys with high a Fe content and low Cr content.

The metallographic cross-sections of the alloys which were severely attacked by metal dusting showed an internally carburized zone and intensive grain boundary attack extending beneath the carburized zone. Internal carbide precipitation happened as result of the failure of an oxide scale to provide a barrier against carbon ingress. Failure of an oxide scale was due to an insufficient supply of Cr to maintain the oxide scale. In addition, carbon may gain access to the alloy surface where the oxide has failed due to inclusions or defects.

The micro-hardness near the surface in the alloys which were severely attacked by metal dusting was very high. In contrast, the hardness values at a distance of about 0.5 mm from the first indent near the surface were found to be much lower and seemed to remain at this level. Further into the alloy cross-section, the hardness values were fluctuating but were not close to the hardness values observed near the surface. The high micro-hardness values measured near the surface are attributed to the carbide precipitation and growth. The process of carbide precipitation and growth occurs as carbon diffuses into the alloys. Thus the average distance between carbides and their sizes increases as the distance from the surface increases. Hardness is a measure of the resistance to deformation when a loaded indenter is forced to penetrate the surface of the alloy during the test. The penetration of the indenter leads to a local deformation which is both plastic and elastic. Since deformation is due to

the motion of dislocations, grain boundaries, carbides within the grains and along the grains would impede the movement of dislocations. Consequently the restriction of the dislocation motion makes the material stronger. Hence the hardness increases. The metallographic cross-section of HR 160 in the as-received condition showed a carburized zone just below the surface whereas no carburized zone was observed for the ground condition. This resulted in a higher hardness for the as-received material. Metal dusting pits observed in these exposure series had often coalesced to form wide irregular pits. At the bottom of the pit, tiny loose metallic particles were often observed. Secondary pits were often observed within the primary pits. Consequently, the pits grew faster and deeper. This suggests, that once the metal dusting process has begun, it will continue until the material is removed from the corrosive environment. The tiny particles also suggests that after disintegration of the metal matrix, carbon continues to dissolve in the small metal fragments and the subsequent nucleation of graphite leads the disintegration of the metal fragments to even smaller fragments. This process seems continues until carbon cannot be dissolved in the tiny fragments.

5.1.2 Alloy Exposures at 500°C (Experiment B and C)

At 500°C all the alloys showed a shorter incubation period prior to metal dusting when compared to experiments conducted at 650°C. Only the ground alloys of HR 160 and Alloy 230 showed good resistance. This phenomenon can be attributed to the relatively good combination of chrome and nickel and low iron content in addition to carbide formers such as cobalt and tungsten and oxide formers such as silicon and aluminium. The ground surface increased their diffusivity path by cold work which provided a high vacancy concentration where the lattice is more open and substitutional diffusion is enhanced. The increased rapid diffusion paths have a small effect on the ingress of carbon since there was already a high probability of empty neighbouring interstitial sites to move through the alloys.

As shown in section 4.3, all alloys that had a carburized zone and intensive carbide precipitation had suffered severe to mild metal dusting attack. Alloys which did not have a carburized zone suffered mild or no attack, as was observed at 650°C. The micro-hardness near the surface was high for alloys with a carburized zone. The high hardness values proved that carbon was supersaturated near the surface and there was a precipitation hardening process due to carbide precipitation and growth. The micro-hardness values of all the alloys were lower in the experiments conducted at 500°C compared to those conducted at 650°C. This was attributed to temperature and exposure time and hence a decreased concentration of carbides due to the faster diffusion of carbon at higher temperature.

The values of the partial pressure of oxygen were much higher than the values of the equilibrium oxygen partial pressure at 650°C and 500°C. Hence the alloys were oxidized. However, the value of the partial pressure of oxygen at 500°C was very low when compared to the value of the partial pressure of oxygen at 650°C. Thus the oxidation process at 650°C was more rapid than at 500°C. Consequently, the oxide film was not formed rapidly to protect the alloy against carbon ingress and hence the alloys were attacked within a short period when compared to alloys at 650°C.

Most of the pits had coalesced to form wide irregular pits. The pits developed from where the oxide scale had failed. It seems that the area where the oxide had failed was never repaired because of insufficient and slow supply of Cr to form a protective scale. Thus the deposition of carbon and super saturation of the alloy matrix process superseded the oxidation process. The metal dusting process continued inside the pits and consequently the pits coalesced.

Szakalos *et al* suggested that there is seldom only one metal dusting mechanism operating on steels or nickel-based alloys [25,42]. As

described in literature in Chapter Two, there are four types of metal dusting mechanisms. The metallic particles observed at the bottom of the pits and coalescing of pits suggested that the metal dusting did continue inside the pits. Thus it is likely that more than one metal dusting mechanism had occurred. Alloy 600, Alloy 230, and Alloy 214 are nickel-based alloys and loose metallic particles were observed inside their pits. These metallic particles had high contents of nickel (73 – 92 wt %) and very low content of other elements. The metallic particles observed at the bottom of the pits may have formed as a result of the continuous fragmentation of nickel particles by graphitization. This phenomenon suggests that Type IV- mechanism may have been involved, although the Type IV- mechanism does not occur alone.

One of the two types of metal dusting mechanisms such as Type II and III could have started the process of dusting. Since Alloy 600, Alloy 230 and Alloy 214 are nickel-based alloys, it is likely that Type II- mechanism has occurred. Type II involves the disintegration of the carbon super saturated phase by internal graphitization. Inside the pits on the sample surface of HR 160 (ARD), the Cr level was higher than at the unaffected surface, suggesting that the products within the pits could have been made up of Cr-carbides or/and oxide. Thus it is likely that Type II and III occurred at same time. The HR 160 (GRD) surface had a higher Cr content than in the pits, suggesting that the Cr_2O_3 was protecting the alloy. Thus HR 160 (GRD) had a better resistance to metal dusting than other alloys except Alloy 230 (GRD).

GR 309 (ARD) and 253 (ARD) had suffered severe metal dusting and severe grain boundary attack. It is well known that austenitic steels are susceptible to inter-granular corrosion at temperatures of between 425-815°C and Cr-carbides (mainly $Cr_{23}C_6$) precipitates at the grain boundaries, depleting the grain boundary and nearby structures of Cr. Cr reacts with carbon within the steel matrix to form $Cr_{23}C_6$. The formation of $Cr_{23}C_6$ may have occurred when the steels were heated to the test temperature at 500°C in each cycle during the exposure.

Precipitation of carbides at the grain boundaries impedes the outward diffusion of Cr to the surface to form a Cr_2O_3 scale since the diffusion of Cr is slower in the bulk material than at the grain boundaries. An unlimited influx of carbon from the environment precipitated more carbide. Hence more Cr is tied up in the carbides and the depletion increases at the grain boundaries. T his severe metal dusting and grain boundary attack was observed by Maier *et al* on Type 304 after 180 hours [9]. The type of meat dusting mechanism that have occurred on GR 309 and 253 MA was Type I, whereby the formation and decomposition of metastable cementite leads to the disintegration of the alloy into metallic iron particles and graphite.

High nickel-contents are ideal since the carbon solubility and diffusivity decreases with increasing Ni-content. However, Grabke *et al* found that alloys with about 30 wt % Ni were attacked more rapidly and effectively than alloys with 20 wt % Ni [54]. In this study, Alloys 601, 800HT, 690, 693, and HR 120 had much higher mass losses for the all alloys than in experiments A and B. The rapid mass loss of Alloys 800HT and HR 120 can be attributed to their low Cr-content. A low Cr-content was not sufficient to rapidly form and repair the oxide film against carbon which lead to metal dusting attack. In addition, the mass loss can be attributed to the fact that they were severely attacked by metal dusting (pitting).

Metallographic cross-sections attested that metal dusting had occurred in Alloy 800HT and HR120 since carburized zone and intensive carbide precipitation were observed below the pits. Alloy 800HT (ARD) suffered uniform wastage. Alloy 800HT (HT) suffered both uniform wastage and local pitting. The onset of metal dusting is rapid for alloys with high Fe-content and relatively low Cr-contents. The type of metal dusting mechanism that occurred in Alloys 800HT and HR 120 is likely to be Type I, since they were iron-based alloys. Alloy 601 showed better resistance to metal dusting than Alloy 800HT despite having the same Cr-content. A high nickel-content, low iron content, and a relatively high aluminium

proved to be beneficial for the resistance of metal dusting of Alloy 601. It has been shown before that Cr in conjunction with a relatively high aluminium content enhances the metal dusting resistance of alloys [33].

The rapid mass loss of Alloy 690 (ARD) can be attributed to the small pits observed on its surface and low Cr (17.2 wt %). Low Cr contents lead to oxide spallation. In contrast, Alloy 690 (HT) also lost mass rapidly but did not suffer any discernible metal dusting attack. Alloy 693 (ARD) and Alloy 693 (HT) showed greater resistance to metal dusting. This is attributed to the high Cr (29.68 wt %) in conjunction with a relatively high Al (1.45 wt %) content. In addition, the resistance was enhanced due to the very low solubility of carbon in Ni (68.9 wt %) and low Fe (4.3 wt %) content. The metallographic cross-sections showed negligible carburization. This means that the protective oxide scale was formed. High Cr (29.68 wt %) was enough to resist excessive oxidation. Despite its high Cr content, oxide scale spallation is likely to have caused high mass loss.

Comparing the heat treated alloys with the alloys that were not heat treated showed no general consistent pattern. Only HR 120 (ARD) and HR 120 (HT) showed a consistent pattern, HR 120 (ARD) performed better than HR 120 (HT). After heat treatment, the grain size of all alloys did not change. This implies that the heat treatment temperature (850°C) was below the recrystallization temperature of the alloys. The only consistent pattern observed was that alloys with more than 60% wt of nickel showed negligible mass loss for 196 hours and suddenly lost significant mass in the last 72 hours of the exposure.

Mass loss can only be caused by disintegration of the alloys or excessive oxidation. Since disintegration of the alloy was not observed in Alloy 690 (ARD) and Alloy 693 in both conditions (heat treated and as-received), it is possible that oxide spallation occurred rapidly after 196 hours and is therefore responsible for mass loss. From this limited exposure series, the influence of heat treatment at 850°C prior to metal dusting is not evident, even though where direct comparison have been possible, there

was some evidence that metal dusting can be more severe, especially for alloys with more than 30 wt % of Fe. It is suggested that more experiments should be conducted to investigate the effect of heat treatment prior to metal dusting exposure and that the heat treatments should not induce grain refinement or growth.

5.2 EFFECTS OF TEMPERATURE AND CARBON ACTIVITY OF THE ATMOSPHERE

In the second exposure series at 500°C, all the alloys were attacked after a shorter time than at 650°C. Carbon deposits and plates grew on the sample surface more rapidly than at 650°C, except for alloys HR 160 and Alloy 230. Rapid mass loss occurred after 4 days of exposure. Nishiyama *et al* suggested that the carbon activity (a_C) and oxygen potential (P_{O_2}) must be considered as an index to represent the metal dusting propensity in the gas atmosphere [16]. In addition, the P_{O_2} has an influence on the formation of the Cr_2O_3 scale which provides protection against metal dusting. The a_C and P_{O_2} at 650°C was 16 and 5.05 $x10^{-26}$ atm, respectively, whereas the a_C and P_{O_2} at 500°C was 500 and 1.96 $x10^{-31}$ atm, respectively. The a_C at 500°C was about thirty times more and the P_{O_2} was five orders of magnitude less than at 650°C. This resulted in graphite forming within a shorter time and the oxide formation was negatively affected by a very low oxygen potential pressure. The oxide forming elements could not be oxidized readily due to the lower oxygen potential. Subsequently, the formation of the protective oxide scale was compromised.

In addition to the factors that accelerated the attack at 500°C, at lower temperatures, the diffusion coefficient of Cr is lower. Two diffusion processes takes place during metal dusting exposure. Firstly, the diffusion of carbon into the alloy to precipitate carbides and possibly to supersaturate the alloy matrix. Secondly, the diffusion of Cr to the

surface to form a protective oxide scale. Cr is a substitutional solute atom, requiring the presence of vacancies for diffusion and carbon is an interstitial solute atom and requires interstitial sites for diffusion. Thus at low temperatures, the diffusion coefficient of Cr is low and cannot be supplied rapidly to the surface to protect the alloy with Cr_2O_3. However, the diffusion of carbon is insignificantly affected by low temperature in this instance since interstitial sites are always present in metals.

5.3 COKE FORMATION

Three types of coke have been observed in this study, carbon plates, coke protrusions and coke nodules. Due to the limitation of this project, a detailed analysis of the corrosion products and carbides formed could not be carried out. However, the physical appearances of the coke deposits were different in shape and size but had similar structures at a microscopic level. The microscopic structure consisted of graphite filaments with metallic particles. The particles found in the corrosion product demonstrate that the metal dusting process had occurred and is the mechanism responsible for the disintegration and wastage of the alloys and steels tested.

5.4 MEASUREMENT OF THE RESISTANCE TO METAL DUSTING

From the results presented, it is interesting to note that the most resistant alloys (viz. Alloy 690 and 693) to metal dusting had higher mass loss than alloys that were severely attacked by metal dusting. These alloys lost mass more than three times as compared to the alloys that were severely attacked by metal dusting at 650°C for 500 hours. In addition, both Alloy 690 and 693 lost more mass than Alloy 601 at 500°C for 268 hours which was severely metal dusted. HR 120 which also suffered severe metal dusting lost less mass when compared to the metal dusting resistant Alloy

693. It seems that this phenomenon has not been reported in the metal dusting literature. It is well known that chromium oxide provide protection against metal dusting and since Alloy 690 and 693 had a considerable high amount of chromium. Thus the resistance of these alloys can only be attributed to the formation of the chromium oxide film even though the mass loss suggest otherwise. In addition, the mass loss maybe attributed to excessive oxidation and spallation. However the mass loss of the alloys that suffered severe metal dusting is attributed to pitting. The mass loss of Alloy 690 and 693 can not be attributed to pitting as they did not show any discernible pits. It is therefore concluded that the mass loss/gain is unreliable to be used as a measure of the resistance to metal dusting corrosion.

5.5 MECHANISMS OF METAL DUSTING

Carbon from the reaction gas mixture CO-H_2-H_2O is absorbed as follows;

$$\mathbf{CO + H_2 = H_2O + C\ (dissolved)}$$

and diffuses into the alloy. Comparing the SEM micrograph of the cross-section of an alloy, as shown in Figure 5.1, with the sketches in Figure 5.2, it seems that during the metal dusting exposure, carbon diffuses through the interstitial sites and grain boundaries. Then, after some time carbon is transformed into graphite. The formation of graphite in the interstitial sites and along the grain boundaries separates the metal matrix. The metal particles generated from the disintegration of the iron-nickel matrix would acts as a catalyst for further carbon deposition from the CO-H_2-H_2O gas mixture leading to more fragmentation of the particles. Hence the coke consists of graphite and the sub micron particles as shown in Figure 5.1. These mechanisms would apply for nickel-based alloys. For iron-based alloys, the mechanism is slightly different since unstable carbides are formed. Subsequent formation of graphite on the cementite renders it to be unstable and decomposes into metallic particles and

graphite as suggested by Grabke *et al* and other researchers [8, 17, 27, 28, 39, 40, 44-46].

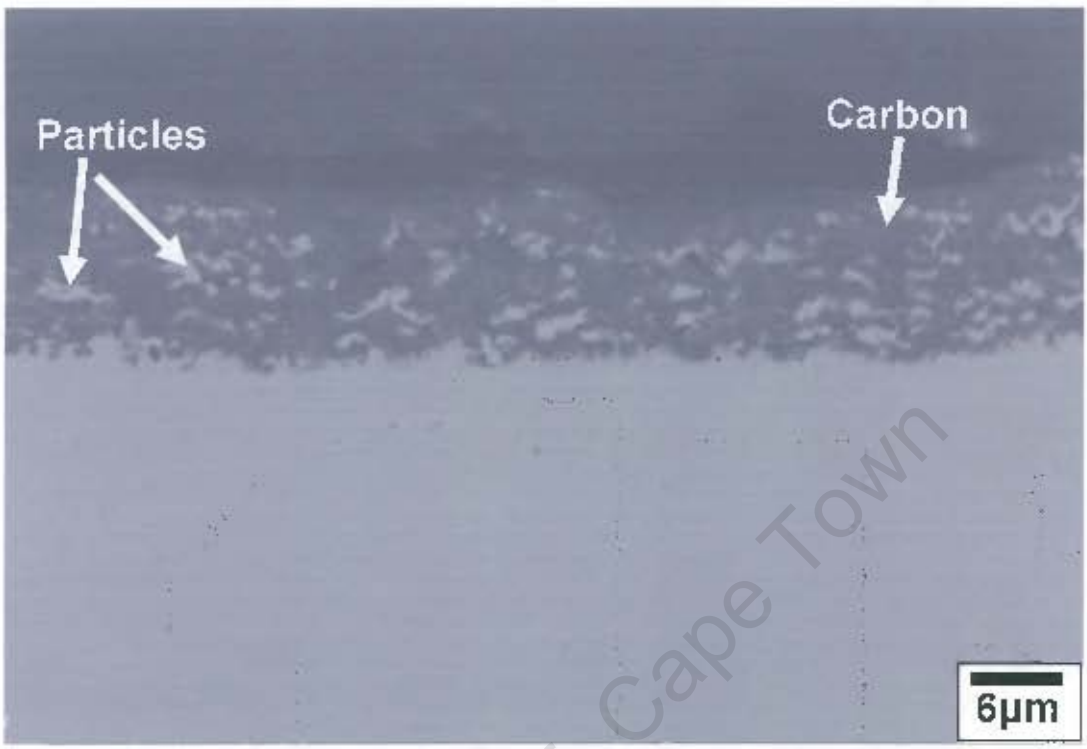

Figure 5.1: Metal dusting of Alloy 214. Metal particles are embedded in the coke.

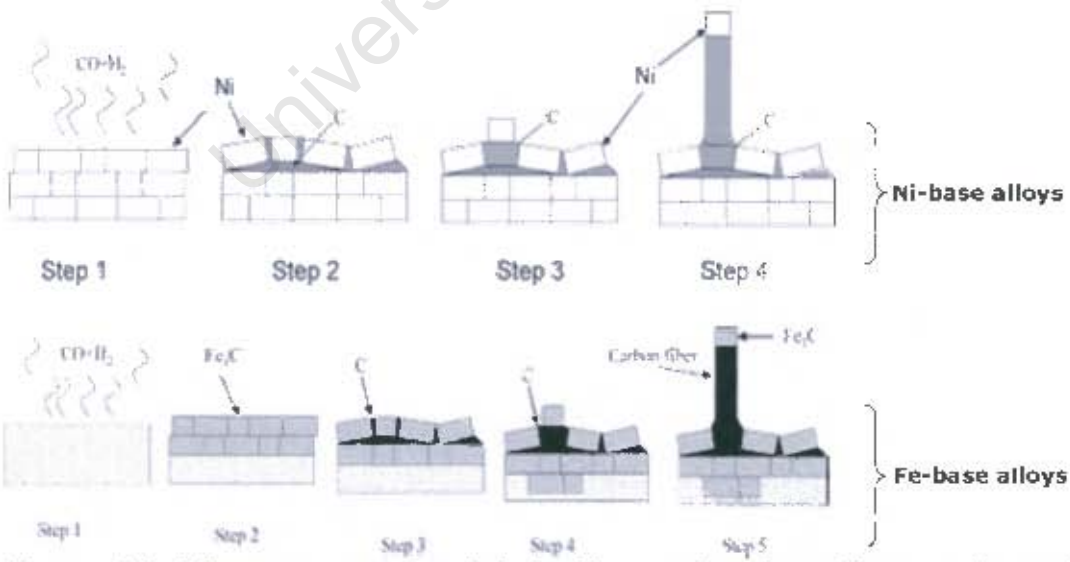

Figure 5.2: The process of metal dusting and carbon filament formation in nickel- and iron-based alloys [24, 67].

5.5 SUMMARY

From the results and discussion presented, it is apparent that metal dusting is affected by oxidation, carburization and temperature. Oxidation is affected by the level of Cr, microstructure of the alloy, oxide spallation, and surface finish. Oxidation processes in the Ni-Fe-Cr alloys leads to the formation of Cr_2O_3 on the surface of the alloys to protect it against carbon ingress.

Defects on the oxide scale and/or oxide spallation provide access for carbon to diffuse into the alloy. When the oxide scale fails, protection against carbon is hindered. The protection can only be retained if the oxide scale is self-repairing. Self-repairing is promoted only if sufficient Cr remains high at the alloy surface. If the alloy surface is depleted of Cr, reparation of the Cr_2O_3 would not occur. A Cr diffusion coefficient is higher in ferritic lattices than in austenitic lattices. Thus Cr will diffuse faster in ferritic alloys than in austenitic alloys. Cr will be supplied at lower rates in the case of austenitic alloys and hence Cr_2O_3 would not form readily and continuously as it was the case in the poor resistance showed by Alloy 600. Ferritic alloys such as GR 309 and 253 MA showed better resistance than Alloy 600 and Alloy 214, which has an austenitic structure.

Carburization is affected by oxide scale formation which forms a barrier for further carbon ingress and addition of strong carbides formers which reduces the dissolved carbon. In addition, carburization is also affected by elements that reduce the solubility and diffusivity of carbon, such as high nickel content. The formation of carbides such as titanium, molybdenum and tungsten carbides consumes dissolved carbon and thus sufficient Cr would be available to form a protective oxide scale. All alloys that were ground in this project showed greater resistance to metal dusting compared to the corresponding as-received alloys with perhaps the exception of alloy 253 MA. This phenomenon is attributed to the increased dislocation density which provided a high vacancy concentration for Cr to diffuse faster to the surface to form a protective oxide scale.

This mechanism was not available for the alloys in the as-received condition. Hence the onset of metal dusting occurred earlier than for the corresponding ground alloys.

Alloy 230 and HR 160 showed better resistance at 650°C due to the combination of oxide forming elements, strong carbides forming elements, low Fe content, and increased diffusion paths for Cr by grinding. The most resistant alloys were Alloy 690 and Alloy 693. The latter did not show any discernible metal dusting attack because of its good combination of high Cr and high Ni content. As far as the temperature is concern, metal dusting becomes more aggressive at low temperatures. The oxygen partial pressure at 500°C was 1.96 $X10^{-31}$ atm whereas at 650°C it was 5.05 $X10^{-26}$ atm. Thus, at 500°C, the oxidation process is affected and becomes sluggish. In addition the oxide scale is not readily formed especially for alloys with a low Cr content. The carbon activity was also affected by temperature since it was very high at 500°C and low at 650°C. Thus a high carbon activity promoted the early carbon deposition on the alloy surface and at the same time oxidation was hindered at low temperature. There was a subtle difference in the onset of metal dusting for all alloys in both conditions. The effect of the present heat treatment did not affect the resistance of the tested alloys to metal dusting.

The shapes of the reproducibility graphs were similar to that of the original test for each of the alloys examined as shown in Figure 4.3 and 4.5 up to 196 hours. The percentage error between the mass change of the original tests and reproducibility tests after 196 hours was very low. A percentage error less than 10% is considered acceptable for long time exposure. Since the percentage error was below 10%, the results are deemed to be reproducible and the simulation rig is able to produce constant severe metal dusting environment.

The present study has demonstrated that high chromium Alloy 693 had much better resistance than low chromium alloys such as Alloy 600. However, high mass loss of Alloy 693, 690 and GR 309 showed that the

severity of metal dusting cannot only be based on the weight loss. Surface analysis is the most accurate way of measuring the severity of metal dusting. Most alloys showed severe pitting with little mass loss and some less pitting with high mass loss as it was the case for Alloy 693 and 690. For this study, comparing the depth penetration from the sample cross-section with the mass change proofed fruitless as no relationship was found and these behaviour can be attributed to narrow and small size of the pits on the surface of the alloys. Thus, the present study has shown that the weight loss/gain is unreliable as a measure of the resistance to metal dusting corrosion. Considering the complex nature of metal dusting, it is of importance to note that metal dusting is governed by oxidation and carburization. Oxidation of ternary alloys is very complicated to understand and it is strongly recommended that the oxidation resistance of Alloy 693 and 690 be tested since the observed mass loss is attributed to oxide spallation.

CHAPTER SIX

CONCLUSIONS

Commercial alloys of ferritic and austenitic structures have been exposed to severe carburizing gas mixture at 500°C and 650°C in order to evaluate factors that affect the resistance to metal dusting. Tests were carried out on samples as-received, prepared with a ground surface or heat treated at 850°C for one hour. The exposure times ranged from 268 to 500 hours in a CO-H_2-H_2O gas mixture under a pressure of 1.2 atm and carbon activity of between 16 and 500. The following conclusions are drawn:

- The simulation rig is able to produce a severe and consistent metal dusting environment.
- Surface treatment by grinding had a strong effect in promoting the resistance to metal dusting.
- The test temperature, carbon activity, and oxygen potential of the gas atmosphere has an influence on propensity of metal dusting.
- The composition of the alloys, particularly those with oxides forming elements such as Cr, Si, and Al can provide protection against metal dusting. In addition, carbide forming elements such as tungsten and molybdenum does enhance the resistance to metal dusting.
- Oxidation of alloys can suppress carburization and metal dusting by the formation of a protective oxide scale which is favoured by with a high Cr (>25 wt %) and surface deformation.
- Metal dusting started from local defects in the oxide film.
- Coking and metal dusting were two processes that promote each other.

- From this limited exposure series, the influence of the present heat treatment which did not alter the microstructure or mechanical properties did not affect the metal's resistance to metal dusting.
- The most susceptible alloys to metal dusting were GR 309, 253 MA, Alloy 600, HR 120, Alloy 601, and Alloy 214 - .these were had either low chrome and / or high iron contents.
- Alloys that showed considerable resistance to metal dusting were HR 160 and Alloy 230 at 650°C. These alloys had very low iron contents and had carbide forming elements.
- The alloy that had the worst resistance to metal dusting was Alloy 800HT. This alloys had a relatively high iron content and no carbide formers.
- The alloys that showed the highest resistance to metal dusting was Alloy 690 and Alloy 693, but Alloy 693 offered better resistance than Alloy 690 due to its high Cr content, high nickel and low iron and oxide forming elements, aluminium and silicon.
- Mass loss/gain is unreliable as a measure of the resistance to metal dusting as shown by Alloy 690 and 693.
- In principle, any material that can dissolve carbon and form carbides will be susceptible to metal dusting.

CHAPTER SEVEN

RECOMMENDATIONS FOR FUTURE WORK

The following further areas of research are recommended:

- Evaluation of the resistance of metal dusting to alloys containing copper, since solubility of carbon in copper is thought to be extremely slow and to be non catalytic to carbon deposition. Hence addition of copper to nickel-chromium alloys might suppress metal dusting.
- Fabrication and evaluation of the following model alloy: 50%Ni-3%Fe-30%Cr-10%W-5%Al. The solubility and diffusivity of carbon in nickel is low when compared to iron, consequently high nickel content in an alloy will help to reduce the solubility of carbon. Higher chromium content would ensure that a protective chromium oxide scale is formed to retard metal dusting whereas the presence of tungsten will help to preserve the chromium level as tungsten will form carbides instead of chromium forming carbides alone. Aluminium can also form a protective oxide scale to retard carbon ingress. A good balanced combination of the above mentioned elements will suppress metal dusting.
- Evaluation of the effects of chromizing and aluminizing metal components to metal dusting resistance. Enriching the surface region of alloys by chromium and aluminium would endow alloys with excellent resistance against corrosion and oxidation.
- Evaluation of the effects of protective coatings against metal dusting. Coatings based on strong oxide formers such as Cr, Si, and Al which are capable of forming protective oxide scales at high temperatures under aggressive reducing environment of metal dusting.
- Investigating how carbon plates and coke protrusions affect the kinetics of metal dusting. Carbon plates seemed to grow rapidly on

alloys with high content of iron and to accelerate the rate of metal dusting. Most alloys which had multiple carbon plates were uniformly attacked whereas alloys which had coke protrusions had erratic pitting.

CHAPTER EIGHT

REFERENCES

1. H.J. Grabke, *Super saturation of iron with nitrogen, hydrogen or carbon and the consequences*, Materials and Technology, 38(5), (2004), 211-222.
2. R.C. Yin, I.M. Allam and A. Al-Farayeddhi, *Carburization behaviour of 310 stainless steel in CH_4/H_2 gas mixture with trace amount of oxygen*, Oxidation of Metals, 60 (3/4), (2003), 315-333.
3. M. Hansel, C.A. Boddington and D.J. Young, *Internal oxidation and carburization of heat-resistant alloys*, Corrosion Science, 45, (2003), 967-981.
4. Y. Cao, F. Ernst and G.M. Michal, *Colossal carbon super saturation in austenitic stainless steels carburized at low temperature*, Acta Materialia, 51(14), (2003), 4171-4181.
5. K. Natesan, Z. Zeng, V .A. Maroni, W.K. Soppet and D.L. Rink, *Metal Dusting Research at Argonne National Laboratory*, International Workshop on Metal Dusting, Argonne National Laboratory, Argonne, IL, http://www.et.anl.gov, (2001).
6. H.J. Grabke and M. Spiegel, *Occurrence of metal dusting-referring to failure cases*, Materials and Corrosion, 54(10), (2003), 799-804.
7. J.H. DeVahn, *Carbon Formation and Metal Dusting in Advanced Coal Gasification Process*, http://www.fischer-tropsch.org, (1997).
8. H.J. Grabke, *Metal dusting of low- and high-alloy steels*, Corrosion, 51(9), (1995), 711-720.
9. E. Pippel, J. Woltersdorf and H.J. Grabke, *Microprocesses of metal dusting on iron-nickel alloys and their dependence on the alloy composition*, Materials and Corrosion, 54, (2003), 747-751.
10. B.A. Baker and G.D. Smith, *Metal Dusting in Laboratory Environment-Alloying Addition Effects*, International Workshop on Metal Dusting, ANL, Argonne, IL, http://www.specialmetals.com, (2001).

11. H.J. Grabke, R. Krajak and E.M. Muller-Lorenz, *Metal dusting of high temperature alloys*, Materials and Corrosion, 44, (1993), 89-97.
12. Z. Zeng and K. Natesan, *Metal dusting problem with metallic interconnects for solid oxide fuel cell*, Materials Research Society, 756, (2003), FF4.2.1-FF4.2.6.
13. B.A. Baker and V.W. Hartmann, *A new nickel-based alloy for resisting metal dusting attack*, www.specialmetals.com.
14. M.L. Holland and H.J. De Bruyn, *Metal dusting failures in methane reforming plant*, International Journal of Pressure Vessels and Piping, 66, (1996), 125-133.
15. M. Maier, J.F. Norton and P. Puschek, *A study of factors contributing to the metal dusting of Fe-Cr-Ni alloys in highly carburizing atmospheres*, Materials at High Temperatures, 17(2), (2000), 347-354.
16. Y. Nishiyama, N. Otsuka, T. Kudu and O. Miyahara, *Metal Dusting of Nickel-Base Alloys in Simulated Syngas Mixture*, Sumitomo Metal Industries, Ltd. Corporate R&D Labs, (2001).
17. H.J. Grabke, *Metal dusting*, Materials and Corrosion, 54(10), (2003), 736-746.
18. H.J. Grabke, E.M. Muller-Lorenz and M. Mike, *Metal dusting behaviour of welded Ni-base alloys with different surface finish*, Materials and Corrosion, 54(10), (2003), 785-792.
19. D. Callister, Jr., Materials Science and Engineering, an Introduction, Fourth Edition, John Wiley and Sons, (1996).
20. D. A. Jones, Principles and Prevention of Corrosion, Second Edition, Prentice Hall, (1996).
21. R.C. John, A.D. Pelton, A. L. Young, W. T. Thompson, I. G Wright and T. M. Besmann, *Assessing corrosion in oil refining and petrochemical processing*, Materials Research, 7(1), (2004), 163-173.
22. D.J. Young and B. Gleeson, *Alloy phase transformations driven by high temperature corrosion processes*, Corrosion Science, 44, (2002), 345-357.
23. K. Salvolaine, J. Mononen, R. Ilola and H. Hanninen, *Materials Selection for High Temperature Applications*, Helsinki university of

technology, Laboratory of Engineering Materials Publications, Espoo, (2005).

24. Z. Zeng and K. Natesan, *Relationship of carbon crystallization to the metal dusting mechanism of nickel*, Chemistry of Materials, 15, (2003), 872-878.
25. H.J. Grabke, *Corrosion by carbonaceous gases, carburization and metal dusting, and methods of prevention*, Materials at High Temperatures, 17(4), (2000), 483-487.
26. A.A. Kaya, *Microstructure of HK40 alloy after high-temperature service in oxidizing/carburizing environment*, Materials Characterization, 49, (2002), 23-34.
27. K.J. Stevens, A. J. Tack, C.W. Thomas and D. Stewart, *Through-wall carburization detection in ethylene pyrolysis tubes*, Journal of Physics D: Applied Physics, 34, (2001), 814-822.
28. P. Szakalos, R. Pettersson and S. Hertzman, *An active corrosion mechanism for metal dusting on 304L stainless steel*, Corrosion Science, 44, (2002), 2253-2270.
29. H. Ackermann, P. Karduck, H. Lucka, L. Lucks and A. Von Richthofen, *Metal dusting in low-NOx recirculation burners for fuel oil*, Corrosion Engineering Science and Technology, 40(3), (2005), 233-238.
30. Alloy Data Sheets, www.haynesintl.com, (2006).
31. Alloy Data Sheets, www.specialmetals.com, (2006).
32. Alloy Data Sheets, www.atlasmetals.com.au, (2006).
33. Alloy Data Sheets, www.multialloys.co.za, (2006).
34. K.J. Stevens, T. Levi, I. Minchington, V. Keast and S. Bulcock, *Transmission electron microscopy of high pressure metal dusted 316 stainless steel*, Materials Science and Engineering, A385, (2004), 292–299.
35. O. Coreno-Alonso, A. Duffus-Scott, C. Zanchez-Cornejo, J. Coreno-Alonso, F. anchez-de Jesus and A. Bolarin-Miro, *On the effect of σ-phase formation during metal dusting,* Materials chemistry and physics, 84, (2004), 20-28.

36. N. Tabet, I. Allam and R.C. Yin, *X-ray photoelectron spectroscopy study of the carburization of nickel-based alloy Haynes 214*, Applied Surface Science, 195, (2002), 166-174.

37. N. Tabet, I. Allam and R.C. Yin, *X-ray photoelectron spectroscopy investigation of the carburization of 310 stainless steels*, Applied Surface Science, 220, (2002), 259-272.

38. R.C. Yin, *Carburization performance of incoloy 800HT in CH_4/H_2 gas mixtures*, Materials Science and Engineering, A380, (2004), 281-289.

39. H.J. Grabke, E.M. Muller-Lorenz and A. Schneider, *Carburization and metal dusting of iron*, Iron and Steel Institute of Japan, 41, (2001), S1-S8.

40. H.J. Grabke, *Mechanism of metal dusting of low and high alloy steels*, Solid State Phenomena, 41, (1995), 3-16.

41. G.W. Han, D. Feng and B. Deng, *Metal dusting and coking of alloy 803*, Corrosion Science, 46, (2004), 443-452.

42. R. Yin, *Thermodynamic roles of metallic elements in carburization and metal dusting*, Oxidation of Metals, 61(3/4), (2004), 323-337.

43. R. Yin, *Thermodynamic aspects of iron in metal dusting*, Oxidation of Metals, 60 (1/2), (2003), 103-116.

44. H.J. Grabke, *Thermodynamics, mechanisms and kinetics of metal dusting,* Materials and Corrosion, 49, (1998), 303-308.

45. E. Pippel, J. Woltersdorf and H. J. Grabke, *Microprocesses of metal dusting on iron-nickel alloys and their dependence on the alloy composition*, Materials and Corrosion, 54, (2003), 747-751.

46. E. Muller-Lorenz, S. Strauss and H. J. Grabke, *Effects of Surface State, Microstructure and Alloying Addition on Metal Dusting Resistance of High Alloy Steels*, Annual Conference of European Federation of Corrosion, Netherlands, (1998).

47. P. Szakalos, M. Lundberg, and R. Pettersson, *Metal dusting of alumina forming Ni-base alloy*, Corrosion Science, 48, (2006), 1679-1695.

48. B. A. Baker and G.D. Smith, *Alloy Solution to Metal Dusting Problems in the PetroChemical Industry*, http://www.specialmetals.com.

49. E.M. Muller-Lorenz and H.J. Grabke, *Coking by metal dusting of steels,* Materials and Corrosion, 50, (1990), 614-619.

50. J. Zhang, A. Schneider and G. Iden, *Characterization of the coke formed during metal dusting of iron in CO-H_2-H_2O gas mixtures,* Corrosion Science, 45, (2003), 1329-1341.

51. J. Zhang, A. Schneider and G. Iden, *Effects of gas composition on cementite decomposition and coke formation on iron,* Corrosion Science, 45, (2003), 281-299.

52. J. Zhang, A. Schneider and G. Iden, *Metal dusting of iron in CO-H_2-H_2O gas mixtures at 600°C,* Journal of Corrosion Science and Engineering, 6(H057), (2003).

53. B.A. Baker and G.D. Smith, *Metal Dusting in Laboratory Environment-Alloying Addition Effects,* International Workshop on Metal Dusting, ANL, Argonne, IL, http://www.specialmetals.com, (2001).

54. S. W. Dean, *Metal Dusting Study,* http://www.corrtech.com, (2002).

55. S. W. Dean, *Estimating Metal Dusting attack on Stainless Steel Alloys in Syngas Environment,* Corrosion/2001, Paper no. 01384, Houston, TX: NACE, (2001).

56. C. Ostwald and H.J. Grabke, *Initial oxidation and chromium diffusion-effects of surface working on 9-20% Cr steels,* Corrosion Science, 46, (2004), 113-1127.

57. H.J. Grabke, E. M. Lorenz, B. Eltester and M. Lucas, *Formation of chromium rich oxide scales for protection against metal dusting,* Materials at High Temperatures, 17(2), (2000), 339-346.

58. D.L. Klarstrom, H.J. Grabke and L.D. Paul , *The Metal Dusting Behavior of Several high Temperature Nickel-based Alloys,* Corrosion/2001, Paper no. 01379, Houston, TX: NACE, (2001).

59. Y. Nishiyama, N. Otsuka and T, Kudo, *Metal dusting of Cr-Ni steels and Ni-base alloys in simulated syngas mixture,* Corrosion Science, (2005), **In press**.

60. S.E. Sadique, M.A.H. Mollah, M.M. Ali, M.M. Haque, S. Basri, M.M.H.M. Ahmad and S.M. Sapuan, *Influence of aluminium addition on the rate of oxidation of iron-chromium alloys,* Journal of Corrosion Science and Engineering, 1(H018),(1999).

61. C.H. Toh, P.R. Munroe and D.J. Young, *Metal dusting of Fe-Cr and Fe-Ni-Cr alloys under cyclic conditions*, Oxidation of Metals, 58(1/2), (2002), 1-21.

62. C. Piehl, Z. Toekei and H.J. Grabke, *Influence of chromium diffusion and different surface finishes on the oxidation behaviour of chromium steels*, Materials at High Temperature, 17(2), (2000), 243-246.

63. P. Perez, *Influence of the alloy grain size on the oxidation behaviour of PM2000 alloy*, Corrosion Science, 44, (2002), 1793-1808.

64. K.T. Voisey, Z. Liu and F.H. Stott, *Inhibition of Metal Dusting of Alloy 800H by laser Surface Melting*, Applied Surface Science, 252, (2006), 3658-3666.

65. A.J.L. Vaughan, Laboratory Simulation of Metal Dusting Corrosion, MSc Thesis, University of Cape Town, (1997).

66. D.R. Gaskell, Introduction to Metallurgical Thermodynamics, Second Edition, Panama, (1981).

APPENDIX A

Experiment A at 650°C

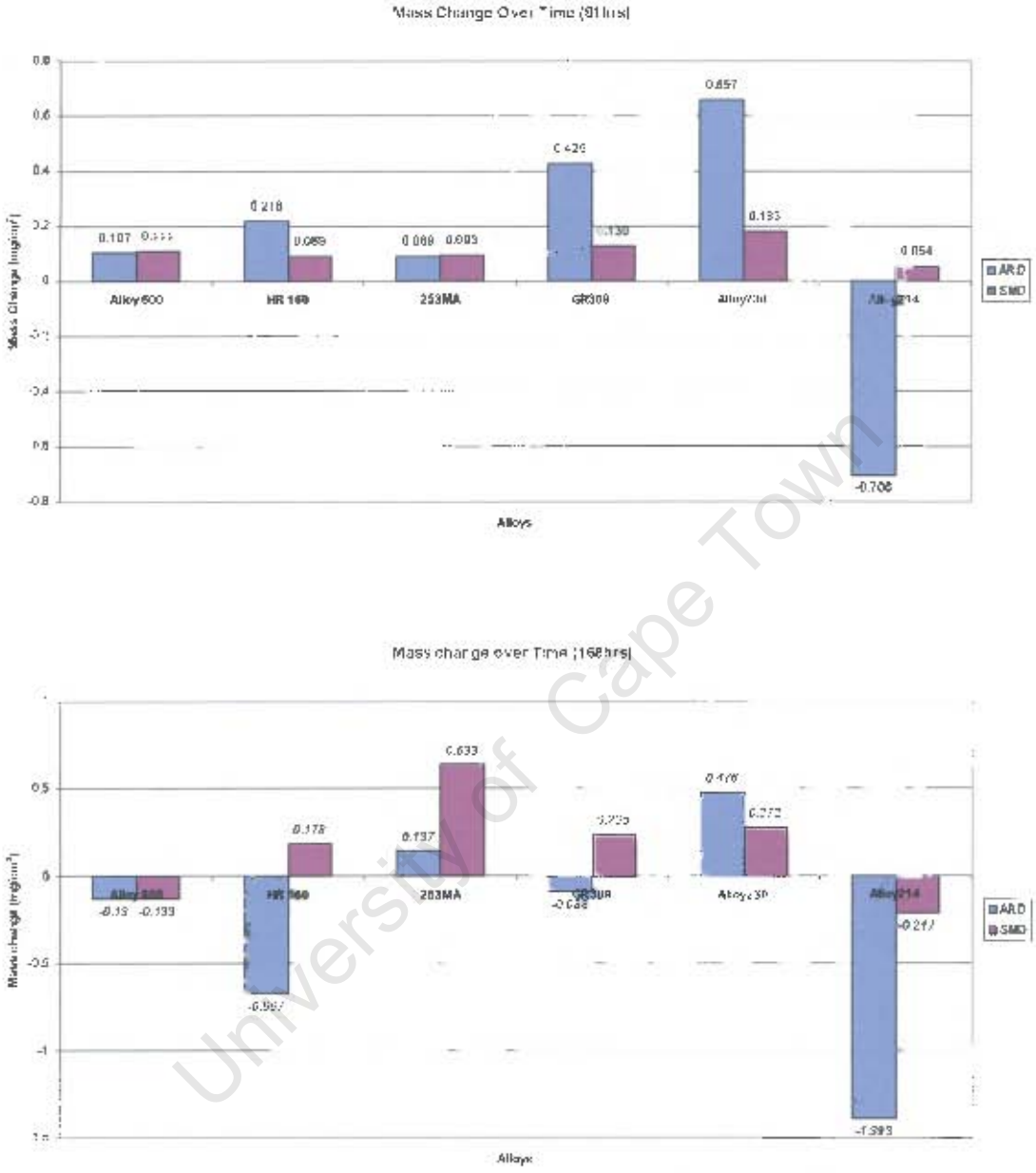

Figure 1: Mass change of exposed alloys after 81 hours and 168 hours in experiment A at 650°C, respectively.

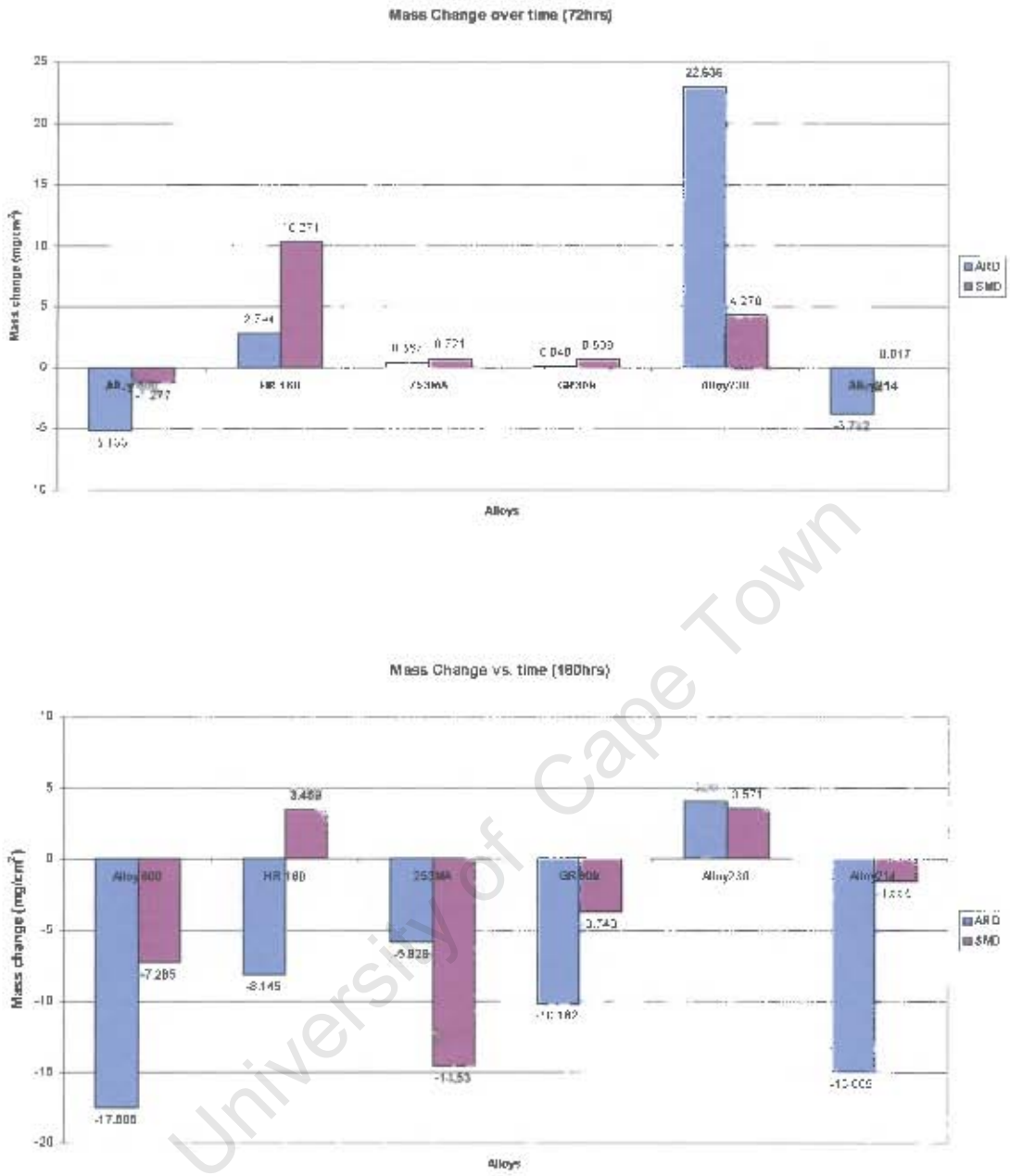

Figure 2: Mass change of exposed alloys after 72 hours and 180 hours in experiment A at 650°C, respectively.

Experiment B at 500°C

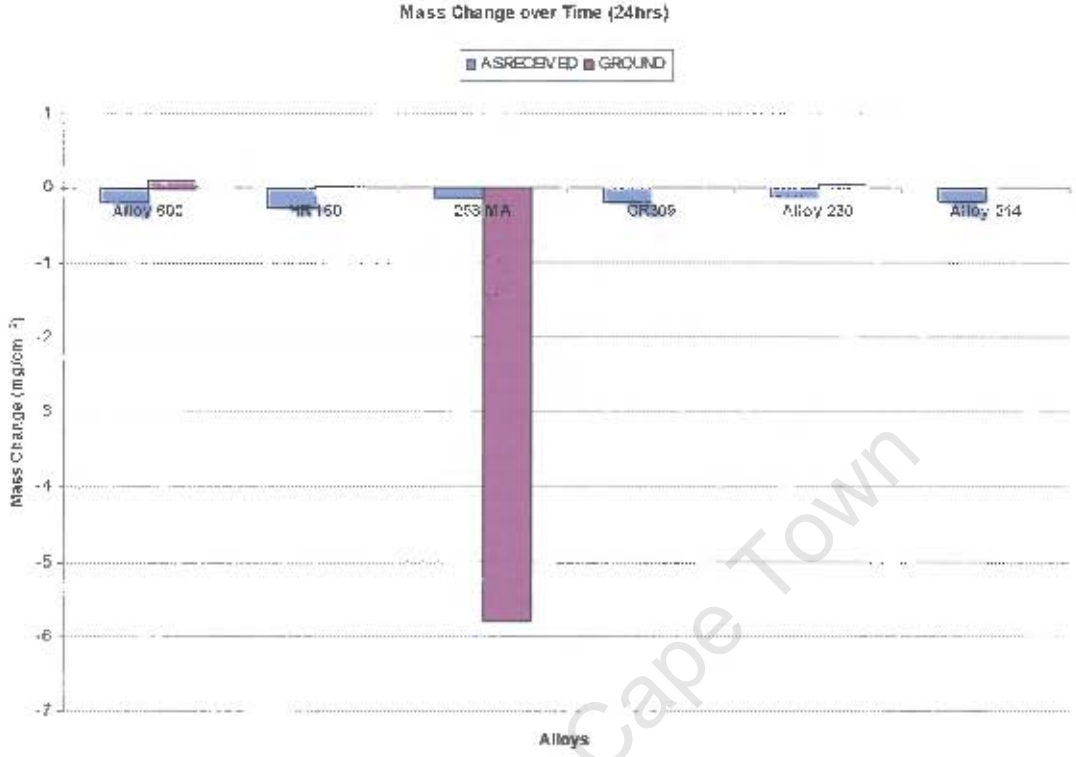

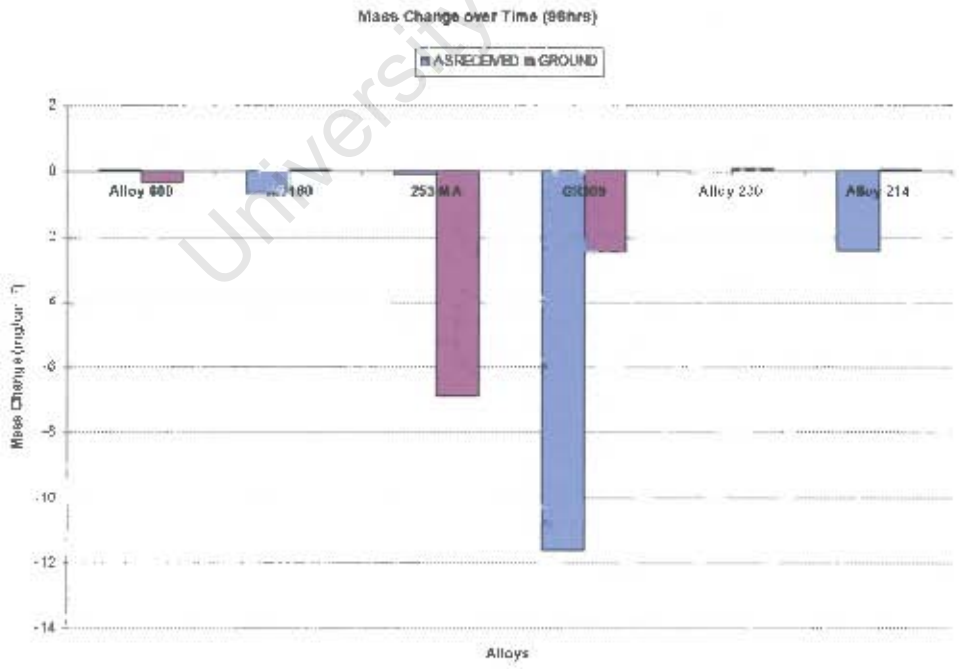

Figure 3: Mass change of exposed alloys after 24 hours and 72 hours in experiment A at 500°C, respectively.

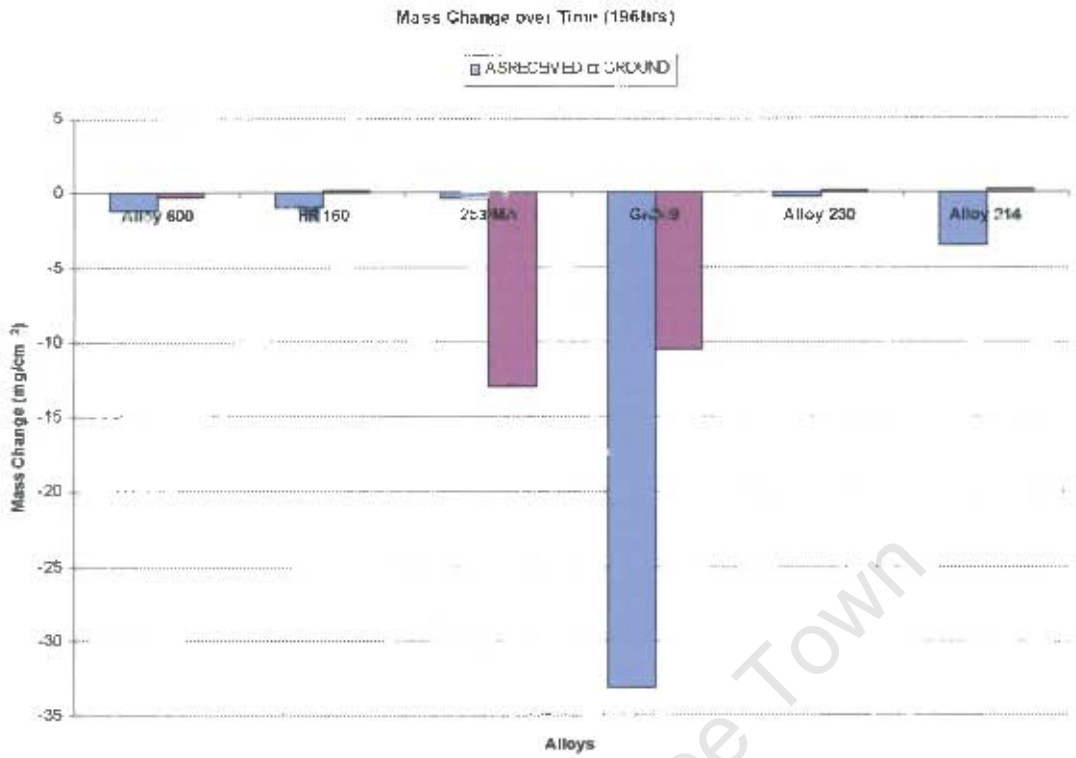

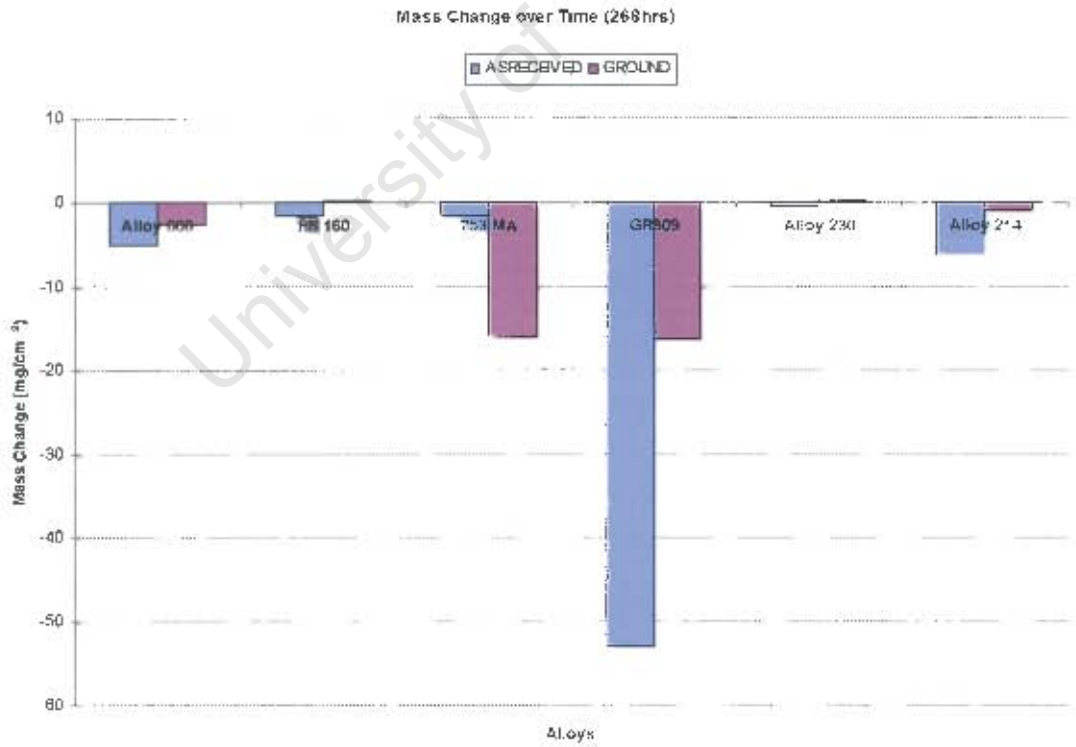

Figure 4: Mass change of exposed alloys after 100 hours and 180 hours in experiment A at 650°C, respectively.

Experiment C at 500°C

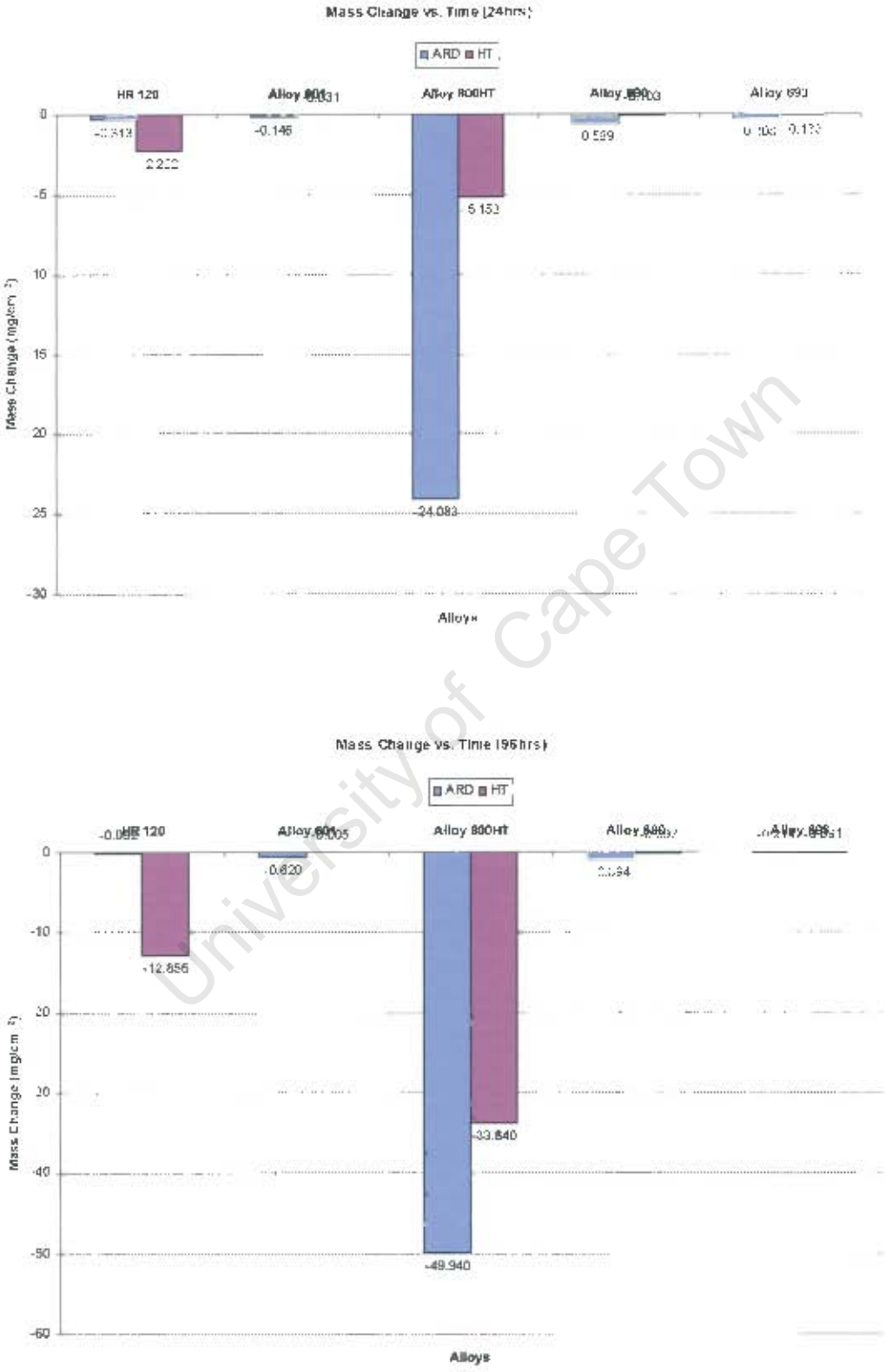

Figure 5: Mass change of exposed alloys after 24 hours and 180 hours in experiment A at 650°C, respectively.

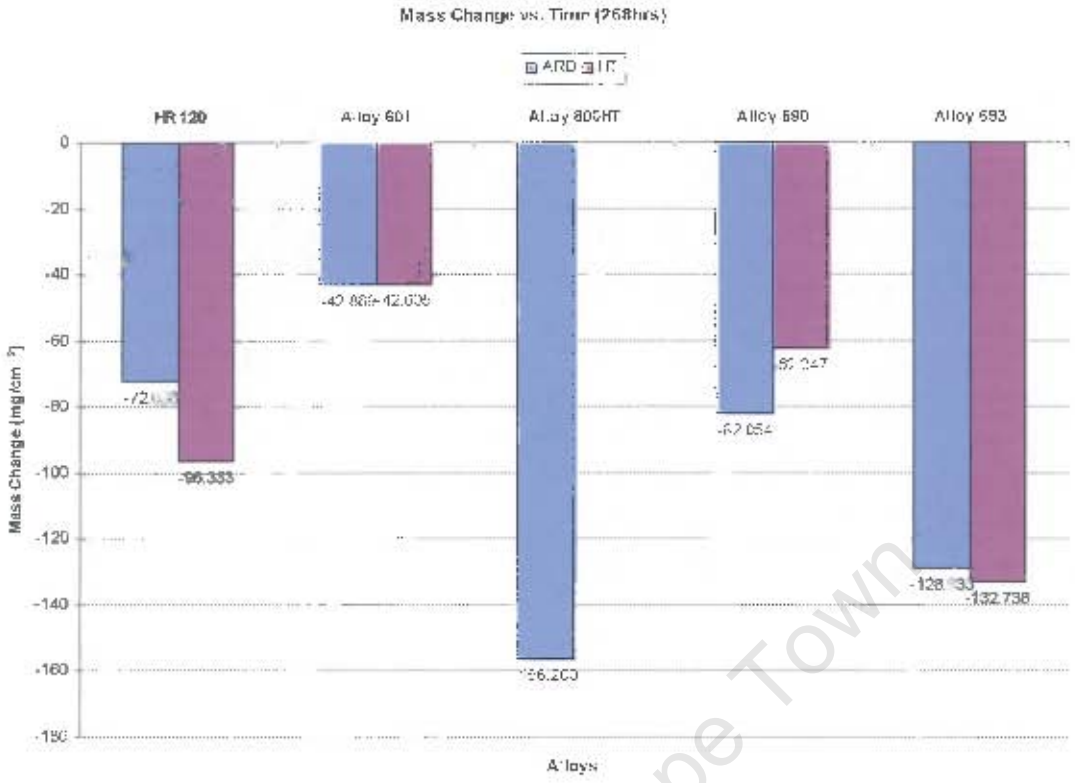

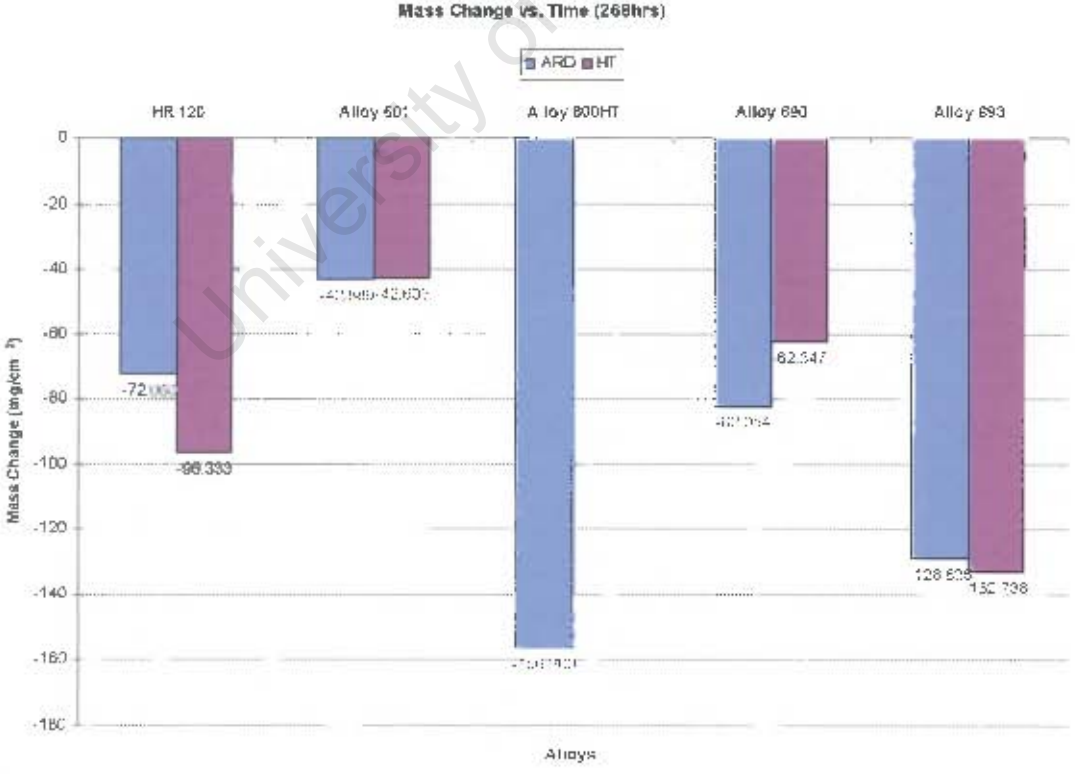

Figure 4: Mass change of exposed alloys after 100 hours and 180 hours in experiment A at 650°C, respectively.

Hardness Measurements for Experiment A at 650°C

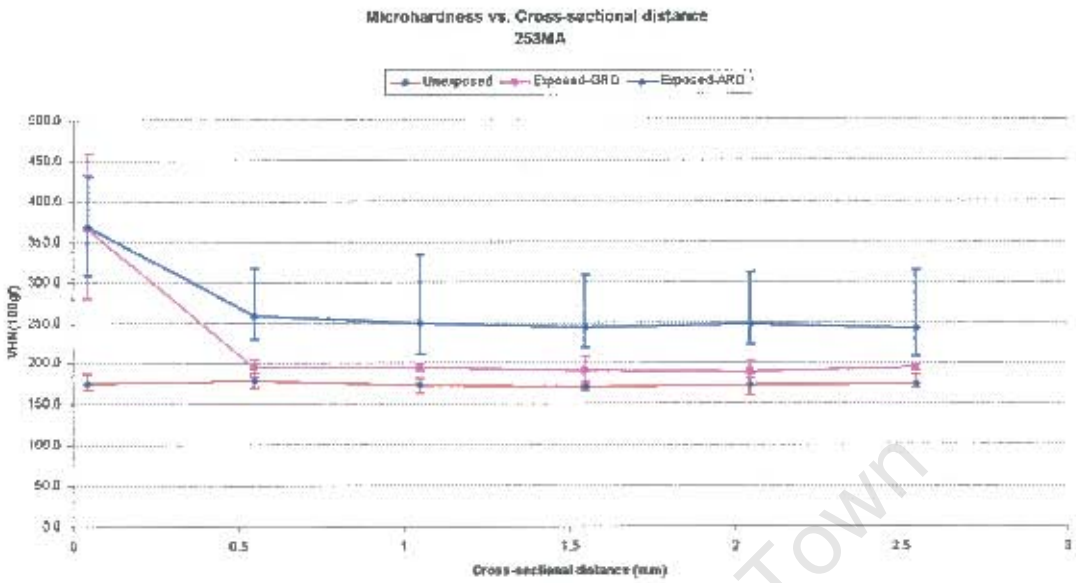

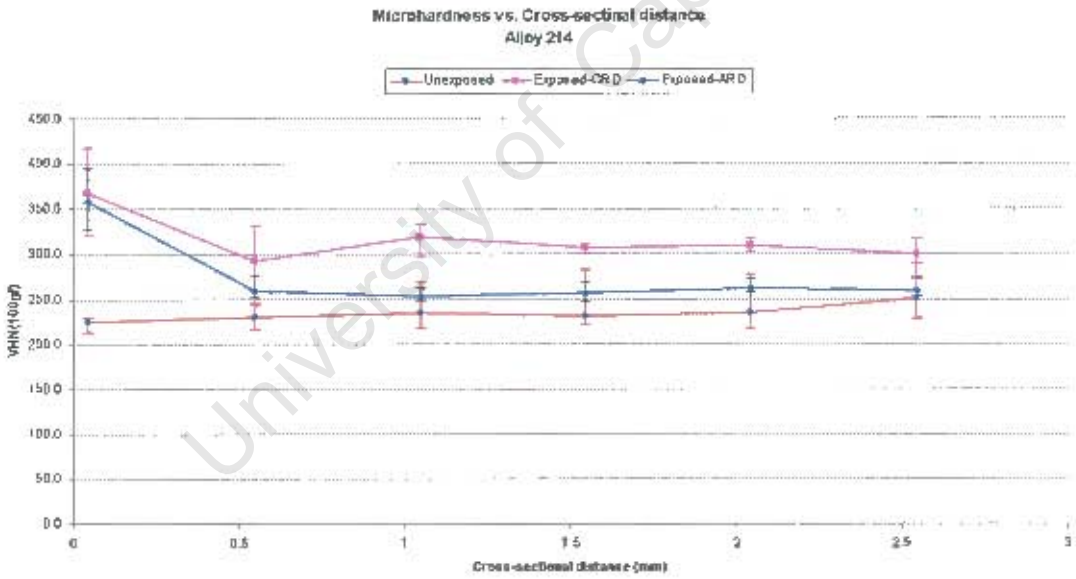

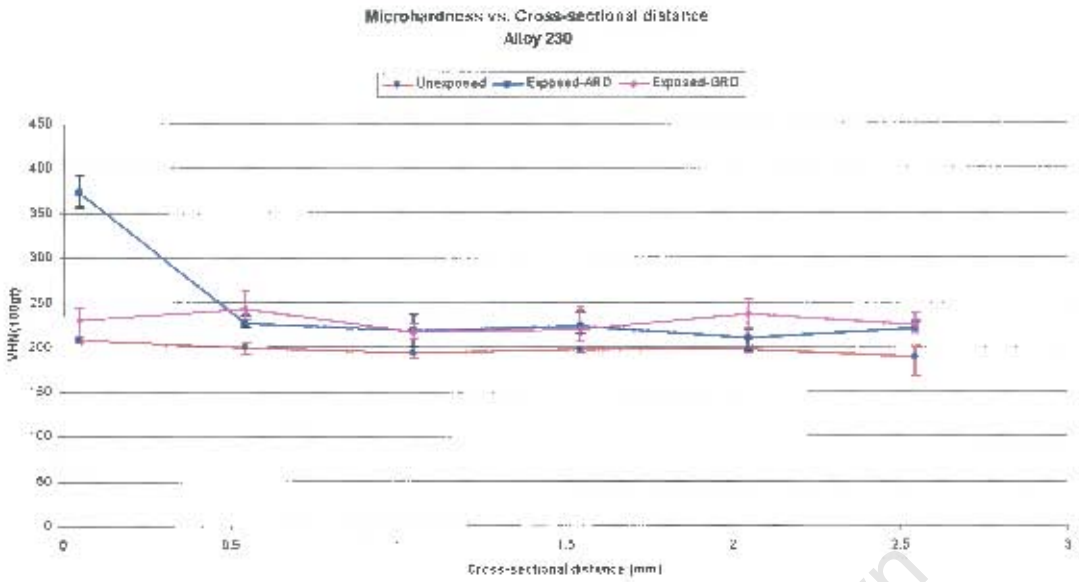

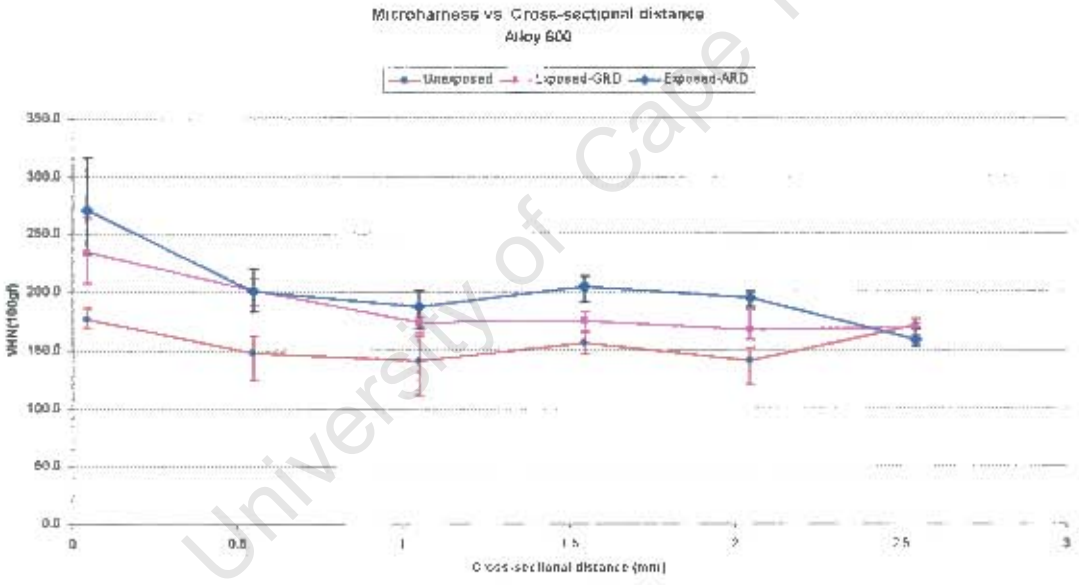

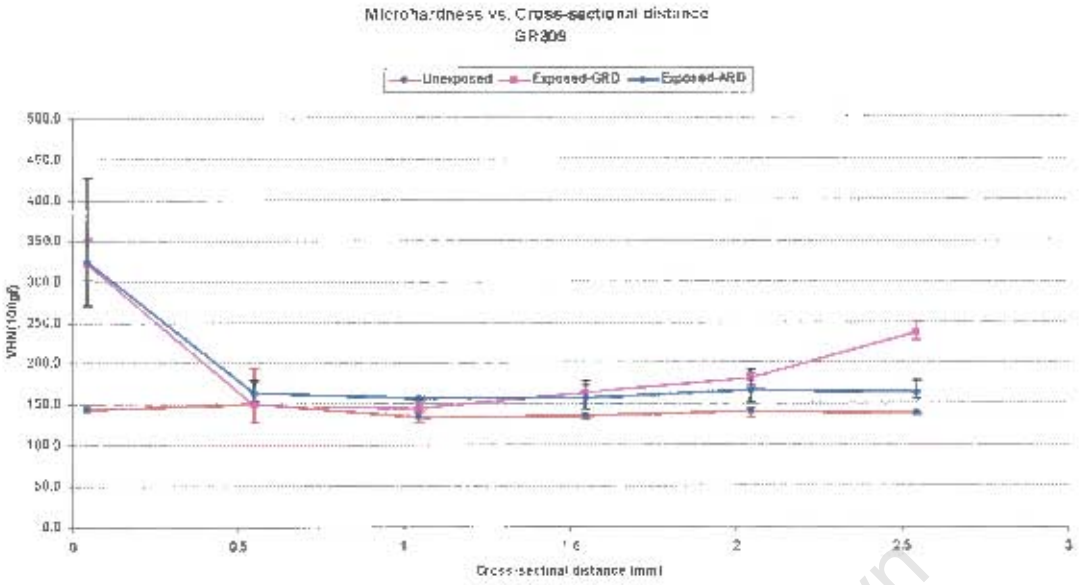

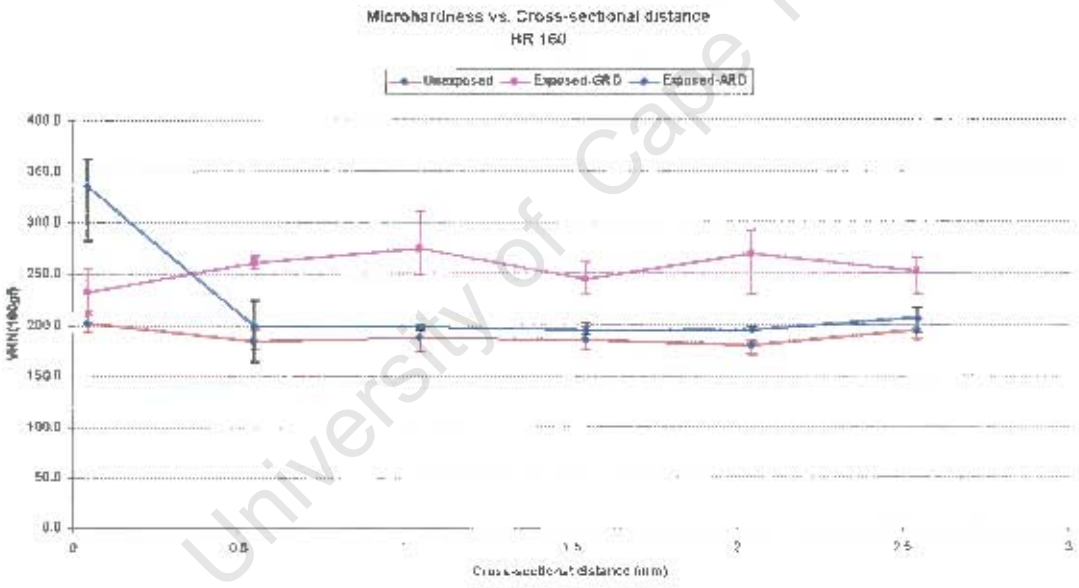

Hardness Measurements for Experiment B at 500°C

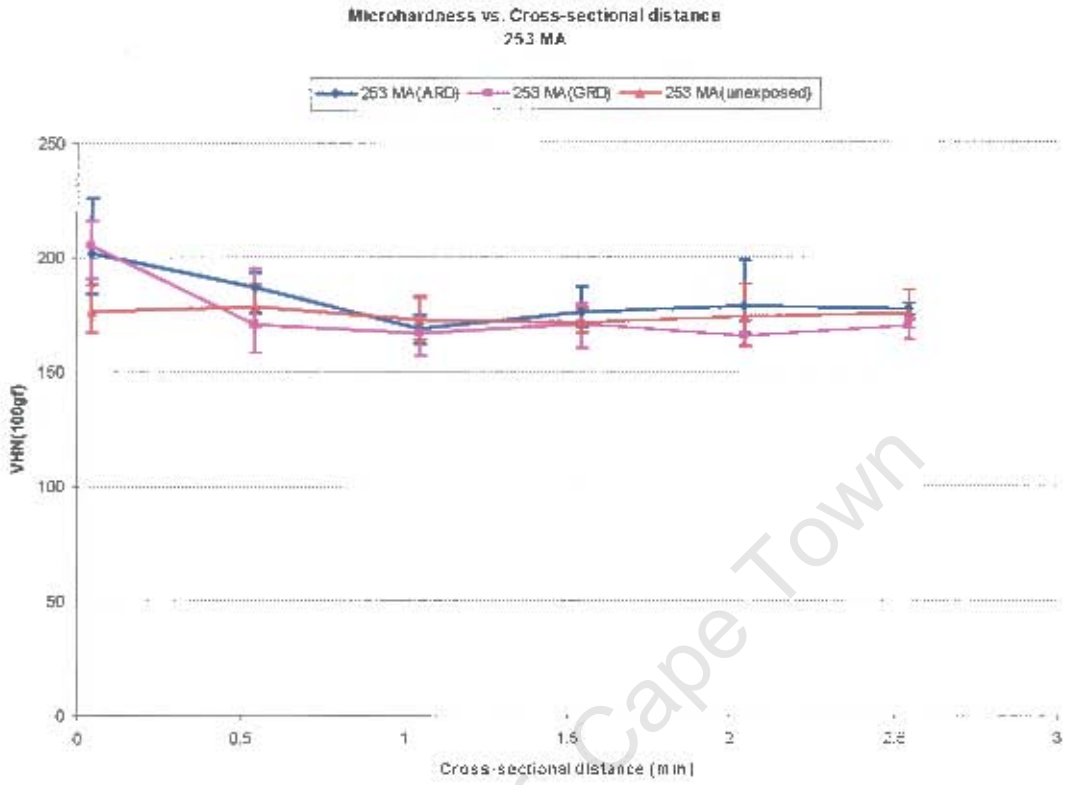

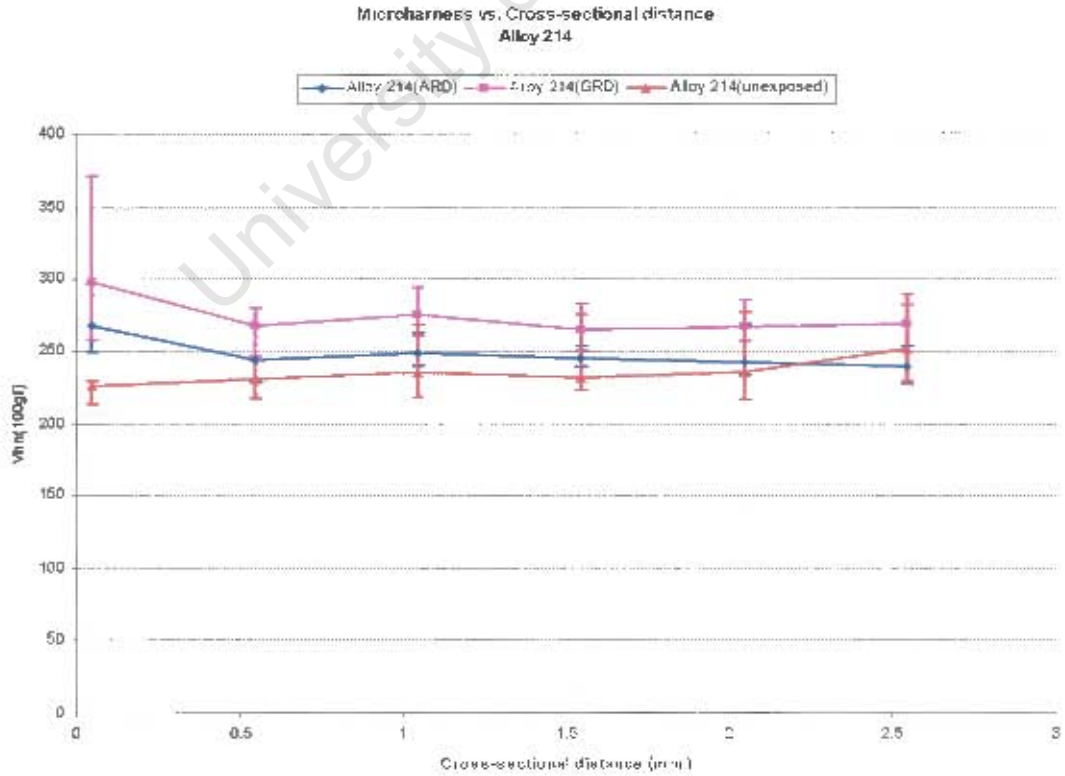

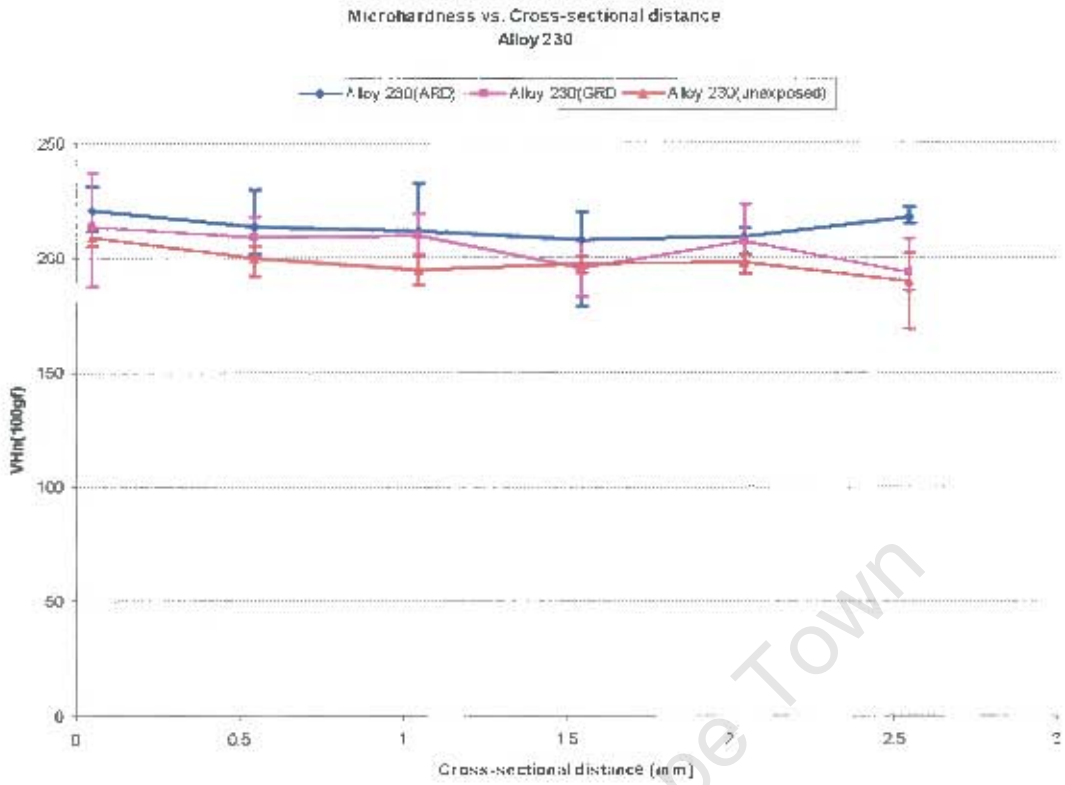

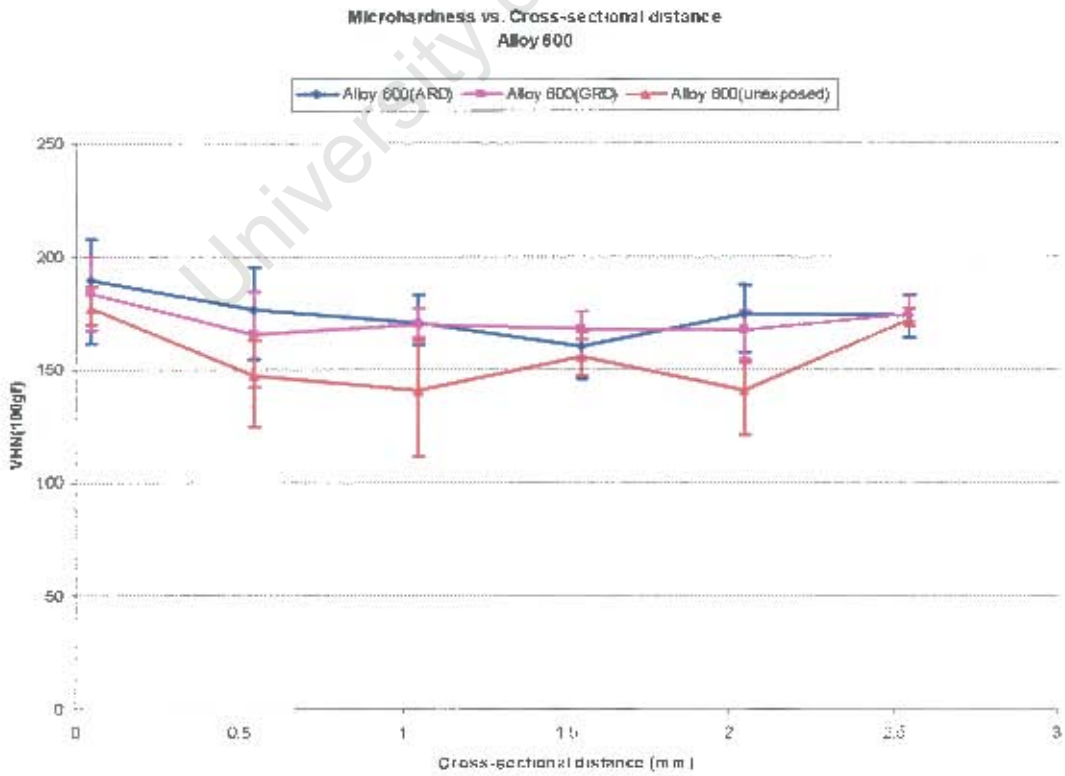

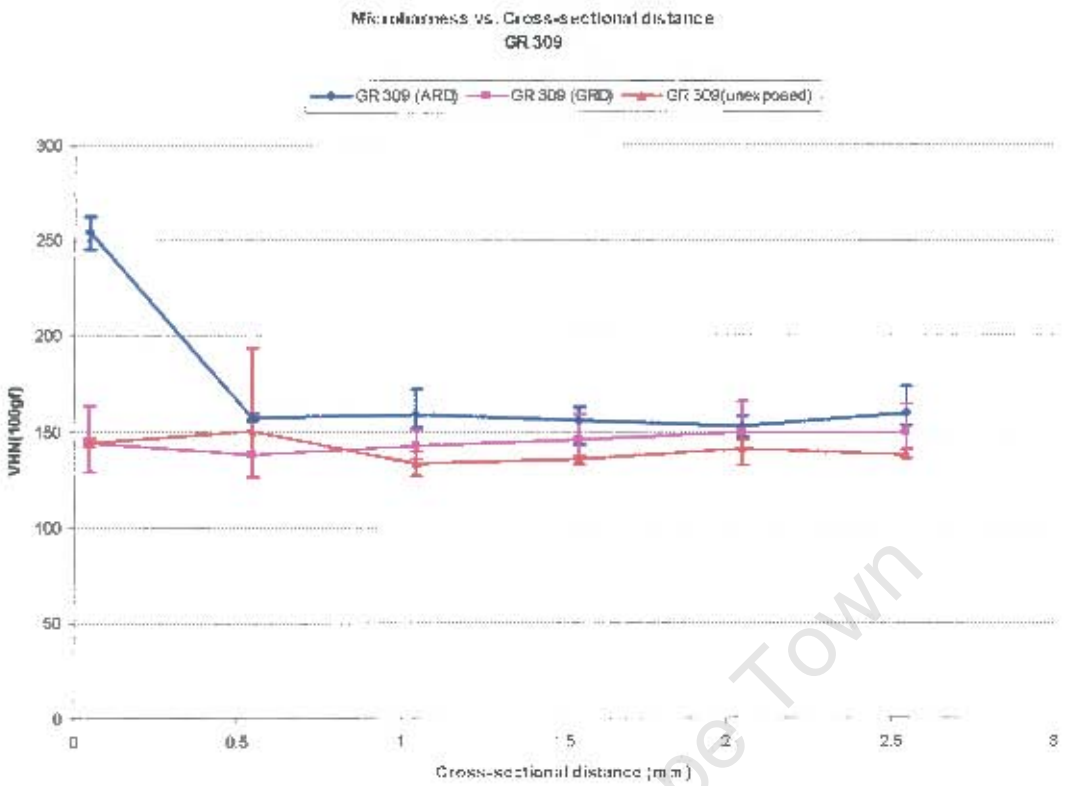

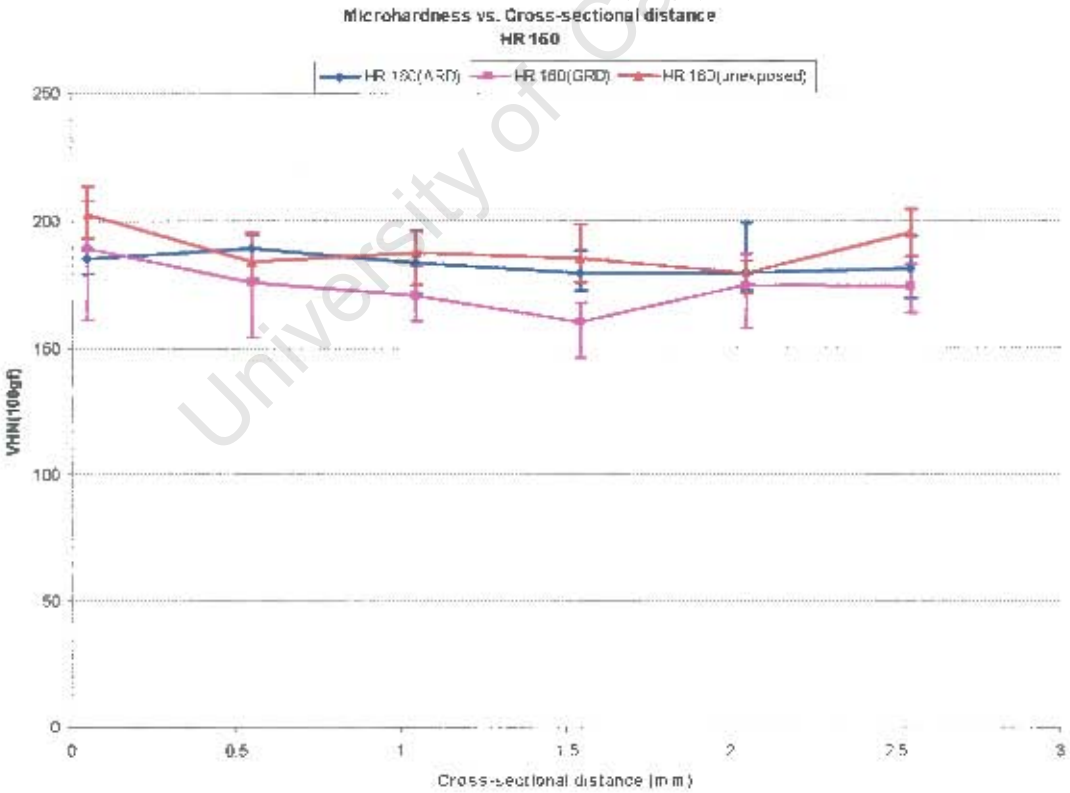

Hardness Measurements for Experiment C at 500°C